

https://dspace.org/

Identification and cellular localization of DD-carboxypeptidase-interacting proteins in mycobacterium smegmatis

Asmal, Rukaya

2015-09-17
http://hdl.handle.net/10539/18689

Downloaded from a DSpace repository. https://dspace.org/

Identification and cellular localization of DD-carboxypeptidase-interacting proteins in *Mycobacterium smegmatis*

Rukaya Asmal (700669)



A dissertation submitted to the Faculty of Health Science, University of the Witwatersrand, Johannesburg, in fulfilment of the requirements for the degree of Master of Science in Medicine.

2015

Declaration

I, Rukaya Asmal declare that this dissertation is my own work. It is being submitted for the degree of Master of Science in Medicine at the University of the Witwatersrand, Johannesburg. It has not been submitted before for any degree or examination at this or any other University.



01/04/2015

(Rukaya Asmal) Date

Dedication

I dedicate this work to the 3 most important, influential and supportive people in my life, my incredibly patient husband Yusuf Docrat and my parents Shameema and Ebrahim Asmal. Without you, none of this would have been possible.

Presentations of this work

Conference:	Wits Research Day and Postgraduate expo
Venue and Year:	University of Witwatersrand, 2012
Type of presentation:	Poster

Conference:	4th SA TB conference
Venue and Year:	Durban, 2014
Type of presentation:	Poster

Abstract

*Mycobacterium tuberculosis (*Mtb), the causative agent of tuberculosis (TB), is responsible for approximately 1.5 million deaths worldwide; a pandemic which is further exacerbated by the emergence of multi- and extensively drug resistant strains. The extensive morbidity and mortality associated with TB has brought about an urgent need for new drugs that promise to shorten treatment duration and reduce the daily pill burden. In this context, the mycobacterial cell wall, particularly the peptidoglycan (PG) layer, is a promising source of new drug targets due to the extensive number of bacterial-specific enzymes that are responsible for biosynthesis of this macromolecular component in bacterial cells. PG biosynthesis and cross-linking involves a number of membrane-bound as well as cytoplasmic enzymes, including penicillin-binding proteins (PBPs), which are the targets for beta-lactam antibiotics. In this study we further elucidate the role of DD-Carboxypeptidases (DD-CPases), a group of low molecular mass PBPs that play a crucial role in the biosynthesis and remodelling of PG in a variety of organisms. These enzymes cleave the terminal D-Alanine residue in PG and are postulated to be involved in preventing the formation of inappropriate cross-links. To identify possible interacting partners for two of the five putative DD-CPases (DacB and MSMEG_2433) in *Mycobacterium smegmatis*, a full-coverage, representative genomic library was constructed as fusions with the Gal4 DNA binding domain in a yeast two-hybrid vector. The genes encoding *dacB* and MSMEG_2433 were cloned as fusions with the Gal4 activation domain and these clones were used to screen the library for putative interacting partners. This analysis identified fifteen possible interacting partners in total for these two DD-CPases. DacB interacting proteins included a tetracycline regulator, an acyltransferase, as well as a subunit of the F_oF_1 ATP synthase. Putative interacting proteins identified for MSMEG_2433 included the same tetracycline regulator that was identified for DacB, a helicase, and PBP1A/1B (PonA2). PonA2 is of particular interest as its identification points

to a role for DacB in PG cross-linking. For cellular localization studies, C-terminal fusions with the mCherry; Venus and rsEGFP fluorescent proteins were created for DacB and MSMEG_2433. Fluorescence microscopy revealed weak or diffused signal from the mCherry and Venus fusion proteins, in contrast, the rsEGFP fusion yielded specific, robust signal and was used for further analysis. Localization studies revealed that both DacB and MSMEG_2433 localized to the cell pole either in a mono-polar or bi-polar fashion similar to that observed with other cell division proteins such as Wag31 and ParB. Furthermore, MSMEG_2433 also localized to the septum in some cases. Collectively, the data from this study suggests that DD-CPases may interact with other PG hydrolysing enzymes to exert their function in mycobacteria. Moreover, localization confirms an important role for these enzymes in cell growth and expansion, which occurs at cell poles in mycobacteria.

Acknowledgements

First and foremost, I would like to thank the **Almighty** for all the favours he has bestowed upon my family and I.

Secondly, to all my funders, the National Research Foundation (**NRF**), the University of Witwatersrand (Postgraduate merit award) and the DST/NRF Centre of Excellence for Biomedical TB Research, for funding me throughout my MSc.

My supervisor, mentor and a true inspiration, **Prof. Bavesh Kana**. You are more than just a supervisor, thank you from the bottom of my heart for your guidance and support. Your kindness and understanding is unsurpassed. You were always willing to listen and advise, whether personal or professional. It has been an honour to be your student, your training took me to a level of science I didn't know I was capable of reaching.

The microscopy unit at the University of Witwatersrand for allowing me to use the Confocal microscope and University of Cape Town, especially **Mohammed Jaffer**, for allowing me to use the TEM and taking the time to teach me the Immunogold technique.

My **colleagues** at the CBTBR, you welcomed me with open arms and gave me a second family. Nikki, Sbu, G, Chris, Zaaheeda, Melissa, Edith, Bhavna and everyone else at the lab who were always there to give recommendations, rejoice with me when experiments worked and to commiserate with me when cultures refused to behave.

To my family and friends, thank you for always being there for me, even when you didn't understand what it is that I do. To my **parents**, I am who I am because of your unwavering support and love. A combination of my dad's push and drive, and my mum's patience and understanding ensured that no matter how difficult things got, giving up was not an option.

Last but not least, to my husband **Yusuf** – no amount of words can express my gratitude to you. You believed in me even when I didn't believe in myself. This is as much yours as it is mine. "Ever thine, Ever mine, Ever ours."

Table of Contents

Declaration ii
Dedication iii
Presentations of this work iv
Abstract v
Acknowledgements vii
List of Figures xi
List of Tables xiii
Nomenclature xiv
1. Introduction 1
1.1. Background 1
1.2. TB Vaccines 2
1.3. Antimicrobial Chemotherapy 3
1.4. TB Pathogenesis 5
1.5. Mycobacterial Cell Wall 8
1.5.1. Peptidoglycan (PG) layer 10
1.6. Mycobacterial Growth 13
1.7. PG Hydrolases 16
1.7.1. Resuscitation Promoting factors (Rpfs) 18
1.7.2. L,D-Transpeptidases (Ldts) 20
1.7.3. Penicillin Binding Proteins (PBPs) 21
1.8. Study Aims and Objectives 26
2. Methods and Materials 27
2.1. Bacterial Strains, Plasmids and growth conditions 27
2.1.1. Growth of Mycobacterial Strains 29
2.1.2. Growth of *E. coli* strains 30
2.2. DNA manipulation 30
2.2.1. Mycobacterial DNA extraction 30
2.2.2. Transformation of bacteria 31
2.2.3. Plasmid preparation 33
2.2.4. Sodium Acetate Precipitation 34
2.2.5. Dephosphorylation of 5'ends 35
2.2.6. Restriction analysis 35
2.2.7. Ligation Reaction 35
2.2.8. Agarose Gel Electrophoresis 36

2.2.9. DNA extraction from Agarose Gels 36
2.2.10. DNA Quantification 36
2.2.11. DNA Sequencing 37
2.4. Library Preparation 37
2.5. Polymerase Chain Reaction (PCR) 38
2.5.1. Roche Fast Start PCR 38
2.5.2. Phusion High Fidelity PCR 38
2.5.3. PCR clean up 38
2.6. Cloning 39
2.6.1. 3-way cloning 39
2.6.2. Blunt-end cloning of DD-CPase-GFP fusions 39
2.7. Microscopy 41
2.7.1. Fluorescence Microscopy 41
2.7.2. Immunogold and Transmission Electron Microscopy (TEM) 41
2.8. Minimum Inhibitory Concentration (MIC) Determination 43
2.9. Assessment of growth and Gene Expression 43
2.9.1. Growth Curves 43
2.9.2. RNA Isolation 43
2.9.3. Reverse Transcriptase (RT) synthesis 44
2.9.4. Quantitative Real Time PCR (qPCR) 45
2.10. Southern Blot 45
2.10.1. Probe synthesis 45
2.10.2. Blotting 46
2.11. Yeast 2-Hybrid system 47
2.11.1. Cloning of bait for yeast interaction libraries 47
2.11.2. Yeast transformation 47
2.11.3. Yeast Mating 49
2.11.4. Plasmid Isolation from Yeast 50
2.11.5. Transformation into *E. coli* 50
2.11.6. Zyppy™ Plasmid Miniprep 51
2.11.7. Confirmations 51
3. Results 52
3.1. Library Preparation 52
3.1.1. Genomic DNA 52
3.1.2. Vector and Fragment Preparation 53
3.2. Cloning of DD-CPase-encoding genes into yeast bait vectors 57

3.2.1. Transformation of DD-CPase genes into the yeast bait vector 58
3.3. Yeast 2-Hybrid Interactions 60
3.3.1. Transformation of library into AH109 yeast cells 60
3.3.2. DD-CPase autonomous activation 61
3.3.3. Yeast Mating 63
3.3.4. DacB and MSMEG_2433 have a number of possible interacting partners 65
3.3.5. Confirmation of interaction in putative clones isolated from yeast mating 69
3.4. Localization of DacB 70
3.4.1. Cloning of DacB-fluorescent protein fusions using crossover PCR 70
3.4.2. 3-way cloning 71
3.4.3. Growth kinetics and Repression of *dacB* 81
3.5. Localization of MSMEG_2433 97
3.5.1. MSMEG_2433-Venus 97
3.5.2 MSMEG_2433-rsEGFP 100
3.6. Single DD-CPase gene knock outs (KOs) have no effect on antibiotic susceptibility 103
4. Discussion 104
5. Appendices 116
Appendix A: Culture media and solutions 116
Appendix B: Molecular weight Markers 118
Appendix C: Primers 119
Appendix D: Library and Yeast Mating 119
Appendix E: PCR confirmation of clones 120
Appendix F: Repeated restriction digests 121
6. References 122

List of Figures

Figure 1.1. Diagram of the mycobacterial cell wall.. 9
Figure 1.2. Diagram of PG synthesis.. 12
Figure 1.3. PG structure and sites of action of a few hydrolases acting on the bonds of PG. 12
Figure 1.4. Diagram of cell division of different rod-shaped organisms.. 14
Figure 3.1. Agarose gel of extracted genomic DNA from WT *M. smegmatis* 52
Figure 3.2. Agarose gel of pGADT7. 53
Figure 3.3. Agarose gels of genomic DNA restrictions.. 54
Figure 3.4. Agarose gel of *Hin*DIII digestion of miniprepped clones. 56
Figure 3.5. Phusion Taq PCR of (A) dacB and (B) MSMEG_2433 using a temperature gradient.. 57
Figure 3.6. Agarose gel of purified products of digested genes and pGBKT7 vector.. 58
Figure 3.7. Restriction profile of pGBKdacB. 59
Figure 3.8. Restriction profile of pGBK2433. 60
Figure 3.9. Spotting of DD-CPase transformants testing for autoactivation. 62
Figure 3.10. Mating clones.. 64
Figure 3.11. Potential positive mating clones.. 65
Figure 3.12. Agarose gel of Zyppy plasmid miniprep and *Hin*DIII digestion.. 66
Figure 3.13. Plates of confirmation reaction of clone 2433_130.. 70
Figure 3.14. Stitch PCR strategy (DacB and GFP). 71
Figure 3.15. Agarose gel of Phusion PCR of dacB and mCherry. 72
Figure 3.16. Restriction profile of dacB and mCherry cloned into pSE100. 72
Figure 3.17. Confocal microscopy of pSEdacB-mCherry construct. 73
Figure 3.18. Agarose gels of Phusion PCR of dacB and Venus.. 74
Figure 3.19. Restriction profile of dacB and Venus cloned into pSE100. 75
Figure 3.20. Fluorescent microscopy of pSEdacB-Venus construct. 76
Figure 3.21. Agarose gels of Phusion PCR of *dacB* and *rsEGFP*.. 77
Figure 3.22. Restriction profile of dacB and rsEGFP cloned into pSE100. 78
Figure 3.23. Immunogold strategy. 79
Figure 3.24. TEM of pSEdacB-rseGFP construct using Immunogold. 80
Figure 3.25. PCR screen for integration of pMC1s. 81
Figure 3.26. Expression data of wild type *M. smegmatis* against the pSEdacB-rsEGFP construct with the pMC1s repressor. 82
Figure 3.27. Confocal microscopy at early log phase.. 86
Figure 3.28. Confocal microscopy during mid-log phase of growth.. 88
Figure 3.29. Graph of localization patterns observed during microscopy.. 89
Figure 3.30. Restriction profile of tetO-*dacB*-rsEGFP cloned into pTweety. 90
Figure 3.31. PCR screen for integration of pMC1s. 91
Figure 3.32. Confocal microscopy of pTw::dacB-rsEGFP with pMC1s construct, at varying concentrations of AHT during log phase. 94
Figure 3. 33. Graph of localization patterns observed during microscopy of pTw::dacB-rsEGFP. 95
Figure 3. 34. Southern Blot analysis of pTw::dacB-rsEGFP construct.) 96
Figure 3. 35. Agarose gels of Phusion PCR of MSMEG_2433 and Venus. 98
Figure 3. 36. Restriction profile of MSMEG_2433 and Venus cloned into pSE100. 98
Figure 3. 37. Fluorescence microscopy of pSE2433-Venus. 99
Figure 3. 38. TEM of Immunogold pSE2433-rsEGFP construct. 100
Figure 3. 39. Agarose gels of Phusion PCR of MSMEG_2433 and rsEGFP. 101

Figure 3. 40. Restriction profile of MSMEG_2433 and rsEGFP cloned into pSE100. t. 101
Figure 3. 41. Fluorescence microscopy of pSE2433-rsEGFP constructs..... 102
Figure 4.1. Model hypothesizing the interaction between MSMEG_2433 and PonA2 in the cell. ... 113
Figure D1: Image of zygote formation during yeast mating.....119
Figure E1: PCR of pSE2433-rsEGFP and pSE2433-Venus clones from *M. smegmatis* colony boil.....120
Figure E2: PCR of pSE*dacB*-mCherry clones from *M. smegmatis* colony boil.....120
Figure E3: PCR of pSE*dacB*-Venus clone from *M. smegmatis* colony boil.....121
Figure E4: PCR of pSE*dacB*-rsEGFP clones from *M. smegmatis* colony boil.....121
Figure F1: Repeated restriction digest of pGBKdacB and pGBK2433.....121
Figure 4.1. Model hypothesizing the interaction between MSMEG_2433 and PonA2 in the cell. .. 113

List of Tables

Table 2.1. Bacterial strains used and/or created in this study 27
Table 2.2. Plasmids used and/or created in this study 28
Table 2.3. Primers used for 3-way cloning 40
Table 3.1. Growth on SD plates lacking specific amino acids 62
Table 3.2. Sequencing results of potential positive mating clones using Blastx 66
Table 3.3. MIC results of single DD-CPase KOs 103
Table C 1: Primers used to check site-specific integration of pMC1s 119

Nomenclature

µ	Micro
3-AT	3-Amino-1,2,4-triazole
AB	Antibody
AD	Activation domain
Ade	Adenine
ADE2	Gene encoding phosphoribosylaminoimidazole carboxylase
AG	Antigen
AHT	Anhydrotetracycline
AIDS	Acquired Immunodeficiency Syndrome
Ami	Amidase
Amp	Ampicillin
attB	$tRNA^{Gly}$ attachment site
ATP	Adenine tri-phosphate
bp	base pair
BCG	Bacille Calmette-Guérin
BD	Binding domain
BSA	Bovine serum albumin
CFU	Colony forming unit
CTAB	Cetyltrimethylammonium bromide
DAP	Diaminopimelic acid
DD-CPase	DD-Carboxypeptidase
DIG	Digoxygenin
DMSO	Dimethylsulphoxide
DNA	Deoxyribonucleic acid
dNTPs	Deoxynucleotide triphosphate
EDTA	Ethylenediaminetetraacetic acid
g	Gram
HCl	Hydrochloric acid
His	Histidine
HIS3	Gene encoding imidazoleglycerol-phosphate dehydratase
HIV	Human-immunodeficiency Virus
hr	Hours
Hyg	Hygromycin
Kan	Kanamycin
kb	Kilo bases
LA	Luria Bertani agar
lacZ	Gene encoding β-galactosidase
LB	Luria Bertani broth
Leu	Leucine
LTBI	Latent TB infection
Lys	Lysine
m	Milli
M	Molar
Mtb	*Mycobacterium tuberculosis*
MDR-TB	Multi-drug resistant TB
$MgCl_2$	Magnesium chloride
min	minutes

MIC	Minimum inhibitory concentration
η	Nano
NaCl	Sodium chloride
NaOH	Sodium hydroxide
NAG	*N*-acetylglucosamine
NAM	*N*-acetylmuramic acid
OD_{600nm}	Optical density at 600 nanometre wavelength
PBP	Penicillin binding protein
PCR	Polymerase chain reaction
PG	Peptidoglycan
PNK	Polynucleotide Kinase
RNA	Ribonucleic acids
Rpf	Resuscitation promoting factor
rpm	Revolutions per minute
RT	Reverse Transcriptase
SD	Synthetic dropout medium
sdH_2O	Sterile distilled water
SDS	Sodium dodecylsulphate
TB	Tuberculosis
Tet	Tetracycline
TetR	Tetracycline repressor
TEM	Transmission Electron Microscopy
Tfb	Rubidium Chloride Compentent Cell solution
Trp	Tryptophan
UDP	Uridine diphosphate
VBNC	Viable but non-culturable
WHO	World Health Organisation
XDR-TB	Extensively drug resistant TB
XXDR-TB	Totally drug resistant TB
X-gal	5-bromo-4-chloro-3-indolyl-D-thiogalactopyranoside
Y2H	Yeast 2-hybrid

1. Introduction

1.1. Background

"Among all infectious diseases that afflict humans, Tuberculosis (TB) remains the deadliest,"

(Ducati et al., 2006).

According to the 2013 report by the World Health Organisation (WHO), 8.6 million new and recurring cases of TB were reported, of which 1.3 million cases resulted in death and 1.1 million were HIV positive (WHO, 2013). TB was previously described as consumption since following transmission, primarily by aerosolized droplets expectorated by infected persons, there is drastic weight loss, night sweats, as well as a violent cough (Glickman and Jacobs, 2001). The global burden of TB disease is exacerbated by a number of factors including a decline in health care systems, overpopulation, accumulation of enclosed working and living areas, HIV/AIDs, economic constraints and drug resistance. TB is a particular source of frustration in Africa due to the high incidence of HIV/AIDs, which results in greater susceptibility to TB, thus leading to an increased prevalence of HIV-TB co-infection. Statistics show that about 75 % of the HIV positive people who developed TB in 2012 were in the African region (WHO, 2013). Furthermore, 3.5 % of new patients and 20.5 % of previously treated individuals developed multi-drug resistant TB (MDR), with 9 % of these being subsequently diagnosed as having extensively resistant TB (XDR) (WHO, 2013).

The causative agent of TB, as identified in 1882 by Dr Robert Koch, is *Mycobacterium tuberculosis* (Mtb), a rod shaped, acid-fast organism that contains a genome with a high G/C content (Sidders and Stoker, 2007). It is non-spore forming, has no evidence of a flagellum, with cell width varying between 0.3 – 0.6 µm and length between 1 – 4 µm (Ducati et al., 2006). Mtb is categorized as a slow growing intracellular pathogen which primarily infects macrophages and can lay dormant in an immuno-competent individual for decades (Sidders

and Stoker, 2007). The genome of Mtb H37Rv is approximately 4.4 x 10^6 bp with ~4000 open reading frames expected to encode genes required for various components of primary and secondary bacteria metabolism (Cole et al., 1998).

1.2. TB Vaccines

There is currently one TB vaccine in use, the Bacillus Calmette-Guérin (BCG) live-attenuated vaccine, which was discovered over a century ago and is administered intradermally. However, there is a high degree of variability in protection between individuals. Even though effective protection has been shown for miliary TB and TB meningitis in children, pulmonary TB protection reduces as adolescence commences and significantly diminishes in adulthood (Fine, 1999). BCG vaccination does not protect individuals against latent infection and in its current format, it cannot be used in a prime-boost manner and hence, cannot exert additive protection in adults (Dietrich et al., 2006). The lack of a protective or prophalyactive vaccine in adults has necessitated the search for new TB vaccines.

Currently, there are three key approaches being utilized in the search and development of novel vaccines: (I) TB subunit vaccines which target specific antigens, (II) live-attenuated vaccines (mycobacterial) which express a broader range of antigens and (III) live Mtb which is substantially attenuated (Lin and Ottenhoff, 2008). At present, 12 vaccine candidates for Mtb are in different phases of clinical trials, most focusing on the prevention of TB either pre- or post- exposure (WHO, 2013). One of the candidate vaccines that recently underwent Phase IIb trials is MVA85A, a poxvirus which expresses the Mtb 85A antigen, it displayed satisfactory protective profile when tested in HIV negative children – i.e. it is immunogenic and tolerated – but demonstrated no major protection with regards to Mtb infection (Tameris et al., 2013). MVA85A is currently undergoing experimentation in HIV negative as well as

positive adolescents and adults with the hope that protection is observed in these cohorts. A novel, successful vaccine in combination with a successful drug regiment is one of the only hopes left to truly combat this disease.

1.3. Antimicrobial Chemotherapy

TB treatment involves the administration of chemotherapy for the duration of 6 months, for drug sensitive TB, using a combination of first line and second line drugs. The current recommended treatment regimens according to WHO guidelines consists of 2 months of combined Pyrazinamide (PZA); Isoniazid (INH); Ethambutol (EMB) and Rifampicin (RIF), followed by four months of INH and RIF (WHO, 2013, Ducati et al., 2006). However, there is a rapid increase in drug resistance, due to various reasons including non-compliance (as patients begin to feel better and do not complete treatment), poor drug availability in certain settings, cross-reactivity with other medications such as anti-retroviral therapy and prescription of inappropriate treatments. This has led to the emergence of MDR, XDR and totally drug resistant (XXDR/TDR) TB (Gandhi et al., 2006, Migliori et al., 2007, Velayati et al., 2009). MDR is defined as a resistance to RIF and INH (first line drugs), XDR comprises MDR, with the added resistance to at least two classes of the second line drugs, a fluoroquinolone and one more class, while XXDR is resistance to all standard drugs, first and second line (Anderson et al., 2012, Velayati et al., 2009).

Drug resistance can occur due to a number of reasons including selective pressure under stressful conditions (changes in pH, low nutrients, etc.), genetic mutations, lateral gene transfer, as well as some microbes having an inherent resistance to specific classes of antibiotics (Depardieu et al., 2007). In mycobacteria, not much has been found regarding gene transfer, but the emergence of resistance to first line drugs has been primarily attributed to mutations in specific drug target genes. The main mutations were associated with genes

such as *embB* (EMB resistance); *rpoB* (RIF resistance); *pncA* (PZA resistance); *katG* and *inhA* (INH resistance) (Telenti et al., 1993, Zhang, 2005, Telenti, 1997, Ramaswamy et al., 2003). There are 5 main classes of TB antimicrobial drugs which are administered either orally or are injected, with some of the second line drugs including Fluoroquinolones, Ethionamides, Aminoglycosides, D-cycloserines and Peptides (Zumla et al., 2013). Second line drugs are quite expensive, not as effective and very toxic with numerous adverse side effects experienced by patients. Consequently, treatment of MDR TB is complicated and requires extended treatment periods with various combinations of second line drugs.

The abovementioned drugs are over five decades old and thus there is a dire need for new drug candidates that would form the basis on new regimens with an associated shortening of the treatment duration and reduction in daily pill burden. With regards to MDR treatment, which may take up to 20 months, new drugs are required to effectively manage this form of TB as well as decrease the side-effects associated with MDR management. There are a number of drugs at different testing phases in the pipeline. One of the most promising new drugs is in phase II and III trials, Rifapentine, which when used in combination with first line drugs, results in culture-negative smears in 8 weeks instead of the 16 weeks it takes with the current treatment (Dorman et al., 2012). Another drug which has gained much interest and is currently in phase II trials is Bedaquiline. This drug is of particular interest with regards to MDR treatment and has already been implemented, thus making it the first new drug to be added to the TB treatment regimen in over 50 years (WHO, 2013). Bedaquiline was added to the current MDR-TB treatment regimen in a double-blinded study which resulted in an increase in sputum culture conversion and a significant decrease in the time it took for sputum conversion to take place (Diacon et al., 2012b). This result was further confirmed by another study using a very similar treatment regimen, this time with the inclusion of XDR patients as well as HIV positive individuals on ARV treatment (Kakkar and Dahiya, 2014).

This drug has also been tested as a combination therapy with pyrazinamide, PA-824 and moxifloxacin, which revealed an accelerated activity of bedaquiline in the presence of pyrazinamide (Diacon et al., 2012a).

1.4. TB Pathogenesis

Pulmonary TB transitions through four stages; beginning with inhalation of tubercle bacteria within infectious aerosol particles, which were expectorated by a diseased individual. At this point, no environmental reservoir for Mtb has been found and transmission occurs direct from person-to-person (Ducati et al., 2006). After inhalation, bacteria are endocytosed by alveolar macrophages and those which escape destruction, proliferate by preventing fusion of the endosome with lysosomes (van Crevel et al., 2002, Dorhoi et al., 2011). The second stage commences with the recruitment of blood monocytes, and other lymphocytes, that have the ability to differentiate into macrophages. This subsequently causes a 'symbiotic stage' where macrophages amass and the bacteria grow exponentially within these cells. Thereafter, development of T cell immunity occurs where immune cells aid in mycobacterial antigen presentation, which eventually results in secretion of cytokines in order to eliminate the bacteria (van Crevel et al., 2002, O'Garra et al., 2013). Once exponential growth ceases, the third stage of disease commences where active disease develops through robust bacterial growth; cell mediated immunity and inflammation which leads to cavity formation (van Crevel et al., 2002, Chao and Rubin, 2010). Alternatively, a clinically latent state is established, with the outcome of disease being dependent on a number of factors, especially the immune status of the individual (Hett and Rubin, 2008, van Crevel et al., 2002, Chao and Rubin, 2010, O'Garra et al., 2013).

Latent TB infection (LTBI) refers to those individuals who are infected with Mtb but do not display any symptoms of the disease. This form of TB is characterized by a PPD positive

result and affects more than 1/3 of the world's population with approximately 10% of these cases developing active disease during the course of their lives (WHO, 2013). A major problem associated with latent TB is that it is asymptomatic and thus goes undetected in the majority of cases. LTBI has been described as an 'equilibrium between host and bacillus' and the term latency is more accurately ascribed to a diseased (or lack thereof) state rather than the growth status of tubercle bacteria (Flynn and Chan, 2001). In the past, latent infection has been associated, albeit with no substantive evidence, with dormancy, which primarily refers to a microbiological state usually found in the laboratory where bacteria enter a reversible state of metabolic inactivity or quiescence (Wayne and Sohaskey, 2001). Whilst it has been demonstrated that Mtb has the ability to enter a state of dormancy *in vitro,* as a survival mechanism, how this relates to latent infection remains a mystery (Deb et al., 2009, Shleeva et al., 2002). For the purposes of this study, we will use the above-mentioned definitions of dormancy and latent infection.

Persistence is defined as, "continuing firmly or obstinately in an opinion or course of action in spite of difficulty or opposition," according to the Oxford dictionary. This has been demonstrated to be an apt description for tubercle bacteria, which are able to survive in cells that are purposed to destroy such organisms and as such, have the ability to evade elimination by the host's immune system as well as the prolonged antibiotic treatment (Gomez and McKinney, 2004). The 'Cornell model' has been used in mice to determine the antimicrobial effect/s in the lungs and spleen in the murine model of TB infection (McDermott, 1959). These studies revealed that initial treatment with drug results in rapid decline of the lung bacillary load to a level that is below detection. However, upon immune suppression, bacteria re-emerge in the lungs of these animals, suggestive of the presence of a bacteria that have persisted in the face of antibiotic treatment. These organisms are still drug-sensitive and are

referred to as persisters (McDermott, 1958). This state can be seen as distinct from the non-replicating, spore forming state that some species adopt.

Bacillus species adapt to unfavourable conditions through the formation of spores which involves global remodelling of metabolism and cell architecture (McKenney et al., 2013). It has been demonstrated that subsequent germination from sporulation is triggered by muropeptides, which are peptidoglycan (PG) breakdown products, probably released during PG remodelling, with muropeptides from a culture of replicating cells proving to be more effective inducers of germination when compared to PG from cells in the stationary phase (Dworkin and Shah, 2010). Although Ghosh and colleagues (2009) reported endospore formation in *M. marinum* and *M. bovis* BCG, the finding was disputed due to the lack of some genes, critical for spore formation, in the mycobacterial genome. The phenotypic similarity of the alleged mycobacterial spores to those observed in *Bacillus* spores, combined with the inability of four separate laboratories to reproduce the result, suggests that the initial report for spore formation is incorrect (Ghosh et al., 2009, Traag et al., 2010). However, mycobacteria do retain the capacity to enter into a viable but non culturable (VBNC) state of non-replicating metabolic quiescence (Shleeva et al., 2004, Wayne, 1994). Moreover, this state is reversible since tubercle bacteria can spontaneously reactivate in these in vitro models of dormancy suggesting that global modulation of metabolism does occur during these shifts in growth state (Chao and Rubin, 2010). However, whether mycobacteria adopt physical changes during the transition to dormancy remains to be investigated. Previous work has demonstrated the presence of ovoid cell forms in cultures of dormant *M. smegmatis* (Anuchin et al., 2009). The abovementioned observations in *Bacillus* provide evidence for a strong link between remodelling of the PG and bacterial dormancy/ reactivation, suggesting that an enhanced understanding of PG remodelling may provide deeper insight into the mechanism of reactivation in mycobacteria. Of particular importance in this regard are the proteins

annotated as resuscitation-promoting factors (Rpfs) which have been implicated in reactivation of Mtb from dormancy. These proteins are also postulated to play an important role in compositional and structural remodelling of the PG layer, thus affecting the growth state of the bacterium (Kana and Mizrahi, 2010). Rpfs are discussed in detail in section **1.7.1**.

1.5. Mycobacterial Cell Wall

The cell envelope in mycobacteria is classified as gram variable since it differs from both gram positive and negative cell wall structures (Glickman and Jacobs, 2001). Structurally, mycobacteria are gram positive due to the presence of a substantial PG layer and no true outer membrane (OM). However they contain porins, a periplasmic-like space and do not retain the gram stain, which are properties shared by Gram negative organisms (Hett and Rubin, 2008).

The cell wall of mycobacteria is unique in the sense that it is lipid rich, hydrophobic and extremely thick (Sidders and Stoker, 2007). The structure, as shown in Figure 1.1, comprises an outer layer (lipids and proteins), and an inner layer which consists of three main components: PG, arabinogalactan (AG) and mycolic acids (MA). These form a complex, comprising the PG layer, followed by a phosphodiester bridge connecting the PG to the AG, to which the MAs are anchored (Jarlier and Nikaido, 1994). This dense core has an impact on the growth of the bacterium, its success as a pathogen, the ability to survive and persist under stress, as well as the bacterium's inherent resistance to antibiotics.

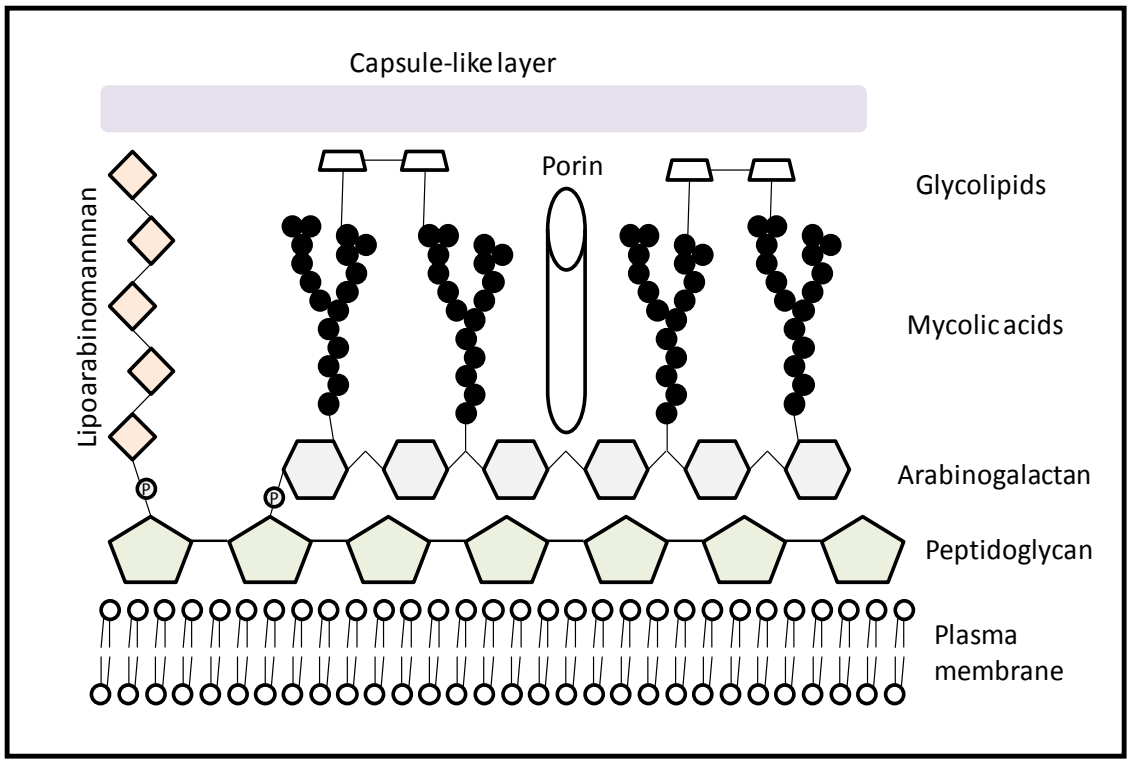


Figure 1.1. Diagram of the mycobacterial cell wall. The wall consists of a lipid bilayer (plasma membrane), followed by the PG to which arabinogalactan and lipoarabinomannan is attached by either a phosphate linker region or phosphatidylinositol anchor, respectively. MAs are esterified to the AG layer. Adapted from (Basso et al., 2005).

MAs are long chain β-hydroxy acids which are substituted by α –alkyl groups, made up of alkelyl or cyclopropyl groups consisting of multiple carbons, generally 60-90 per chain (Anderson et al., 2012, Hett and Rubin, 2008). These lipid chains lie alongside each other at a 90-degree angle to the cell surface. The MA comprises the outer layer of the cell wall and constitutes the major determinant of cell permeability in mycobacteria (Jarlier and Nikaido, 1994, Sani et al., 2010). A few other mycolic acids of interest have been identified, these include the Cord factor and trehalose-6,6'-dimycolate (TDM), which is the lipid molecule responsible for the cord-like formations or clumping viewed when mycobacteria are grown in liquid culture and has been associated with pathogenicity (Lederer et al., 1975, Brennan and Nikaido, 1995, Takayama et al., 2005). Other such lipids gaining interest include phtiocerol dimycocerosate (DIM/pDIM), lipoarabinomannan (LAM) etc. (Brennan and Nikaido, 1995).

MAs are esterified to AG and thus AG plays a role of anchorage of the MAs to the PG (Hett and Rubin, 2008). This layer is generally referred to as the mycolyl-AG layer. AG is the major polysaccharide of the mycobacterial cell wall and adopts a branched-chain structure with non-reducing termini formed by the arabinose (Ara) residues (Brennan, 2003). Both the arabinose (Ara_f) and galactose (Gal_f) are in the furanose confirmation with branching occurring at specific positions in this structure (Crick et al., 2001). MA attachment occurs in clusters of four, with two thirds of the total MAs being attached to the terminal Ara motifs (Brennan and Nikaido, 1995). Attachment of this matrix to the PG occurs by linkage of muramic acid on PG (via a phosphodiester link) to position 6 of Gal_f via a 'linker region' (McNeil et al., 1990). There are 3 main forms of MAs, α-; keto- and methoxy- MAs, which play different roles in pathogenicity and their ability to stimulate immune responses (Verschoor et al., 2012). In *C. glutamicum*, the presence of mycolic acid has been associated with the process of glutamate excretion (Gebhardt et al., 2007). In mycobacteria, mycolic acids are pivotal for growth and have been implicated in antimicrobial resistance (Marrakchi et al., 2014).

1.5.1. Peptidoglycan (PG) layer

The PG layer functions as a protective layer for the bacterial cell and plays an important role in determining cell shape and size. Due to this layer being unique to bacteria and the vast number of enzymes associated with it, it is an important target for antimicrobial drugs. The mycobacterial PG layer consists of repeating *N*-acetyl muramic acid (NAM) and *N*-acetyl glucosamine (NAG) residues held together by β-1,4-glycosidic linkages with peptide chains attached to the NA/GM residues of the glycan backbone. The peptide chains are made up of different residues, with L-alanine (L-Ala) at position 1, D-glutamine (D-iGln) at position 2, *meso*-diaminopimelic acid (*m*-DAP) at position 3, and D-alanine (D-Ala) at positions 4 and 5, Figure 1.2. and Figure 1.3. A unique feature in mycobacteria is the presence of *N*-

glycolylated muramic acid (in addition to *N*-acetylated muramic acid), Figure 1.3 (Vollmer et al., 2008a). The *N*-glycolylation has been attributed to a hydrolase, encoded by the *namH* gene, with deletion of this gene causing only *N*-acetylation to take place (Raymond et al., 2005). Specific enzymes act on the above-mentioned residues to yield cross-links between the peptide chains of the PG layer, thus connecting the glycan strands to create a three dimensional matrix (Park, 1995). Linkage of the peptide side-chains results in the formation of either a 4→3 cross-link or 3→3 cross-link between the side chains, Figure 1.3. Mycobacterial cell walls contain both 4→3 and 3→3 cross-links between the peptide chains which are generated by DD-transpeptidation or LD-transpeptidation, respectively (Lavollay et al., 2008). LD-transpeptidases are discussed in detail in section **1.7.2.**

It is hypothesized that mycobacterial PG synthesis occurs in a step-wise fashion with numerous reactions. The initial reaction involves synthesis of the uracil diphosphate (UDP) - NAM from UDP-NAG, followed by synthesis of the UDP-NAM-pentapeptide side chain beginning with L-Ala and ending with D-Ala. At this point the subunit is transferred to the cell membrane where UDP of the NAM is released by attachment of bactoprenol phosphate (lipid I), thereafter lipid I is converted to lipid II and the resultant PG subunit (lipid II) is flipped across the membrane, Figure 1.2. (Crick et al., 2001). It is at this stage that PG assembly, cross-linking, remodeling etc. can take place in the periplasmic compartment (Sobhanifar et al., 2013, Gee et al., 2012). The constant growth and cell division processes demand that PG remains a dynamic structure which is constantly remodelled to allow for a variety of functions including shape maintenance, replication and division of cells. This process of PG turnover is facilitated by PG hydrolases.

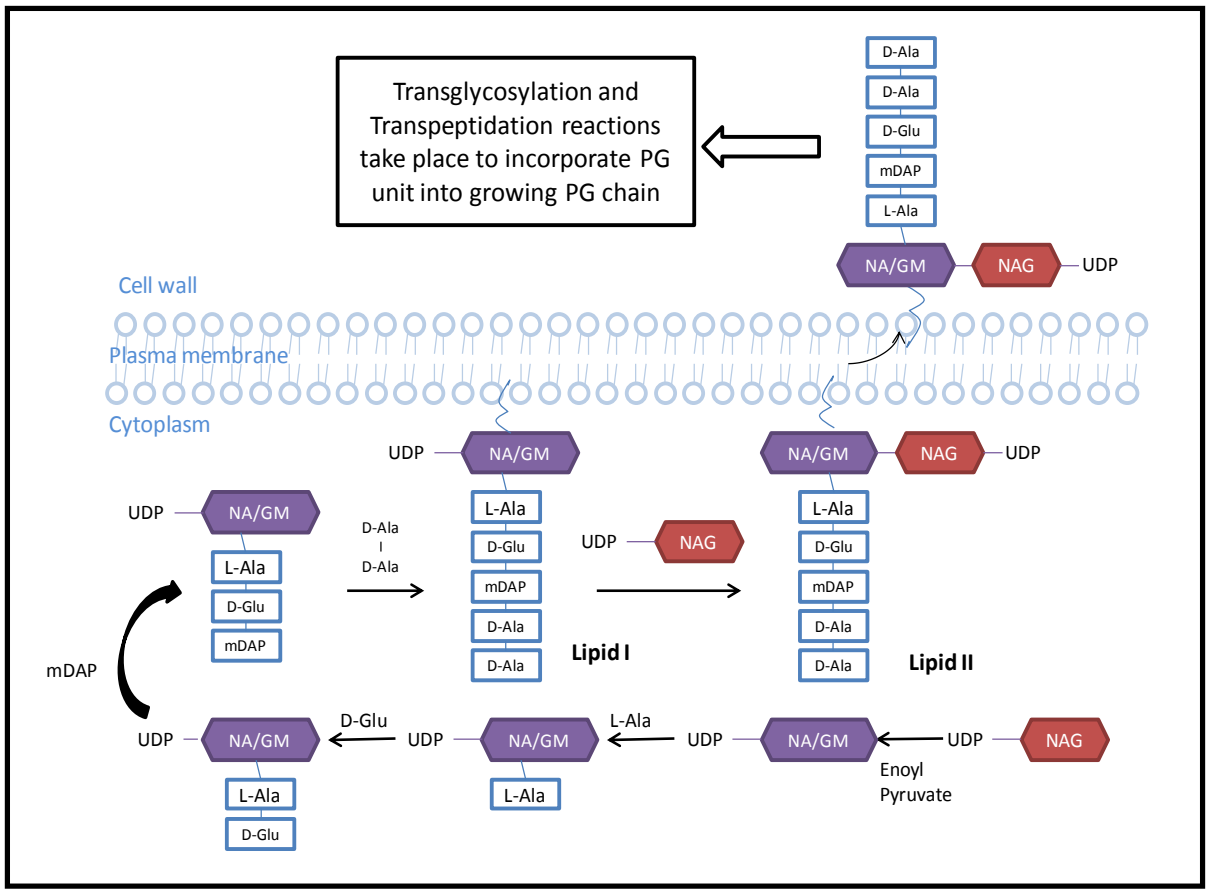


Figure 1.2. Diagram of PG synthesis. Biosynthesis of a PG subunit occurs in the cytoplasm and it is thereafter flipped into the periplasm where incorporation of the subunit into the PG chain occurs. Adapted from (Pinho et al., 2013, Vollmer et al., 2008b).

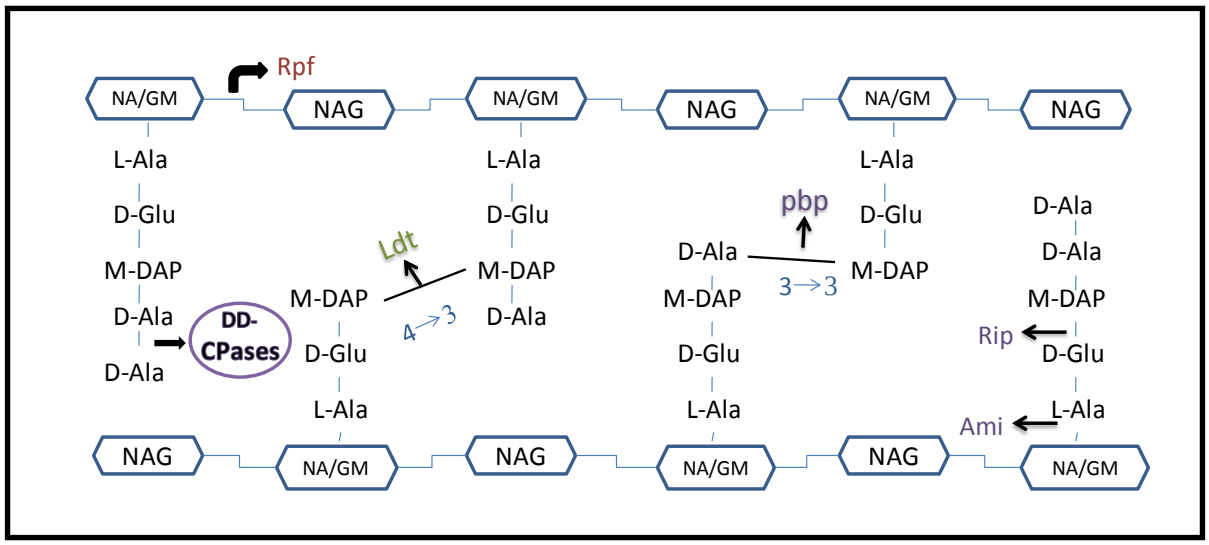


Figure 1.3. PG structure and sites of action of a few hydrolases acting on the bonds of PG. Cross-links are formed either by Ldts (LD-transpeptidases) or high molecular weight PBPs. DD-CPases (DD-Carboxypeptidases) cleave the terminal D-Ala, freeing the terminal residue. Adapted from (Vollmer et al., 2008b, Kana and Mizrahi, 2010).

1.6. Mycobacterial Growth

The constant remodeling of PG, i.e. the breakdown and synthesis, is a key process for successful bacterial growth and cell division. In rod-shaped bacteria such as *E. coli* and *B. subtilis*, which are the best studied, new PG is inserted along the cells axis with a left- or right- handed helical pattern, respectively, Figure 1.4 (Wang et al., 2012, Mendelson, 1976). These organisms have two modes of growth which occur separately; i.e. cell division controlled by the divisome and cell elongation controlled by the elongasome, with each mode containing a specific set of proteins present in complexes to efficiently carry out these processes (Cabeen and Jacobs-Wagner, 2005, Jacobs and Shapiro, 1999).

Elongation of *E. coli* is determined by an actin-like protein MreB which plays an important role in localization of new PG synthesis and has a role in maintaining the rod-shape of these organisms (Wang et al., 2012). MreB also functions in a complex with other Mre proteins as well as RodA, which aids and allows FtsZ-ring co-ordination to take place (Young, 2010). FtsZ is a tubulin-like protein. *B. subtilis* has MreB as well as Mbl, with MreB implicated in the control of the width of the cell and Mbl involved in the control of the length of the linear axis of the cell (Jones et al., 2001). Due to the manner in which these organisms grow, inert PG is found at the poles, which is not the case in mycobacteria (Hett and Rubin, 2008).

The divisome of both *E. coli* and *B. subtilis* is initiated by FtsZ, which works in concert with approximately eleven other proteins in a complex in order to form the Z-ring at the mid-cell position for initiation of cell division (Bi and Lutkenhaus, 1991, Adams and Errington, 2009). The precise placement of the Z-ring in these organisms is dependent on ‘negative control systems’, namely the Min system (made up of MinCDE/ MinCD DivIVA) and the nucleoid occlusion system (Noc/SlmA) which function by either preventing the formation of the Z ring or prevents FtsZ polymerization, respectively (Hu and Lutkenhaus, 2000). These functions

are triggered by the length of the cell, thus producing a division event which results in symmetrical cells, each of which contains a nucleoid, Figure 1.4 (Trueba, 1982).

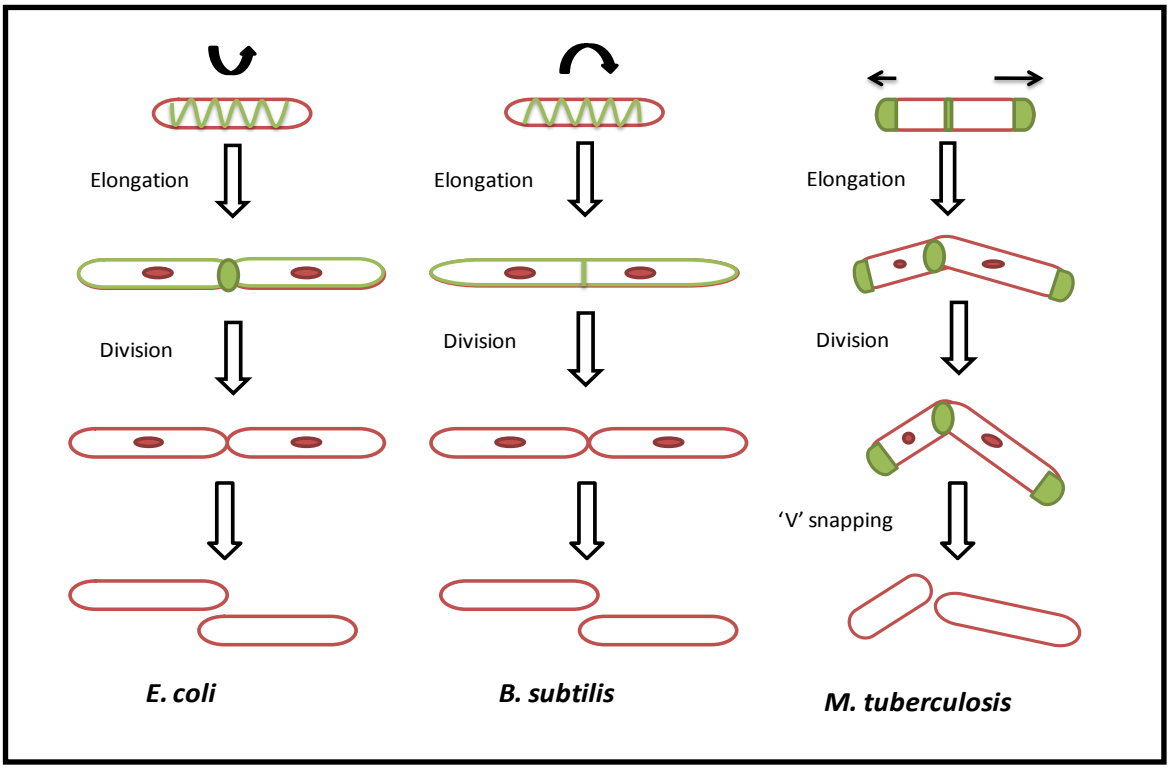


Figure 1.4. Diagram of cell division of different rod-shaped organisms. *E. coli* incorporates new PG in a left-handed helix along the cell wall, while *B. subtilis* incorporates PG in a right-handed helix along the cell wall to produce cells of the same length. Mycobacteria incorporate new PG at the poles and separate by 'snapping' which produce cells of different lengths. Adapted from (Adams and Errington, 2009, Santi et al., 2013).

Mycobacterial cell division differs greatly from other rod-shaped bacteria. The main difference being that mycobacteria grow from the poles instead of along the axis, which results in two cells in a V-shaped confirmation that divide by a mechanism referred to as 'snapping' (Thanky et al., 2007). Mycobacteria seem to be missing many of the proteins described for the division of *E. coli* and *B. subtilis*. While a homologue of FtsZ is present, the difference is that the MreB proteins described are absent and although there may be other actin-like proteins which could serve the function of the MreB family, none have been described in mycobacteria yet. Hett and Rubin (2008) hypothesized that due to these features, FtsZ is the determining factor of both elongation and septation. Other cell division proteins that are not found in mycobacteria include FtsA and potentially ZipA, which act to stabilize

the Z-ring. Another interesting feature of the FtsZ of mycobacteria is its inherently slow polymerization, the role for which has not been fully elucidated yet (Hett and Rubin, 2008). FtsZ in mycobacteria seems to function in a similar fashion as in other rod-shaped bacteria with the presence of multi-protein complexes. One such complex is demonstrated by FtsZ-FtsW-PBP3 (FtsI), where the FtsZ and FtsW directly interact and thus FtsW acts as a connecting molecule, together suggesting that cell division and synthesis of septal PG is dependent on the interaction of a multitude of proteins which form complexes (Datta et al., 2006, Rajagopalan et al., 2005). DivIVA plays a role as a polar determinant in other organisms, and its homologue in mycobacteria, Wag31, acts as a guide for growth at the poles (Cava et al., 2013, Meniche et al., 2014). This protein interacts with FtsI (PBP3), and acts to protect FtsI from oxidative stress re-iterating the importance of protein complexes in cell division (Mukherjee et al., 2009).

Mycobacteria lack the Z-ring negative regulator systems, i.e. the Min system and nucleoid occlusion and is possibly the reason that the mycobacterial Z-ring does not always form at the mid-cell (Singh et al., 2010). In *E. coli* and *B. subtilis*, these systems are dependent on cell length in order to produce symmetrical cells (Trueba, 1982). Studies have shown that mycobacteria produce mostly symmetrically dividing cells of different lengths (Joyce et al., 2012, Vijay et al., 2014). Singh and colleagues (2013) stated that to compensate for the absence of these regulators, DNA translocation is directional and polar growth occurs unevenly following FtsZ ring assembly. They also showed that the daughter cells all produced viable cells, even though growth and division occurred at varying rates, with the presence of both bi- and uni- polar growth (Singh et al., 2013). A recent study has shown that Mtb also has a small percentage of cells with asymmetric mid-cell placement (defined as > 10 % septum position deviation) producing a short and long cell – in this case due to septum placement, and not growth of the poles (Vijay et al., 2014). All resultant cells, including the

short cells, as well as division events contained intact nucleoids with the short cells being neither VBNC cells nor spores, as they divide normally (Vijay et al., 2014). *M. smegmatis* cells have been shown to produce a higher degree of asymmetric cells when compared to *E. coli* and *B. subtilis* with growth occurring preferentially at one pole (Aldridge et al., 2012). This gives rise to 'accelerator' and 'alternator' cells, depending on which daughter inherits the growing pole and cell division in mycobacteria is controlled/triggered by time instead of size of the cells (Aldridge et al., 2012). Another study focusing on division events of XDR and XXDR Mtb strains demonstrated that asymmetric division occurrence increased in XDR and XXDR strains compared to susceptible and MDR strains (Farnia et al., 2010). This study also revealed that the highly resistant strain produces 'round bacilli' and branching, with the round cells hypothesized to disseminate faster and could be a driving force in the virulence of these strains (Farnia et al., 2010).

As demonstrated, cell division is dependent on a number of enzymes working collectively, many of which are hydrolases, which function to breakdown certain components in the cell wall.

1.7. PG Hydrolases

The PG hydrolases in bacteria act by hydrolyzing different bonds in the PG matrix which facilitate a number of processes including cell growth and division, shape maintenance, PG remodeling for insertion of secretion apparatus etc. In gram negative bacteria they also play a role in PG recycling, while in the gram positive *Bacillus* sp. they have been shown to play a role in spore germination and release of muropeptides, which could act as signaling molecules for resuscitation of dormant cells (Shah et al., 2008, Dworkin and Shah, 2010, Nikitushkin et al., 2013).

The cell requires a variety of PG hydrolases with diverse modes of action in order to carry out the array of activities described. There are generally a number of hydrolases with similar function (referred to as functional redundancy), with these functions being essential in maintaining the integrity of the cell. There is a hydrolase which could act on every bond present in PG (Sobhanifar et al., 2013). PG hydrolases act on the three types of bonds present in the PG sacculus – glycosidic (glycosidases), amide (amidases) and peptide (peptidases) bonds. Glycosidases are involved in glycan backbone cleavage, and consist of *N*-acetylglucosamidases and *N*-acetylmuramidases which are sub-divided, based on cleavage products, into lysozymes and lytic transglycosylases (LTs) (Frirdich and Gaynor, 2013). LT-cleavage of PG results in the terminal NAM residue containing a 1,6-anhydro ring while products of lysozyme cleavage lack this ring.

Amidases (*N*-acetylmuramyl-L-alanine amidases) on the other hand, remove the entire peptide side chain by cleavage between NAM and L-Ala (Schomburg and Salzmann, 1991). In a bioinformatics analysis by Machowski et al. (2014), four amidase homologues were identified in Mtb and annotated as *ami1*, *ami2*, *ami3* and *ami4*, with the former two containing an amidase_3 domain, while the latter two contain an amidase_2 domain. Amidases play a role in cell communication, cell separation and antibiotic resistance in other organisms, as well as sporulation and germination in *Bacillus* sp. (Heidrich et al., 2001, Smith et al., 2000). A recent study demonstrated that based on the structural and biochemical properties of Mtb *ami1* (Rv3717), as well as the ability of Rv3717 to act on PG fragments and accept transposon insertions, this enzyme could play a role in the recycling of PG, which has not been described in Mtb as yet (Prigozhin et al., 2013, Griffin et al., 2011). A second distinct study has shown Ami2 to be essential in the environmental strain *M. smegmatis* and further demonstrate that Ami1 plays a pivotal role in cell division (Senzani and Kana, Unpublished).

Peptidases, which cleave within the peptide side chain, are generally penicillin binding proteins (PBPs) and include endopeptidases and carboxypeptidases. One of the best characterized endopeptidases in Mtb is RipA (Rpf-interacting protein A) which, together with RipB, contains a NlpC/p60-like domain (Both et al., 2011). RipA (Rv1477) and RipB (Rv1478) were shown to hydrolyze the bond between D-Glu (position 2) and mDAP (position 3) and thus have a role in cell-wall remodeling (Both et al., 2011). However, they have differences in both substrate specificity and N-terminal fragments. RipA, an essential gene in Mtb, is a zymogen (requires proteolytic cleavage to activate the protein) whose expression must be tightly regulated as studies in *M. smegmatis* have shown that depletion causes chaining of cells and over-expression causes lysis (Chao et al., 2013). RipA is hypothesized to play a role in exit from dormancy as it interacts with and forms a complex with RpfB or RpfE and this hydrolysis is controlled/modulated by a high molecular weight (HMW) PBP, PBP1, by competition between RpfB/E and PBP1 for RipA (Hett et al., 2007, Hett et al., 2010, Patru and Pavelka, 2010, Hett et al., 2008). A bioinformatics analysis of the genome of Mtb revealed 3 other endopeptidase homologues – Rv0024, RipD and Rv2190 (Machowski et al., 2014).

1.7.1. Resuscitation Promoting factors (Rpfs)

Rpf, a secreted protein, was first described in *Micrococcus luteus* as an essential gene which plays a role in resuscitation of dormant forms of the bacterium (Mukamolova et al., 1998). In 2006, Mukamolova et al showed this enzyme to be muralytic. Consistent with this, Rpfs bear strong structural similarity to lysozymes and are hence hypothesized to cleave between the NAM and NAG residues (β 1-4 glycosidic bond) of PG and accordingly are classified as lytic transglycosylases (Cohen-Gonsaud et al., 2005, Ruggiero et al., 2009, Mukamolova et al., 2006). Mycobacteria retain multiple *rpf* homologues with *M. smegmatis* containing four (*rpfA*, *rpfB* and a duplication of *rpfE* – based on gene synteny), whereas Mtb contains five:

rpfA-rpfE which are collectively dispensable for growth but are required for virulence in the murine model of TB infection (Kana et al., 2008, Machowski et al., 2014). Furthermore, while these genes are dispensable under normal *in vitro* conditions, they become important for growth in the presence of cell wall stress.

There is evidence to indicate a level of functional specialization within the *rpf* gene family in Mtb (Gupta and Srivastava, 2012). This has been demonstrated by deletion studies, where *rpfB* deletion alone and *rpfB* in combination with *rpfA* deletion caused colony forming defects as well as delayed reactivation of growth in mice (Tufariello et al., 2006, Russell-Goldman et al., 2008). Triple *rpf* deletion mutants defective for different combinations resulted in resuscitation impairment and varying attenuation effects in mice (Downing et al., 2005). With regards to a functional hierarchy, Kana et al (2008) demonstrated that *rpfB* and *rpfE* rank highest in terms of their ability to restore a plating defect in the quintuple *rpf* deletion mutant, which is particularly significant as both enzymes have been shown to interact with RipA for enhanced PG hydrolysis (Hett et al., 2008). This interaction is hypothesized to play a role as the driving force of resuscitation in Mtb as dormant cells have been shown to contain a thicker cell wall (Mukamolova et al., 1999).

A study by Mukamolova and colleagues (2010) confirmed that sputum from patients with smear positive TB contains an Rpf dependent population of Mtb, leading to the hypothesis that Rpfs may play a role in the transmission of TB disease (Mukamolova et al., 2010). The mechanism of reactivation by Rpfs is still largely unknown, however a recent study has shown that high molecular weight PG fragments have the ability to induce resuscitation in specific media (Nikitushkin et al., 2013). This led to the theory that Rpfs could produce signalling molecules in the form of muropeptides in order to trigger resuscitation, which is an attractive idea since Mtb contains PrkC and PknB homologues as well as the PASTA-binding

domain, all involved in muropeptide recognition in other organisms such as *Bacillus* sp. (Foulquier et al., 2014, Squeglia et al., 2013)

As cells approach stationary phase, the growth of BCG was enhanced through supplementation with Rpfs, whereas these same proteins had no effect on exponentially growing cells (Mukamolova et al., 2002). This is consistent with the role of Rpfs in resuscitation. Entry into stationary phase also increases 3→3 cross-links in mycobacterial sp., which could also be the case in dormant bacteria, resulting in a cell wall that is more resistant to hydrolases (Lavollay et al., 2008).

1.7.2. L,D-Transpeptidases (Ldts)

Ldts are responsible for the formation of the 3→3 cross-links between stem peptides by cleavage between D-Ala at position 4 and mDAP at position 3 of the peptide stem and subsequent linkage between mDAP residues (Mainardi et al., 2005). 3→3 cross-links have been implicated in adaptation to stationary phase in mycobacteria and thus to cells with a decreased metabolic rate as mentioned in the previous sections (Lavollay et al., 2008). These observations point to a role for Ldts in adapting to growth phase-specific needs. However, a recent study reported evidence that 3→3 cross-links predominate at all stages of growth and hypothesized that transpeptidases identify amidation of the desired residues and control cross-linking in this way, with Ldts containing a preference for the substrate of an ε-carboxyl donor stem which is unamidated (Kumar et al., 2012). Hence, a definitive conclusion requires further analysis, but most studies support the former hypothesis, as this is consistent with experiments conducted in other organisms.

Mtb contains five putative Ldts annotated Ldt_{Mt1}-Ldt_{Mt5}, with Ldt_{Mt1} and Ldt_{Mt2} being the best studied (Gupta et al., 2010). Kumar and colleagues (2012) demonstrated that Ldts, as well as DD-CPases, are sensitive to carbepenems. Carbepenems act on the cell wall by inhibiting

synthesis and have the added advantage of containing an inherent resistance to β-lactamases (Papp-Wallace et al., 2011). Loss of Ldt_{Mt2} only and both Ldt_{Mt1} and Ldt_{Mt2} resulted in a number of defects including morphological alterations; reduced growth in liquid culture; decreased virulence; altered localization of a number of proteins (including a number of low molecular weight proteins); increased vulnerability to vancomycin, as well as a combination of amoxicillin-clavulanate (Gupta et al., 2010, Schoonmaker et al., 2014). These defects were much more pronounced in the double mutant, pointing to a potential functional redundancy between the *ldt* genes. The above-mentioned results suggest that Ldts, and possibly other low molecular weight PBPs are associated.

1.7.3. Penicillin Binding Proteins (PBPs)

PBPs are implicated in PG synthesis/assembly and are thus named due to their ability to bind β-lactam antibiotics (Spratt, 1983). PBPs are acyl-serinetransferases whose molecular weights vary between 25000-100000 Daltons (Ghuysen, 1991). There are 3 main classes of PBPs – Class A and Class B, which consist of high molecular weight PBPs, and Class C, which consist of low molecular weight PBPs. Class A high molecular weight PBPs are bi-functional enzymes which contain both transpeptidase (PB domain) and transglycosylase (n-PB domain) activity, whereas Class B high molecular weight PBPs contain only transpeptidase activity (Spratt, 1983). With regards to class B PBPs, mycobacteria encode three – PbpA, PbpB (FtsI) and PBP-lipo, with the former two being implicated in *M. smegmatis* cell division (Machowski et al., 2014, Dasgupta et al., 2006). In other organisms such as *E. coli*, FtsI forms part of the divisome assembly complex in concert with other cell assembly proteins (Muller et al., 2007).

Two class A PBPs have been identified in mycobacteria, *ponA1* (PBP1) and *ponA2* (PBP1A). A PBP1 mutant in *M. smegmatis* displayed an increased susceptibility to β-lactam antibiotics; increased permeability; as well as slower growth in liquid media (Billman-Jacobe et al.,

1999). PonA2, which contains a PASTA domain, has been implicated in anaerobic and stationary phase adaptation with mutational studies resulting in increased susceptibility to antibiotics, as well as a number of discrepancies at the onset of stationary phase including the formation of spherical cells, cell surface changes, and survival and recovery defects (Patru and Pavelka, 2010). *M. smegmatis* contains a duplication of PonA2, which has been annotated as PonA3. PBP1 has also been shown to interact with the endopeptidase RipA as described in section 1.7 (Hett et al., 2010). PBP1 homologues in *E. coli* and *B. subtilis* have been shown to be involved in cell division and elongation and play similar roles in mycobacteria (Basu et al., 1996, Claessen et al., 2008, Banzhaf et al., 2012).

Class C low molecular weight PBPs consist of endopeptidase and carboxypeptidases. Endopeptidases have been discussed at the beginning of section 1.7, while the main focus of the current MSc is the carboxypeptidases.

1.7.3.1. DD-Carboxypeptidases

DD-CPases, class C low molecular weight PBPs, act to modify PG by cleavage of the terminal D-Ala residue of the pentapeptide side chain, Figure 1.3. These enzymes have a role in controlling cross-linking of PG (Ghuysen, 1991). Most organisms encode a number of DD-CPases which are said to be enzymatically redundant with most being annotated as non-essential genes. Studies have shown that while these enzymes control cross-linking, they are not directly involved in synthesizing them (Hammes and Seidel, 1978).

DD-CPase activity has not been characterized in most organisms, with best studied DD-CPase genes being those of *E. coli* and, to a lesser extent, *B. subtilis*. *E. coli* encodes four DD-CPases – PBP4, PBP5, PBP6 and DacD, with PBP4 containing bifunctional activity i.e. endopeptidase and carboxypeptidase activity, its primary activity being as an endopeptidase (Ghosh et al., 2008). PBP5, encoded by *dacA*, is the most studied DD-CPase. Mutation of

PBP5 resulted in severe growth and morphological defects, while over-expression resulted in the formation of spherical cells (Ghosh and Young, 2003, Markiewicz et al., 1982). None of the other LMW PBPs can compensate fully for loss of PBP5, whereas in mutants lacking other DD-CPases, genetic complementation with PBP5 alone is able to reverse cell defects (Nelson and Young, 2001). The activity of this gene has been attributed to the presence of a Ω-loop in its Domain I region (Nelson et al., 2002). PBP6 shares a significant sequence homology to PBP5 and both are controlled by BolA (a transcriptional regulator), however their biological roles seem to differ as PBP6 has been implicated to have a function in the stationary phase (van der Linden et al., 1992, Ghosh et al., 2008, Chowdhury et al., 2012). DacD has the ability to partially compensate for loss of resistance to β-lactams in a PBP5 mutant and its expression increases during mid-log phase of growth (Santos et al., 2002). It has been hypothesized that the differing DD-CPases function at different growth phases which points to these genes playing specific roles, dependent on which growth phase they are most active (Ghosh et al., 2008).

B. subtilis encodes a number of DD-CPases including PBP4a (*pbp*), PBP5, PBP5* and DacF. PBP5* (*dacB*) is the most well characterized DD-CPase in this organism. It is synthesized only at later stages of sporulation, specifically stage III, and its role is hypothesized to be in the synthesis of the spore cortex (Todd and Ellar, 1983, Buchanan and Ling, 1992). The *dacA* gene encodes PBP5 – the vegetative DD-CPase which is expressed at the exponential phase of growth and is suggested to play a role in promoting the maturation of PG (Atrih et al., 1999). PBP4a (*dacC*), a DD-CPase with thiolesterase activity, is active during late stationary phase and retains sequence homology to *E. coli* PBP4 (Pedersen et al., 1998, Duez et al., 2001). Not much is known regarding DacF. It is expressed within the bacillus fore-spore during the stationary phase of growth and has been hypothesized to play a role during sporulation by

modifying PG (Popham et al., 1999). These findings are consistent with the premise that the action of different DD-CPases is indeed growth phase dependent.

There have not been many studies focusing on DD-CPases from other organisms. There are a number of homologues which have been identified in different organisms, and this section will just highlight a few of the better characterized homologues. PBP3 of *Neiserria gonorrhea* contains homology to PBP4 of *E. coli* and has a role in PG biogenesis (Ghosh et al., 2008). PBP6b (DacD) of *Salmonella enterica* has sequence homology to *E. coli* DacD and both are hypothesized to play similar roles in the cell since DacD mutants in both organisms result in biofilm defects (Brambilla et al., 2014). PBP3 (*dacA*) of *S. pneumonia* seems to function in a similar fashion as *E. coli* PBP5, since mutants have severe morphological defects as well as a cell division defect (Severin et al., 1992, Morlot et al., 2004). In *P. aeruginosa,* PBP5 also shows homology to *E. coli* PBP5 with the inclusion of carbapenemase (confers reisistance to the carbapenem class of antibiotics) action (Smith et al., 2013). Recently, the *dacB* gene of *V. parahaemolyticus* has been implicated in the initiation of VBNC cells through the production of irregularly shaped cells (Hung et al., 2013). The presence of DD-CPases with conserved sequence homologies in a variety of microorganisms indicates the importance of these genes in the cell and the pivotal role they play in cell wall homeostasis.

A recent analysis of the mycobacterial genome has revealed that Mtb has three DD-CPase homologues, namely Rv3627c; *dacB1* and *dacB2* (Machowski et al., 2014). The environmental mycobacterial sp., *M. smegmatis*, contains five putative homologues, *dacB* (Rv3627c homologue); MSMEG_2432; MSMEG_2433 (duplication of *dacB2*); MSMEG_1661 and MSMEG_1900 (Ealand and Kana, unpublished). Recent studies have focused on DacB2 of Mtb which, when over-expressed, caused a number of defects including biofilm and sliding motility defects, as well as alterations in colony morphology and a

reduction of growth (Bourai et al., 2012). Mutational studies resulted in a reduction of growth in minimal media under stressful conditions. The mutant strain also showed increased endurance in macrophages, which could indicate a function in pathogenesis (Bourai et al., 2012). Kumar and colleagues (2012) demonstrated the ability of carbapenems (meropenem in particular) to inhibit DacB2, as well as one Ldt, and in turn cause pentapeptide accumulation, pointing to the possibility of these genes/proteins as targets for new drugs.

This study focused on further elucidation of DD-CPases in *M. smegmatis*, a close homologue of Mtb routinely used as a model organism for TB research. As previously stated, bioinformatics analysis was conducted by Ealand and colleagues, who also tested expression levels of these genes, showing increased expression during logarithmic growth, with the MSMEG_2433 gene being the most highly expressed. Attempts were made to delete the DD-CPase -encoding genes from the *M. smegmatis* genome, which confirmed the essentiality of *dacB* in *M. smegmatis*. These results form the backbone of this study since the essentiality of *dacB* combined with the increased expression of MSMEG_2433 during log-phase of growth prompted the selection of these two genes for further characterization in this study. The aims are outlined below.

1.8. Study Aims and Objectives

Aim

The aim of this study was to identify interacting partners for two putative DD-CPase-encoding genes in *M. smegmatis*, *dacB* and MSMEG_2433, and to determine the localization of these proteins. Interacting partners were identified using a yeast-two hybrid system, the results of which could point to the presence of a protein complex that could have a pivotal role in the cell. Antibiotic susceptibility of single DD-CPase deletion mutants was also carried out to determine any changes in drug susceptibility profiles with regards to these genes.

Objectives

1. To construct two vectors carrying either the *dacB* or MSMEG_2433 genes as fusions to the Gal4 DNA binding domain (bait)
2. To construct a library of the genome of *M. smegmatis* in a vector to create a library of fusion proteins to the Gal4 Activation Domain which will then serve as the prey for the screen.
3. To identify the protein/s interacting with the *M. smegmatis dacB* and MSMEG_2433 using the yeast two-hybrid system.
4. To determine the localization of the DD-CPases in the cell by constructing in-frame fusions to a fluorescent protein.
5. To determine the antibiotic susceptibility profiles of single gene DD-CPase knockouts (MSMEG_2432, MSMEG_2433 and MSMEG_1600).

2. Methods and Materials

2.1. Bacterial Strains, Plasmids and growth conditions

All bacterial strains and plasmids constructed and/or used in this study are listed in Tables 2.1 and 2.2. Glycerol stocks of all strains were prepared using 33 % glycerol and stored at -70°C.

N.B. All centrifugation steps were carried out at room temperature unless otherwise stated.

Table 2.1. Bacterial strains used and/or created in this study

Strain	Genotype	Reference
E. coli		
Escherichia coli DH5α	*SupE44 ΔlacU169 hsdR17 recA1 endA1 gyrA96 thi-1 relA1*	Promega, Madison, WI
Escherichia coli Dam-	*ara-14 leuB6 fhuA31 lacY1 tsx78 glnV44 galK2 galT22 mcrA dcm-6 hisG4 rfbD1 R(zgb210::Tn10)* Tet^S *endA1 rspL136* (Str^R) *dam13::Tn9* (Cam^R) *xylA-5 mtl-1 thi-1 mcrB1 hsdR2*	New England Biolabs, Ipswich, MA
M. smegmatis		
mc^2155	High frequency transformation mutant of *M. smegmatis* ATCC 607	(Snapper et al., 1990)
SRS	Derivative of mc^2155 carrying pMC1s, which encodes the tetracycline repressor, integrated at the *attB* bacterial phage attachment site, Kan^R	C. Ealand (CBTBR)
Δ1661	Derivative of mc^2155 carrying an unmarked MSMEG_1661 deletion of 1158 bp	C. Ealand (CBTBR)
Δ2433	Derivative of mc^2155 carrying an unmarked MSMEG_2433 deletion of 855 bp	C. Ealand (CBTBR)
Δ2432	Derivative of mc^2155 carrying an unmarked MSMEG_2432 deletion of 792 bp	C. Ealand (CBTBR)

Yeast		
AH109	*MATa, trp1-901, leu2-3, 112, ura3-52, his3-200; gal4Δ, gal80Δ, LYS2 : : GAL1$_{UAS}$-GAL1$_{TATA}$-HIS3, GAL2$_{UAS}$-GAL2$_{TATA}$-ADE2, URA3 : : MEL1$_{UAS}$-MEL1 $_{TATA}$-lacZ*	(James et al., 1996) Clontech Laboratories Inc.
Y187	*MATα, ura3-52, his3-200, ade2-101, trp1-901, leu2-3, 112, gal4*Δ, *met–, gal80*Δ,*URA3::GAL1*UAS-*GAL1*TATA-*lacZ*	(Harper et al., 1993) Clontech Laboratories Inc.

Table 2.2. Plasmids used and/or created in this study

Plasmids	**Genotype**	**Reference**
pGADT7	Y2H vector to produce AD fusions, GAL4 (768-881) AD, LEU2, HA epitope tag; Amp^R	*Clontech Laboratories Inc.*
pGBKT7	Y2H vector to produce BD fusions, GAL4(1-147) DNA-BD, TRP1, c-MYC epitope tag; Kan^R	*Clontech Laboratories Inc.*
pSE100	*E. coli*-Mycobacterium shuttle vector carrying Pmyc1^{tetO}; Hyg^R	(Ehrt et al., 2005)
pTweety (pTTP1BG)	Integration vector carrying an integrase gene; Genta^R	(Pham et al., 2007); Nicole C. Narrandes (CBTBR)
pMC1s	Shuttle vector carrying PSMYC–*tetR*, integrates at the *attB* site on the mycobacterial genome; Kan^R	(Ehrt et al., 2005)
mCherry (pSB1C3**)**	*E. coli* vector carrying mRFP, Kan^R	(Shaner et al., 2004)
Venus (pMK)	*E. coli* vector carrying Venus, Kan^R	(Petreanu et al., 2007)
rsEGFP	*E. coli* vector carrying rseGFP, Kan^R	(Grotjohann et al., 2011)
pGBKdacB	Derivative of pGBKT7, carrying the 1443 bp *dacB* gene cloned as an in-frame fusion to the *gal4* promoter DNA binding domain Kan^R	This study

pGBK2433	Derivative of pGBKT7, carrying the 891 bp MSMEG_2433 gene cloned as an in-frame fusion to the *gal4* promoter DNA binding domain Kan^R	This study
pSEdacB-mCherry	Derivative of pSE100, carrying the *dacB* gene with an in-frame C-terminal fusion to the mCherry fluorescent gene Hyg^R	This study
pSEdacB-Venus	Derivative of pSE100, carrying the *dacB* gene with an in-frame C-terminal fusion to the Venus fluorescent gene Hyg^R	This study
pSEdacB-rsEGFP	Derivative of pSE100, carrying the *dacB* gene with an in-frame C-terminal fusion to the *rseGFP* fluorescent gene Hyg^R	This study
pSE2433-Venus	Derivative of pSE100, carrying the MSMEG_2433 gene with an in-frame C-terminal fusion to the Venus fluorescent gene Hyg^R	This study
pSE2433-rsEGFP	Derivative of pSE100, carrying the MSMEG_2433 gene with an in-frame C-terminal fusion to the *rseGFP* fluorescent gene Hyg^R	This study
pTw::dacB-rsEGFP	Derivative of pTweety carrying the tetO, *dacB* gene and *rseGFP* fluorescent gene $Genta^R$	This study

Kan^R (Kanamycin resistant); Amp^R (Ampicillin resistant); $Genta^R$ (Gentamycin resistant); Hyg^R (Hygromycin resistant)

2.1.1. Growth of Mycobacterial Strains

M. smegmatis was grown in Middlebrook 7H9 supplemented with 0.5 % glycerol, 0.085 % NaCl, 0.2 % glucose and 0.05 % tween 80 (referred to herein at 7H9), as well as the appropriate antibiotic, at 37 ºC overnight at a shaking speed of 100 rpm. For growth on solid media, Middlebrook 7H10 supplemented with 0.2 % glycerol, 0.085 % NaCl, 0.5 % glucose (referred to herein as 7H10) and the appropriate antibiotic was used with incubation at 37 ºC

for 3-4 days. Antibiotic concentrations used were as follows: 50 µg/mL hygromycin (Hyg), 25 µg/mL Kanamycin (Kan) and 10 µg/mL Gentamycin (Genta).

2.1.2. Growth of *E. coli* strains

E. coli was grown in Luria-Bertani broth (LB) supplemented with the appropriate antibiotic at 37 ºC overnight (unless otherwise stated). Luria-Bertani agar (LA) was used for growth on solid media. Antibiotic concentrations used were as follows: 200 µg/mL Hyg, 50 µg/mL Kan and 25 µg/mL Genta.

2.2. DNA manipulation

2.2.1. Mycobacterial DNA extraction

2.2.1.1. Cetyltrimethylammonium bromide (CTAB) method

Mycobacterial cells were initially heat killed at 65 ºC for 35 min followed by harvesting using centrifugation (3500 × *g*) for 10 min and the pellet was resuspended in 100 µL TE. Thereafter, 50 µL lysozyme (10 mg/mL) was added to each tube and incubated at 37 ºC for 1 hour. A combination of 70 µL 10 % SDS and 6 µL proteinase k (10 mg/mL) was added to the tubes and incubated at 65 ºC for 2 hours. Following this, 100 µL 5M NaCl was added, mixed, and 80 µL pre-warmed NaCl/CTAB was then added to the mixture and vortexed. This was incubated at 65 ºC for 10 min. Approximately 800 µL chloroform:isoamyl alcohol (24:1) was added to each tube, mixed and centrifuged for 5 min. Aqueous layer was transferred to a clean tube, 0.6 volumes of isopropanol was added to this, tubes were inverted, placed on ice for 20 min and then centrifuged (16500 × *g*) for 20 min. The resulting DNA pellet was then washed twice with cold 70 % ethanol and pellet was dried in the speed vac for approximately 15 min. Each pellet was resuspended in 40-60 µL TE buffer, quantified using the Nanodrop (Inqaba Biotech, South Africa) and stored at 4 ºC.

2.2.1.2. Colony boil for small-scale mycobacterial DNA extractions

Half of the desired colony was picked and resuspended in 100 µL sterile water (sdH_2O). Thereafter, 50 µL chloroform was added and the tube inverted 6 times. This was boiled at 65 ºC for 15 min and centrifuged (16500 × *g*) for 2 min. The supernatant was transferred to a clean eppendorf tube and used immediately.

2.2.2. Transformation of bacteria

2.2.2.1. Chemical Transformation of E. coli

E. coli DH5α or Dam^- cells (only used when enzymes sensitive to methylation were subsequently used on plasmid DNA) were made chemically competent using the rhubidium chloride method. Briefly 2 mL of an overnight *E. coli* culture was inoculated into 200 mL 2 × TY (tryptone and yeast extract, Appendix A) broth and incubated at 37 ºC with shaking at 200 rpm until the cell density reached an OD_{600} = 0.5. This was then placed on ice for 15 min and the cells harvested at (3500 × *g*) for 5 min. The supernatant was discarded and 20 mL TfbI (transformation buffer I, Appendix A) was added per 50 mL culture volume, the pellet was gently resuspended and placed on ice for 15 min. Cells were harvested as indicated before, resuspended in 2 mL TfbII (transformation buffer II, Appendix A) per 50 mL culture volume and placed on ice for 15 min. Quick freeze in ethanol was carried out at -70 ºC, in 500 µL aliquots, and stored at the same temperature.

For the transformations, up to 1µg of plasmid DNA was added to 200 µL of competent cells (thawed on ice). This was chilled on ice for 15 min, thereafter heat shocked at 42 ºC for 90 sec and placed on ice for 2 min. Following this, 700 µL LB was added to the transformation and the reaction was rescued at 37 ºC for an hour. Rescued transformations were plated on LA with the appropriate antibiotic/s and incubated overnight at 37 ºC.

2.2.2.2. Electroporation of E. coli

Lucigen E. cloni 10F Supreme cells were used according to manufacturer's instructions. Briefly, cuvettes were pre-chilled on ice and 25 µL competent cells (thawed on ice) were aliquoted into the cuvettes. Thereafter, 1 µL sodium acetate precipitated ligation reaction or plasmid DNA (resuspended in 0.5× TE buffer) was added to the appropriate cuvette. After electroporation, 975 µL recovery medium was added to the cuvette following rescue of cells at 250 rpm for 1 hour at 37 ºC. Settings for electroporations were as follows: 600 Ohms resistance, 1800 V voltage, 10 µF capacity and a 1 mm cuvette. Plating was the same as for chemical transformation.

2.2.2.3. Electroporation of M. smegmatis

One hundred mL *M. smegmatis* culture was grown in 7H9 overnight at 37 ºC to OD_{600nm} 0.5-1.0. Cultures were incubated on ice for 30 min and thereafter transferred to chilled 50 mL conical tubes and spun down at 3500 rpm at 4 ºC for 10 min. The supernatant was discarded and pellet resuspended in 30 mL cold 10 % glycerol. Cells were spun down again and resuspended in 15 mL cold 10 % glycerol, followed by a third wash in 5 mL 10 % ice cold glycerol and stored on ice. Cells were used immediately.

For electroporations, 400 µL of the competent cells were aliquoted into chilled electroporation cuvettes. Up to 1 µg of plasmid was added to the appropriate cuvette and incubated on ice for 5 min. Cells were electroporated and 1 mL 2 × TY was added to the cuvettes and the bacteria rescued overnight at 37 ºC. Electroporation settings were as follows: 2500 v voltage, 1000 Ω resistance, 25 Ω capacity and 2 mm cuvette. After rescuing the cells, bacteria were harvested by centrifugation (3500 × *g*) for 10 min and resuspended in 400 µL 2 × TY. Thereafter 10^1-10^2 dilutions were made and 100 µL of the dilutions, and the remainder of the undiluted cells, were plated on 7H10 with the appropriate antibiotic. Plates were incubated at 37 ºC for 3-5 days.

2.2.3. Plasmid preparation

2.2.3.1. Plasmid Miniprep of E.coli (alkaline lysis method)

For plasmid preparation, 2 mL overnight cultures grown in LA with the appropriate antibiotic were centrifuged (16500 × *g*) for 5 min. The cell pellets were resuspended in 100 µL cold Solution I (Appendix A), to which 200 µL Solution II (Appendix A) was added, inverted to mix, and placed on ice for 5 min. Thereafter 300 µL cold Solution III (Appendix A) was added, mixed by inversion, and incubated on ice for a further 5 min. Following incubation, the cell lysate was centrifuged (16500 × *g*) for 10 min and the supernatant was transferred to a sterile eppendorf tube, to which 2 µL RNase A was added. Tubes were incubated at 37 ºC for 20 min, followed by addition of 450 µL isopropanol to the tubes, which were mixed by inversion and centrifuged at 16500 × *g* for 20 min. The pellet was washed twice with 70 % ethanol and dried in the Eppendorf Concentrator 5301. The pellet was resuspended in 20 – 30 µL sdH_2O and quantified using the Nanodrop 1000 (Nanodrop technologies, USA).

2.2.3.2. Plasmid Maxiprep of E. coli

2.2.3.2.1. Alkaline lysis method

For bulk preparation of plasmid DNA, 50 mL overnight cultures were centrifuged (3500 × *g*) for 10 min at 4 ºC and resuspended in 1mL cold Solution I, which was split into 200 µL aliquots and transferred to eppendorf tubes. The cells were harvested by centrifugation (16500 × *g*) for 30 seconds. The cell pellet was resuspended in 200 µL cold Solution I, followed by addition of 400 µL Solution II, mixing by inversion and incubation on ice for 5 min. Thereafter, 300 µL cold Solution III was added, mixed and returned to ice for 10 min. The tubes were then centrifuged at 16500 × *g* for 10 min. The supernatant was transferred to a sterile eppendorf, to which 2 µL RNase (10 mg/mL) was added and incubated at 42 ºC for 20 min. Thereafter, 650 µL isopropanol was added to each tube, allowed to cool at room

temperature for 10 min, followed by centrifugation for 20 min at 16500 × *g*. The DNA pellet was washed twice with 70% ethanol and dried in an Eppendorf Concentrator at 60 ºC for 15 min. The pellet was resuspended in 200 µL sdH_2O. For further purity, sodium acetate precipitation was used to clean the plasmid DNA as described in section 2.2.4.

2.2.3.2.2. Bulk plasmid preparation using the Nucleobond Plasmid extraction kit

In some cases, bulk plasmid preparations were made using the Nucleobond plasmid extraction kit, which was used according to the protocol provided by the manufacturer. Briefly, 50 mL of cells were harvested by centrifugation at 3500 × *g* for 15 min at 4 °C. Cells were resuspended in 8 mL Buffer S1 + RNase by vortexing and then lysed using 8 mL Buffer S2. Cells were neutralised by the addition of 8 mL Buffer S3 and the lysate cleared by centrifugation for 30 min at 3500 × *g* (4 °C). The cleared lysate was then loaded onto an equilibrated Nucleobond N100 column (equilibrated using Buffer N2), the flow through discarded and column was then washed twice with 10 mL Buffer N3 and flow through discarded. Plasmid DNA was eluted using 5 mL Buffer N5. The plasmid DNA was then precipitated by the addition of 0.8 volumes of isopropanol, followed by centrifugation, washing and quantification using the Nanodrop 1000.

2.2.4. Sodium Acetate Precipitation

For precipitation of DNA, 0.1 volume 3M sodium acetate buffer (pH 5.2) and 2 × volume cold 100 % ethanol was added to desired tube/s and mixed. Tubes were placed on ice for 20 min and thereafter centrifuged (16500 × *g*) for 10 min. The pellet was then washed with 70 % ethanol, centrifuged for 5 min and dried in an Eppendorf Concentrator at 60 ºC for 15 min. The pellet was then resuspended in 20-40 µL TE or sdH_2O.

2.2.5. Dephosphorylation of 5'ends

For cloning, the vector is required to be dephosphorylated in order to reduce the possibility of the vector ligating to itself without the inclusion of the desired insert, leading to false positives. For this the Roche Fast AP phosphatase was used as per the manufacturer's protocol (Roche, South Africa). Briefly, following restriction digest of the vector, 1 µL Roche Fast AP was added to the reaction along with 1/10 volume Fast AP buffer. The reaction was incubated at 37 ºC for a minimum of 2 hours. Reactions were heat inactivated at 65 ºC for 15 min.

2.2.6. Restriction analysis

For restriction digest, up to 2 µg of DNA or plasmid was digested using 1 unit of the appropriate enzyme and 10 × buffer as per manufacturer's instructions, in a 20 µL reaction. Enzymes used were from Roche, Fermentas (USA) or New England Biolabs (NEB, UK). NEB buffers were supplemented with 10 µg/mL BSA as required.

2.2.7. Ligation Reaction

For the ligation reactions, the vector:insert ratio was calculated using the following formula:

$$Amount\ of\ insert\ (ng) = \frac{50\ \eta g\ vector\ x\ insert\ size\ (bp)}{Vector\ size\ (bp)}$$

Molar ratios of 1:1 or 1:2 were used, using 50 ηg of vector, as these produced the optimum results. T4 ligase from Fermentas was used according to manufacturer's protocol using the appropriate calculated vector:insert concentrations in a 20 µL reaction. Reactions were incubated at room temperature for 30 min - 1 hour. For blunt cloning, PEG4000 was added to the reaction (1/10 volume), with an incubation time of 1 hour at room temperature. Reactions were then heat inactivated at 75 ºC for 15 min.

2.2.8. Agarose Gel Electrophoresis

To resolve DNA, 0.8-1 % gels were used for high molecular weight fragments (>500 bp). Gels were made using 1× TAE (1 mM EDTA, 40 mM Tris-acetic acid pH 8.5) buffer, agarose and 0.5 µg/mL ethidium bromide. Gels were run at 80-100 voltage and DNA molecular weight markers were run alongside all samples. Gels were viewed under a UV light using the GeneSnap system (Biorad, South Africa).

2.2.9. DNA extraction from Agarose Gels

QIAquick gel extraction kit was used according to the provided protocol. Briefly, the agarose gel slice was weighed in a sterile eppendorf tube, to which thrice the volume of Buffer QG was added and this was incubated at 50 ºC until the gel slice was completely dissolved. Once dissolved, one volume isopropanol was added with this mixture being subsequently transferred to a QIAquick column in order to bind the DNA. The sample was centrifuged (17900 × *g*) for 1 min and flow-through discarded. The column was then washed by the addition of 750 µL Buffer PE, centrifuged (17900 × *g*) for 1 min, flow-through discarded and centrifugation repeated. The QIAquick column was then placed in a clean 1.5 mL eppendorf tube and DNA was eluted using 40 µL Buffer PE and quantified using the Nanodrop-1000.

2.2.10. DNA Quantification

Quantification of genomic DNA, plasmid DNA, as well as RNA was carried out using the Nanodrop ND-1000 Spectrophotometer (Nanodrop Technologies) which measures absorbance at 260 nm and 280 nm. Agarose gel electrophoresis was also used to quantify DNA by comparing the intensity of the desired bands against the intensity of the molecular weight markers used; Roche/Fermentas markers II, III and IV were used in this study (Appendix B).

2.2.11. DNA Sequencing

Sequencing was outsourced to the Sequencing facility at Stellenbosch University, using the Big Dye terminator v3.1 Cycle Sequencing kit and Bioline Half Dye Mix. The sequencing data was analyzed using the Lasergene programme suite, specifically EditSeq and Seqman™.

2.4. Library Preparation

For genomic DNA libraries, 1 µg of DNA was digested by a serial dilution of the enzymes *Hpa*II and *Aci*I. An aliquot of the restriction digests were run on a 0.8 % gel and the fragments in the correct size range (0.5 kb – 3 kb) were excised and purified (as described above) followed by cleaning using a sodium acetate precipitation. pGADT7 was simultaneously restricted with *Cla*I, dephosphorylated, sodium acetate precipitated and dephosphorylated a second time. Ligation reactions were set up according to size differences between the vector and average size of insert. A 5.3 × concentration difference was used and a reaction was set up using 300 ηg of vector and 60 ηg of insert. The ligation reaction was incubated overnight at 22 ºC and was subsequently heat inactivated, sodium acetate precipitated and resuspended in 5 µL of 0.5 × TE buffer. Thereafter, 1 µL of this reaction was used for electroporation into Lucigen E. cloni 10F Supreme cells (as previously described) and plated on LA/Amp. Plates were incubated overnight at 37 ºC and 10 colonies were picked, a plasmid miniprep was carried out and the plasmid was digested with *Hin*DIII to ensure presence of insert. The rest of the cells were then scraped into LB media. An aliquot was frozen at -80 ºC and plasmid isolation was carried out using the Nucleobond kit for the remainder of the cell mixture. Purified plasmid was stored at – 20 ºC until further use.

2.5. Polymerase Chain Reaction (PCR)

2.5.1. Roche Fast Start PCR

Screening/ confirmation of *M. smegmatis* clones were achieved by using the appropriate primers in a Roche FastStart PCR reaction. A 30 µL reaction was set up using 8 µL 10 mM dNTPs, 3 µL 10× PCR buffer with $MgCl_2$, 6 µL 5× GC rich solution, 2.5 µL 10 mM forward primer, 2.5 µL 10 mM reverse primer, 0.5 µL FastStart Taq Polymerase, up to 5 µL template DNA, and sdH_2O up to 30 µL. Cycling conditions were as follows: one cycle of an initial denaturation at 94° C for 4 min; 30-35 cycles of 30 s denaturation at 94° C, 30 s annealing at 55-70° C and 30-90 s elongation at 72° C which was followed by a final elongation step at 72° C for 5-7 min.

2.5.2. Phusion High Fidelity PCR

Amplification of genes for cloning was carried out using Phusion high fidelity PCR. A 50 µL reaction was set up using 10 µL 5 × HF buffer, 1.5 µL DMSO, 8 µL 10 mM dNTPs, 2.5 µL 10 mM forward primer, 2.5 µL 10 mM reverse primer, 0.3 µL Phusion Taq Polymerase, DNA up to 0.1 µg, and sdH_2O up to 50 µL. Cycling conditions were as follows for 35 cycles: initial denaturation at 98 ºC for 3 min, denaturation at 98 ºC for 10 s, annealing between 55 ºC-70 ºC for 30 s, elongation at 72 ºC for 45 s and final elongation at 72 ºC for 7 min.

2.5.3. PCR clean up

QIAquick PCR clean-up kit was used according to the provided protocol. Briefly, 5 volumes buffer PBI was added to 1 volume of the PCR sample, mixed, and transferred to a QIAquick column. In order to bind the DNA, sample was then centrifuged (17500 × *g*) for 1 min and flow-through discarded. Thereafter, 750 µL buffer PE was added to the column and centrifugation step was repeated twice. Column was then placed in a clean 1.5 mL eppendorf tube and DNA was eluted using 40 µL buffer EB. DNA was subsequently quantified using the Nanodrop-1000.

2.6. Cloning

2.6.1. 3-way cloning

The *dacB* gene and MSMEG_2433 were cloned either with mCherry, rsEGFP or Venus into pSE100. Primers used for amplification of genes are outlined in Table 2.3. The vector, pSE100, was restricted with *Pac*I and *Pst*I for the *dacB* and mCherry cloning, *Pac*I and *Hin*DIII for *dacB* and Venus cloning, as well as for the MSMEG_2433 and Venus cloning, *Bam*HI and *Hin*DIII for *dacB* and rseGFP cloning, and finally, *Pst*I and *Hin*DIII for the MSMEG_2433 and rsEGFP cloning. pSE100 was digested, dephosphorylated and fragments were digested with enzymes indicated above. These were then run on a 0.8 % gel; the fragments were excised and extracted using the Nucleospin gel extraction kit. Cloning was achieved using a ligation ratio of 1:2:2 (pSE100: gene: fluorescent gene). Ligations were transformed into *E. coli* DH5α and plated on LA + Hyg. Potential positive clones were screened by restriction analysis and one putative clone was taken forward by inoculation into 50 mL LA + Hyg and plasmid maxiprep was achieved using the Nucleobond kit. The plasmid was then electroporated into *M. smegmatis*, plated on 7H10 + Hyg and incubated at 37ºC for 3 days. A colony was picked and small scale DNA extraction was carried out followed by confirmation using PCR (with primers of the appropriate genes). The repressor pMC1s was electroporated into electrocompetent *M. smegmatis* carrying pSE*dacB*-rsEGFP and confirmed using PCR with the pMC1s primers (Appendix C). Freezer stocks of all clones were made using 33 % glycerol and stored at -70 ºC.

2.6.2. Blunt-end cloning of DD-CPase-GFP fusions

For cloning of the blunt ended *dacB*-rsEGFP cassette, with the tetO, the cassette was cut out of the pSE100 background using *Pci*I and *Hin*DIII. The fragment ends were blunted using the Klenow fragment from NEB, as well as Polymerase I (NEB), according to the manufacturer's instructions. Briefly, a 30 µL reaction was set up using the 20 µL restriction digest, 3 µL 10

mM dNTPs, 3 µL NEB buffer 2 with BSA, 1 µL Klenow fragment (NEB), 1 µL T4 Polymerase I (NEB) and sdH_2O up to 30 µL. The reaction was incubated at 22 ºC for 15 min. pTweety was restriction digested with *Sma*I and dephosphorylated using FastAP. Blunt cloning was followed using a ligation insert:vector ratio of 1:2. Ligations were transformed into *E. coli* DH5α and plated on LA + Genta. Potential positive clones were screened by restriction analysis (using *Xba*I) and one clone was taken forward by inoculation into 50 mL LA + Genta. Plasmid maxiprep was achieved using the Nucleobond kit. The resulting plasmid, as well as the repressor pMC1s was then electroporated into *M. smegmatis*, plated on 7H10 + Genta for the plasmid only, and 7H10 + Genta + Kan for the plasmid with pMC1s, and incubated at 37ºC for 3 days. A colony was picked and small scale DNA extraction was carried out and vector incorporation was confirmed using PCR (with primers of the appropriate genes as well as primers for pMC1s). Freezer stocks of all clones were prepared.

Table 2.3. Primers used for 3-way cloning

Gene	**Primer (5' – 3')**
dacB (mCherry) F	GCGCTTAATTAA*PacI*ATGAGCGATAGGCTGACG
dacB (mCherry) R	GCGCGGATCC*BamHI*TGCGCCGCATCCGCAGCT
dacB (Venus) F	GCGCTTAATTAA*PacI*ATGAGCGATAGGCTGACG
dacB (Venus) R	GCGCAGATCT*BglII*TGCGCCGCATCCGCAGCT
dacB (rsEGFP) F	GCGCGGATCC*BamHI*ATGAGCGATAGGCTGACG
dacB (rsEGFP) R	GCGCGAATTC*EcoRI*TGCGCCGCATCCGCAGCT
2433 (Venus) F	GCGCTTAATTAA*PacI*ATGTGGAGGTACGCCTTC
2433 (Venus) R	GCGCAGATCT*BglII*GAGCGCCCCGATGCTCGC
2433 (rsEGFP) F	GCGCCTGCAG*PstI*ATGTGGAGGTACGCCTTC
2433 (rsEGFP) R	GCGCGAATTC*EcoRI*GAGCGCCCCGATGCTCGC
mCherry F	GCGCGGATCC*BamHI*ATGGCTTCCTCCGAAGAC
mCherry R	GCGCCTGCAG*PstI*TTATTAAGCACCGGTGGA
Venus F	GCGCAGATCT*BglII*ATGGTTTCAAAGGGTGAA

Venus R	GCGCAAGCTT^{HinDIII}TTATTACTTGTATAATTC
rsEGFP F	GCGCGAATTC^{EcoRI}ATGGTGAGCAAGGGCGAG
rsEGFP R	GCGCAAGCTT^{HinDIII}TTACTTGTACAGCTCGTC

Restriction enzyme sites are underlined.

2.7. Microscopy

2.7.1. Fluorescence Microscopy

Cells were prepared by growing a 5 mL culture in 7H9 supplemented with the appropriate antibiotic at 37 ºC overnight, to an OD_{600nm} = 0.3 – 0.5. The culture was centrifuged (3500 × *g*) for 10 min (4 ºC). The pellet was resuspended in 1 mL 7H9 and transferred to a sterile eppendorf tube. Cells were spun down, harvested at 16500 × *g* for 5 min and washed twice with 400 µL 7H10. Cells were then resuspended in 50 µL 7H9. For staining, following the initial spin step, 1 µg/mL vancomycin (cold) and 1 µg/mL fluorescent vancomycin (BODIPY label) was added to the resuspended pellet and incubated at 37 ºC for 1.5 hours.

A 2 % agarose gel was used to prepare a pad where approximately 250 µL of gel mix was spread onto a slide. Another slide was placed over in order to ensure an even surface. The top slide was removed and 2 - 5 µL of cells were spread onto the agarose bed and a cover slip placed over. Slides were viewed immediately on the Zeiss LSM-780 Confocal microscope and images processed with ZEN black Ver. 11 software (Zeiss, Germany).

2.7.2. Immunogold and Transmission Electron Microscopy (TEM)

pSEdacB-rsEGFP and pSE2433-rsEGFP cells were scraped off 7H10/Hyg plates and fixed using 4 % paraformaldehyde and 0.5 % glutaraldehyde in PBS (pH 7.4) at 4 ºC for 4 hours. Cells were centrifuged at 3500 × *g* for 10 min (4ºC), the pellet was washed with PBS and centrifuged again followed by resuspension in 4 % low melting agarose and subsequently allowed to set on ice. Cubes of approximately 1 mm^3 were then cut, washed with PBS and

thereafter washed with sdH_2O. Samples were then dehydrated through a graded series of ethanol as follows; 50 % ethanol at 4 ºC for 10 min, 75 % ethanol at 4 ºC for 10 min, 95 % ethanol at 22 ºC for 10 min and 100 % ethanol at 22 ºC for 30 min. A 1:1 mixture of LR white:100 % ethanol was added and mixed for 1 hour. The mixture was poured out and 100 % LR white was added and mixed overnight (on a Rotamix) at 4 ºC. The resin was replaced with 100 % LR white and mixed at room temperature for 1 hour. Samples were then embedded in Beem capsules and polymerized at 50 ºC for 24 - 36 hours. Ultrathin sections were cut using Relchert Ultracut Ultramucrotome (Circa Scientific, Canada) and mounted onto formvar-carbon coated nickel grids and allowed to dry overnight.

Subsequent immunolabelling was performed by incubating the grids in small reagent droplets on parafilm at room temperature. The free aldehyde was quenched by incubating the grids in 0.1 M glycine solution for 20 min. Sections were then rinsed twice using TBS-Tween for 2 min and were subsequently incubated in blocking buffer for 30 min, thereafter on droplets of primary antibody (1:50, 1:100, or 1:500 dilution) for 2 hours at room temperature. Sections were rinsed, 6 times, on droplets of TBS-Tween for 2 min. Sections were then rinsed on droplets of 1:50 dilution of secondary antibody for 1 hour at room temperature and rinsed again on large droplets of TBS-Tween, 6 times for 2 min. Slides were then dried completely prior to fixing. Post-fixation of sections were then carried out on droplets of 2 % glutaraldehyde in 0.1 M PBS for 10 min and followed by rinsing 6 times with TBS-Tween for 2 min. Sections were then rinsed in 3 × 20 dips of sdH_2O and subsequently stained with uranyl acetate for 5 min and lead citrate for 5 min. Grids were viewed using a Tecnai F20 TEM.

2.8. Minimum Inhibitory Concentration (MIC) Determination

Wild type *M. smegmatis*, ΔMSMEG_1661, ΔMSMEG_2433 and ΔMSMEG_2432 were grown in 7H9 at 37 ºC to an OD_{600nm} of 0.3. A 1:10 dilution of the cultures was carried out, which was then diluted a further 1:50. The experiment was set up using a 96 well plate with the broth microdilution method (Domenech et al., 2005). The following antibiotics were used: Ampicillin (Amp), Vancomycin (Vanc), Erythromycin (Ery), Rifampicin (RIF), Cefamandole (Cad), Cefoxitin (Cox), Cefotaxime (Cot), Ceftriaxone (Ctx) and Cefapirin (Cap). Plates were incubated at 37 ºC for 5 days and thereafter viewed visually with the MIC being determined as the lowest drug concentration which inhibited growth by 90 %.

2.9. Assessment of growth and Gene Expression

2.9.1. Growth Curves

A 5 mL pre-culture of *M. smegmatis* mc^2155 (pSEdacB-rsEGFP), i.e. repressor-less (R-), and pSEdacB-rsEGFP::pMC1s 0 ηg tet, including repressor (R+), were started from freezer stocks, which was then used to inoculate a 30 mL pre-culture. This 30 mL culture was then used to inoculate 150 mL cultures of (i) R-; (ii) R+ supplemented with 0 ηg AHT; (iii) R+ supplemented with 0.5 ηg AHT; (iv) R+ supplemented with 5 ηg AHT; (v) R+ supplemented with 50 ηg AHT; and (vi) R+ supplemented with 100 ηg AHT, at an OD_{600nm} of 0.02. Samples were taken at 6 hours, 9 hours and 18 hours (i.e. from early to mid-log growth) from which OD_{600nm} readings, fluorescent microscopy and quantitative PCR was carried out.

2.9.2. RNA Isolation

For preparation of RNA for gene expression analysis, 50-100 mL aliquots of culture were spun down for 10 min at 3500 × *g*. The cells were resuspended in 1 mL 7H9, spun down again and resuspended in 500 µL 1 × TE buffer. Thereafter, 50 µL lysozyme (10 mg/mL) was added to each tube and incubated at 37 ºC for 30 min. The cultures were then aliquoted into

ribolyzing tubes and ribolyzed at a speed of 4.0 for 45 seconds and placed on ice for 2 min. The ribolyzing step was repeated thrice. The supernatant was transferred to an eppendorf tube, to which 355 µL lysis buffer was added, vortexed and stored at -80 ºC until RNA isolation. RNA isolation was carried out according to the Nucleospin RNA II kit according to the protocol. Briefly, the lysate was filtrated, to which 350 µL 70 % ethanol was added. Samples were then loaded onto a column to bind RNA and centrifuged at 11000 × *g* for 30 seconds. The silica membrane was desalted by the addition of 350 µL membrane desalting buffer and centrifugation at 1000 × g for 1 min. DNA digestion was then carried out using 95 µL DNase (made up of 10 µL rDNase reconstituted as per manufacturer's instructions) reaction mixture and incubated at room temperature for 15-30 min. The silica membrane was washed initially with 200 µL RA2, centrifuged at 11000 × *g* for 30 seconds, thereafter with 600 µL RA3, centrifuged and 11000× g for 30 seconds, and finally with 250 µL RA3, centrifuged at 11000 × *g* for 2 min. RNA was then eluted with 50 µL RNase free H_2O and quantified using the Nanodrop. One µg of RNA was then treated with DNase1 using 1 µL Turbo DNase, incubated at 37 ºC for 30 min, followed by the addition of another 1 µL Turbo DNase and 30 min incubation. DNase inactivation was carried out using 7 µL DNase removal resin and centrifuged at 13000 rpm for 5 min. A 23 µL volume of the sample was then removed and used for RT-PCR.

2.9.3. Reverse Transcriptase (RT) synthesis

A 2.5 µM reverse primer mix of *dacB* and *sigA* reverse primers were made up and 2 µL was added to the Turbo DNase treated RNA. The *sigA* gene was included as a normalizer since expression of this house keeping gene remains consistent throughout growth. Reactions were run as follows: 94 ºC for 30 seconds, 65 ºC for 3 min and 57 ºC for 3 min. RT+ and RT- reactions were set up using SuperScript III according to the manufacturer's protocol. Briefly, a 25 µL reaction was set up using 5 µL first strand buffer, 4 µL 25 mM $MgCl_2$, 2 µL 0.1 M

DTT, 1 µL 10 mM dNTPs and 0.8 µL SuperScript III, to which 12.5 µL of the annealed product was added. A RT negative control was set up that excluded the SuperScript III, which was replaced with sdH_2O. Reactions were placed in the PCR machine, incubated at 50 ºC for 50 min and inactivated at 85 ºC for 5 min, the resulting cDNA was then taken forward for qPCR.

2.9.4. Quantitative Real Time PCR (qPCR)

qPCR was carried out using the SsoFast Evergreen Supermix (Biorad). For this, 20 µL reactions were set up using 10 µL SsoFast Evergreen Supermix, 0.75 µL forward primer (10 µM), 0.75 µL reverse primer (10 µM), 1 µL cDNA and 7.5 µL sdH_2O. A standard curve was also set up using the same reaction, with the addition of 2 µL genomic DNA instead of cDNA. Reactions were placed into a CFX96 Real-Time PCR detection system (Bio-Rad Laboratories) and carried out with two sets of reactions with the following cycling parameters: The first set commences with an enzyme activation step of 95 ºC for 30 s, followed by, ten cycles of denaturation at 95 ºC for 10 s, touchdown annealing commencing at 65 ºC for 10 s and decreasing by 0.5 ºC following each cycle, and finally elongation at 72 ºC for 10 s. Thereafter, the second set of reactions consisting of 35 cycles commences as follows: a denaturation step at 95 ºC for 10 s, an annealing step at 60 ºC for 10 s and an elongation step at 72 ºC for 10 s. Thereafter, melt curve analysis was conducted from 50 ºC and gradually increasing to 95 °C. N.B. SYBR Green quantification was carried out following each cycle at all stages.

2.10. Southern Blot

2.10.1. Probe synthesis

DIG-dUTP labelled probes were synthesized using a DIG-dNTP mix in a Roche FastStart PCR reaction. Briefly, a 50 µL reaction was set up using 5 µL 10 × PCR buffer with $MgCl_2$,

10 µL 5 × GC rich solution, 2.5µL 10 mM forward primer (*dacB*), 2.5µL 10 mM reverse primer (*dacB*), 5 µL DIG-dNTP mix or 8 µL 10 mM dNTPs for the negative control or a mixture of both as an extra control, 0.5 µL FastStart Taq Polymerase, 50 ηg template DNA, and sdH_2O up to 50µL. Cycling conditions were as previously described in section 2.5.1. Reaction and controls were run on the same agarose gel as a molecular weight shift is caused by DIG-labelling.

2.10.2. Blotting

Restriction digests of 500 ηg of chromosomal DNA using 2 U of the enzymes *Bcl*I and *Stu*I were carried out overnight at 37 ºC. These were run on a 0.8 % agarose gel with Roche marker IV for 2 hours at a voltage of 80 v. The gel was photographed using the G-Box SYNGENE system and was thereafter depurinated in 0.2 M HCl solution for 10 min with gentle shaking. Gels were then denatured in 0.5 M NaOH/ 1.5 M NaCl for 30 min with gentle shaking. Gels were washed in 1 × TBE buffer (89 mM Tris Borate, 2 mM EDTA, pH 8.3), overlaid with Hybond^{TM}-N nitrocellulose membrane and thereafter sandwiched between 2 thick Whatman filter papers and 2 pre-soaked sponges (in 1 × TBE) in a gel cassette. This was transferred to an SB10 tank (Bio-Rad) containing 1 × TBE. DNA transfer to the nitrocellulose membrane was carried out for 2 hours at 600 mA. Crosslinking was carried out by UV irradiation at 2500 mJ/cm^3 twice. Membrane/s were then added to hybridization bottles containing 12 mL DIG-EASY-HYB and incubated at 54 ºC for 30 min. The probe was then denatured at 95 ºC for 5 min and added to the DIG-EASY-HYB in the bottle. Hybridization was carried out at 54 ºC overnight. The membrane was then washed with 20 mL solution I (2 × SSC, 0.1 % SDS) by gentle tilting for 5 min, and thereafter washed twice with pre-warmed solution II (0.5 × SSC, 0.1 % SDS) at 68 ºC for 15 min in the hybridization oven. The membrane was then rinsed in washing buffer (0.1 M maleic acid buffer, 0.3 % $Tween_{20}$) for 5 min, incubated in 20 mL blocking solution (1:10 dilution of 10 × blocking

solution in 0.1 M maleic acid buffer) for 30 min at room temperature, incubated in 20 mL Antibody solution (20 mL 1 × blocking solution, 2 µL Anti-DIG-AP) for 30 min at room temperature, washed twice in wash buffer for 15 min and finally equilibrated for 5 min in 20 mL detection buffer. The membrane was placed in a hybridization bag and 1 mL CSPD was spread over the membrane. The membrane was then incubated at 25 ºC for 5 min, excess liquid was squeezed out and incubated at 37 ºC for 10 min. Membranes were then exposed to X-ray film for 30 min and developed in an automated Axim developer.

2.11. Yeast 2-Hybrid system

2.11.1. Cloning of bait for yeast interaction libraries

The *dacB* gene and MSMEG_2433 were amplified by Phusion high fidelity PCR using the following primers, GCGCGGCGCCATATAG^{NdeI}CGATAGGCTGACG & GCGCCGGGATCC^{BamHI}TCATGCGCCGCATCCGCA; GCGCGGCGCCATATG^{NdeI}TGGAGGTACGCCTTC & GCGCCGCTGCAGTCAG^{PstI}AGCGCCCCGATGCT respectively. pGBKT7 was digested with *Nde*I and *Bam*HI for *dacB* cloning, and *Pst*I and *Nde*I for MSMEG_2433 cloning and thereafter dephosphorylated. Ligation reactions were followed using an insert:vector ratio of 1:2. Transformations and plasmid preparations were followed as previously described in sections 2.2.2 and 2.2.3.

2.11.2. Yeast transformation

2.11.2.1. Bait construction

Several 1-3 week Y187 colonies (approximately 2.5 mm in diameter) were inoculated into 1 mL YPDA media, vortexed and transferred to a flask containing 50 mL YPDA. This was incubated at 30ºC for 16-18 hours shaking at 250 rpm to OD_{600nm} =1.80 – 2.00. The overnight culture was subsequently transferred to 300 mL YPDA, the cell density adjusted to an

OD_{600nm} = 0.25 and incubated at 30ºC for 3 – 4 hours, shaking at 230 rpm, to OD_{600nm} = 0.5 ± 0.1. Cells were transferred to 50 mL Falcon tubes and centrifuged at 1000 × *g* for 5 min at 22ºC. Cells were washed twice with sdH_2O and thereafter each 50 mL Falcon tube pellet was resuspended in 5mL sdH_2O, pooled, and centrifuged at 1000 × *g* for 5 min at 22ºC. The supernatant was discarded and cell pellet was resuspended in 1.5 mL freshly prepared 1 × TE/LiAC.

For the transformation, 0.1 µg of the bait (*dacB* or MSMEG_2433) and 0.1 mg Herring testes carrier DNA were added to 1.5 mL eppendorf tubes, to which 100 µL prepared yeast competent cells were added and vortexed. Following this, 600 µL freshly prepared PEG/LiAC solution was then added to the tubes and vortexed to mix. Reactions were then incubated at 30 ºC for 30 min with shaking at 200 rpm. Thereafter 70 µL DMSO was added and mixed gently by inversion. This was then heat shocked for 15 min at 42 ºC. Reactions were then placed on ice for 2 min and centrifuged for 30 seconds at 16500 × *g*. Cells were resuspended in 500 µL 1 × TE buffer, 100 µL was plated on SD/-Trp and incubated at 30 ºC for 3 – 5 days.

2.11.2.2. Autoactivation

To test for autonomous histidine activation, a transformation reaction was carried out as for the bait, with the addition of 0.1 µg empty pGADT7 (prey) with the 0.1 µg bait. Following resuspension, 100 µL aliquots of cells were plated on SD/-Leu, SD/-Trp and SD/-Leu/-Trp dropout media. Colonies that emerged on SD/-Leu/-Trp were picked and resuspended in 500 µL 1 × TE buffer. The OD_{600nm} was adjusted to 0.5 and 10 µL was spotted on SD/-Leu/-Trp, SD/-Leu/-Trp/-His, SD/-Leu/-Trp/-His + 0.5 mM 3AT, SD/-Leu/-Trp/-His + 1 mM 3AT and SD/-Leu/-Trp/-His + 1.5 mM 3AT. Plates were incubated at 30 ºC for 3 - 5 days.

2.11.2.3. Construction of yeast library of M. smegmatis genomic fragments

AH109 was made competent using the same procedure as for Y187 (section 2.11.2.1), but up-scaled to library scale. Briefly, the overnight culture was transferred to 1 L YPDA and resuspended in 8 mL freshly prepared 1 × TE/LiAC. For the transformation, 0.3-0.4 mg sodium acetate precipitated library DNA and 20 mg Herring testes carrier DNA (denatured) was added to a 500 mL flask to which 8 mL AH109 competent cells was added and mixed vigorously. Then, 60 mL freshly prepared PEG/LiAC was added and vortexed to mix. This was incubated at 30 ºC for 30 min with shaking at 200 rpm, 7 mL DMSO was added and mixed by gentle swirling, heat shocked at 42 ºC for 15 min in a water bath and chilled on ice for 2 min. Cells were then centrifuged at 1000 × *g* for 5 min and the pellet was resuspended in 10 mL 1 × TE buffer. Thereafter, 200 µL aliquots were plated on approximately 55 SD/-Leu plates and incubated at 30 ºC for 3 - 5 days. Plates were scraped into freezing media (YPDA + 25 % glycerol), transferred to 2 mL cryovials and placed at -80 ºC.

2.11.3. Yeast Mating

One fresh 2-3 mm colony of transformed bait (*dacB* cloned into Y187 or MSMEG_2433 cloned into Y187) was inoculated into 50 mL SD/-Trp media and incubated shaking (250 rpm) at 30 ºC overnight to an OD_{600nm} = ~0.8. Cells were centrifuged at 1000 × *g* for 5 min and the pellet was resuspended in 3.5 - 4 mL SD/-Trp to a cell density of $>1\times10^8$ cells/mL. An aliquot of the *M. smegmatis* library was thawed in a room temperature water bath and a 1:100 dilution made to obtain a cell density of $>2\times10^7$ cells/mL. The library was combined with the bait strain in a 2 L flask, to which 45 mL of 2 × YPDA supplemented with Kan was added. The flask was then incubated at 30 ºC for 24 hours, shaking at 40 rpm. Following incubation, a drop of the culture was viewed under the Zeiss phase contrast microscope (40×) to check for the formation of zygotes. Cells were transferred to 50 mL conical tubes and centrifuged at 1000 × *g* for 10 min. The 2 L flask was rinsed twice with 25 mL 0.5 × YPDA

supplemented with Kan and this was used to resuspend the cell pellet from the previous step. The cells were centrifuged at 1000 × *g* for 10 min and the resulting pellet was resuspended in 10 mL 0.5 × YPDA/Kan media. Thereafter, 10^1 to 10^4 dilutions were made and 100 µL of each was plated on SD/-Trp, SD/-Leu and SD/-Leu/-Trp. The remainder was plated in 200 µL aliquots on SD/-Leu/-Trp/-His. All plates were incubated at 30 ºC for 6 days. All colonies which grew on SD/-Leu/-Trp/-His were picked, resuspended in 200 µL 0.5 × YPDA and spotted on SD/-Leu/-Trp, SD/-Leu/-Trp/-His/X-α-Gal and SD/-Leu/-Trp/-His/-Ade. Colonies which were blue on SD/-Leu/-Trp/-His/X-α-Gal were picked, resuspended in 500 µL 0.5 × YPDA, OD_{600nm} adjusted to 0.1 and 10 µL was spotted on SD/-Leu/-Trp/-His/X-α-Gal, SD/-Leu/-Trp/-His/-Ade and SD/-Leu/-Trp/-His/-Ade/X-α-Gal. Plates were incubated at 30 ºC for 6 days.

2.11.4. Plasmid Isolation from Yeast

Potential positive clones were picked and grown in 2 mL SD/-Leu (to select for the prey) overnight at 30 ºC. Cells were spun down at 16000 × *g* for 1 min and the supernatant was discarded. The cell pellet was resuspended in 230 µL DNA lysis buffer (10 mM Tris HCl, 0.1 M NaCl, 1 % SDS, 1 mM EDTA, 2 % Triton X-100). The suspension was transferred to a screw cap tube containing 0.4 g acid-washed 0.75 – 1 mm glass beads, to which 200 µL phenol:chloroform:isoamyl alcohol (25:24:1) was added. Tubes were vortexed at top speed for 2 min to isolate the plasmid DNA and thereafter spun down at 16000 × *g* for 5 min. The top aqueous layer was transferred to a sterile eppendorf tube and sodium acetate precipitation was followed. The pellet was resuspended in 30 - 40 µL 0.5 × TE buffer.

2.11.5. Transformation into *E. coli*

One µL of the isolated plasmid DNA isolated from yeast was electroporated into Lucigen E. cloni 10F Supreme cells as previously described, with the entire transformation being plated on LA/Amp and incubated overnight at 37 ºC.

2.11.6. Zyppy™ Plasmid Miniprep

One colony from each successful electroporation was picked and grown in LB/Amp overnight at 37 ºC. Zyppy plasmid miniprep was followed according to the provided protocol. Briefly, 2 mL of the *E. coli* culture was spun down at 16500 × *g* for 5 min and the pellet was resuspended in 600 µL LB, to which 100 µL 7 × lysis buffer was added and inverted 6 - 8 times to mix. Thereafter, 350 µL cold neutralization buffer was added, mixed by flicking, and centrifuged at 16500 × *g* for 2 min. The supernatant was transferred to a Zymo-spin™ column and centrifuged for 15 seconds. Two hundred µL of Endo-wash buffer was added to the column and centrifuged for 15 seconds. Thereafter 400 µL Zyppy™ wash buffer was added to the column and centrifuged for 30 seconds (16500 × *g*). The column was then transferred to a clean eppendorf tube and 30 µL Zyppy™ elution buffer was added to the column, incubated at room temperature for 2 min and thereafter centrifuged at 16500 × *g* for 30 seconds. Plasmid DNA was sent for sequencing using the T7 region primers.

2.11.7. Confirmations

Sequences from positive clones were analyzed using the NCBI website, namely nucleotide BLAST (BLASTn) and subsequently protein BLAST (BLASTx) in order to determine the presence and identity of any interacting proteins. Once potential interactions were found, the small scale yeast transformations using 100 ηg of vector into AH109 were carried out using a combination of either pGBKT7/bait (MSMEG_2433 or *dacB)* + pGADT7/prey (potential interacting partner); or empty pGBKT7 + pGADT7/prey. pGADT7 and pGBKT7 vector only were also transformed as controls. These were subsequently plated on SD/-Leu/-Trp, SD/-Leu/-Trp/X-α-Gal, SD/-Leu/-Trp/-His, SD/-Leu/-Trp/-His/X-α-Gal, SD/-Leu/-Trp/-His/-Ade, SD/-Leu/-Trp/-His/-Ade/X-α-Gal and incubated at 30 °C for 6 days.

3. Results

3.1. Library Preparation

3.1.1. Genomic DNA

For construction of the library, a high concentration of genomic DNA was required in order to obtain enough fragments for full coverage. Hence, a stationary phase culture of *M. smegmatis* was used for DNA isolation, which resulted in a high yield of genomic DNA that was not sheared and ran at a molecular weight > 20 kb, Figure 3.1.

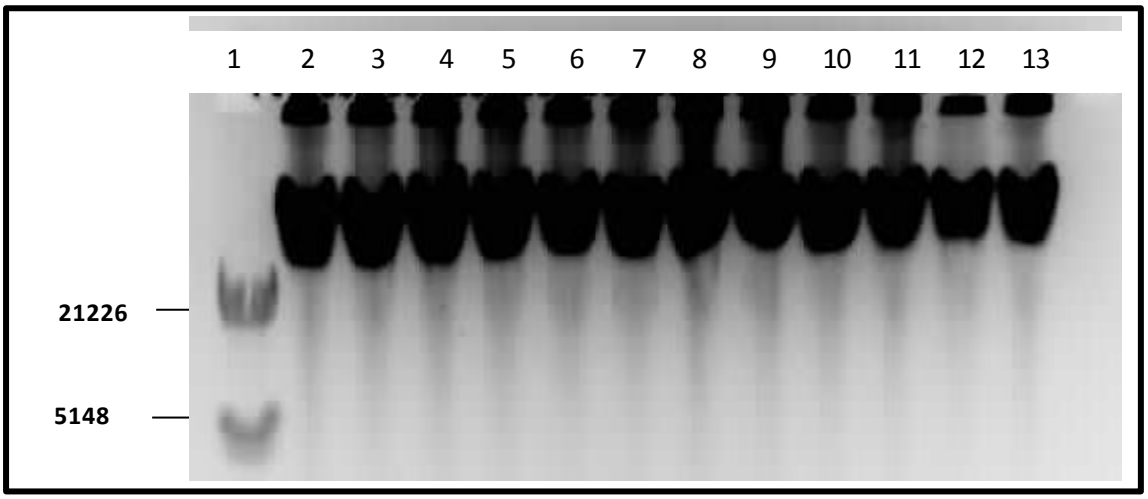


Figure 3.1. Agarose gel of extracted genomic DNA from WT *M. smegmatis*. **[Lane 1]** Roche Marker III, **[Lanes 2-13]** Isolated *M. smegmatis* genomic DNA.

A variety of enzymes including *Hin*DIII, *Bgl*II, *Sac*I, *Bam*HI and *Cla*I were utilized to digest genomic DNA, with the enzymes *SacI* and *Bgl*I showing the best frequency in cutting for the construction of a library (moderate cutters – data not shown), while *Bam*HI showed a high frequency of cutting, indicating that a partial digestion would yield appropriately sized fragments as well. The vector into which this DNA was cloned (pGADT7) contained unique restriction sites for proper insertion of the fragments, which included the *Bam*HI site, as well as the *Cla*I site, for constructing fusions with a *Hpa*II/*Aci*I digested genomic DNA library (James et al., 1996). Considering the previously published *M. smegmatis* genomic libraries in

yeast vectors, we decided to use the *Cla*I site for pGADT7 linearization and *Hpa*II/*Aci*I for fragment preparation (Steyn et al., 2002).

3.1.2. Vector and Fragment Preparation

The prey vector (pGADT7) was transformed into Dam- *E. coli* cells and the plasmid was isolated. The vector was subsequently digested using *Cla*I in order to linearize the vector, which was then phosphatased in order to prevent vector re-ligation. The linearized vector is shown in Figure 3.2.

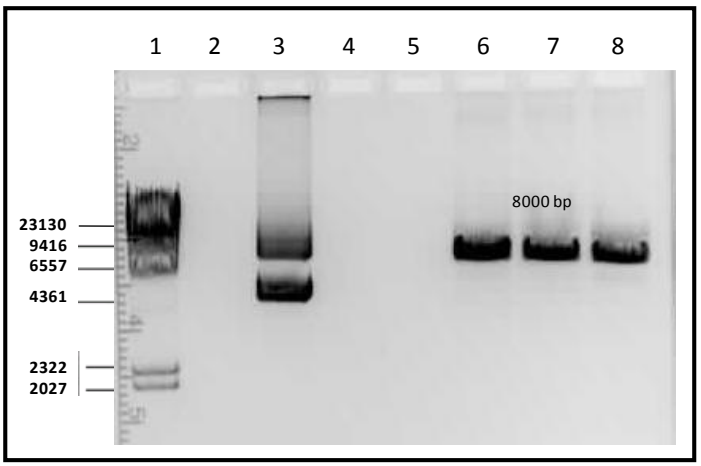


Figure 3.2. Agarose gel of pGADT7. **[Lane 1]** Roche Marker II, **[Lanes 2, 4, 5]** Empty, **[Lane 3]** Uncut pGADT7, **[Lanes 6-8]** *Cla*I digested pGADT7.

Restriction of pGADT7 with *Cla*I resulted in linearization of the vector as expected, Figure 3.2. A ligation control was carried out to assess vector re-ligation background colonies following phosphatase treatment. A negligible number of vector re-ligation products were obtained (data not shown). The linearized product was then taken forward for library preparation.

M. smegmatis DNA fragments for cloning were obtained with either *Hpa*II or *Aci*I restriction digest using an enzyme dilution series. A range of 500-5000 bp was chosen, Figure 3.3.

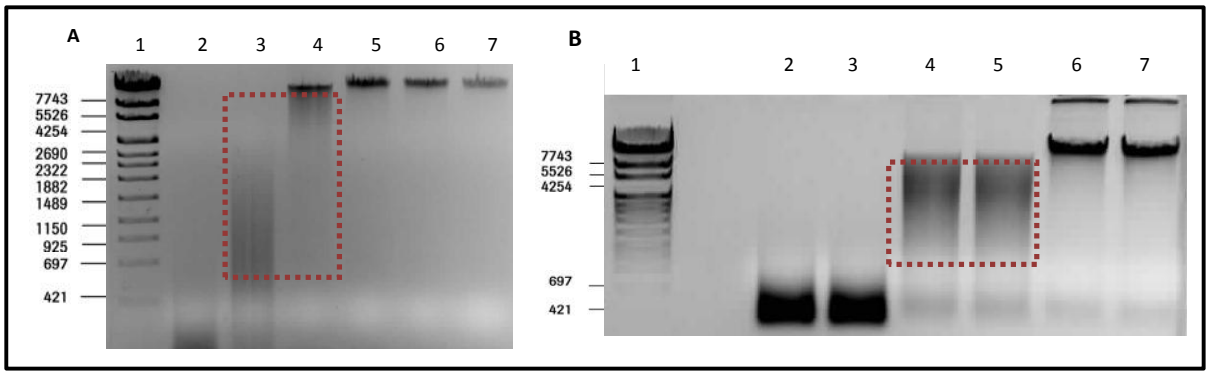


Figure 3.3. Agarose gels of genomic DNA restrictions. **(A)** *Hpa*II restriction by using a 3 fold dilution series of the enzyme **[Lane 1]** Roche Marker IV, **[Lanes 2-7]** *Hpa*II restriction of genomic DNA at each dilution. **(B)** *Aci*I restriction by using a 3 fold dilution series of the enzyme **[Lane 1]** Roche Marker IV**, [Lanes 2-7]** *Aci*I restriction of genomic DNA at each dilution.

Initial attempts at construction of the library were not met with success. Many different methods were attempted to optimize the approach and obtain a high enough efficiency. *Hpa*II and *Aci*I restrictions were ligated separately with ligations set up to target a range of sizes: 500 bp; 2500 bp and 5000 bp. However the highest efficiency reached was 10^4 CFU/mL, which was insufficient for full coverage (we required at least 10^5 - 10^6 CFU/mL). Transformation efficiency calculation is shown in Appendix D. Transformations were carried out with chemically competent cells prepared freshly using a variety of approaches. However, this did not improve efficiency (data not shown).

Commercially available *E. coli* chemically competent cells were then used, which retained an efficiency of $> 2 \times 10^8$ CFU/mL on purified plasmid DNA. When this did not work, vector and fragments were prepared in bulk and the ligase was heat inactivated following the ligation reaction. Efficiency still did not improve. The *Aci*I and *Hpa*II fragments were then combined into one reaction and T4 ligase was replaced with FastLink DNA ligase. A bulk ligation was then attempted and all reactions pooled together and dried but the efficiency remained low. Fragments were then concentrated using sodium acetate and ethanol (fragments were run on a gel to confirm their presence). A 1:3 vector:insert ratio was then attempted using 1µg of vector. The results revealed that only the 500 bp targeted reaction

gave a 10^4 CFU/mL efficiency, while the 2500 bp and 5000 bp reactions resulted in negligible efficiencies (< 10 CFU/mL), as fewer colonies were observed than the background for the above-mentioned reactions. This was attributed to the large size of the fragments in latter ligations. Thus, a 1:3 ratio was followed for the 500 bp and 1:1 for the 2500 bp and 5000 bp targeted reactions. Whilst the efficiencies improved, they remained at 10^3 - 10^4 CFU/mL. The ligations were then repeated, but this time using fragments in the range of 500-3000 bp with ligations targeted to 1000 bp and 3000 bp in a 1:1 ratio. The efficiency remained at 10^4 CFU/mL. Takara ligase was then used and electroporation was carried out instead of chemical transformation. Initially the reactions sparked, thus dialysis (to remove salts) was carried out on all ligation reactions prior to electroporations using 2 day old electro-competent cells. All ligations were carried out with fragments previously obtained. This resulted in an efficiency of 10^5 CFU/mL, a 10 fold increase to previous reactions. To increase the yield of fragments used for the ligation, digested fragments were isolated with agarase instead of spin columns following gel extractions. Reactions were run on a 0.7 % low melting agarose gel, the desired sizes were cut out and agarase was used to purify the fragments. The resulting concentrations of fragments were much higher than the spin column. A ligation was again attempted. This was also unsuccessful. A few more attempts were made to obtain fragments using low melting gels and ligation reactions as previously described, with no improvement in the result.

Following these unsuccessful attempts, the library construction was carried out in Dr Adrie Steyn's lab (K|RITH), by Ms Rukaya Asmal who spent 6 weeks at K|RITH to construct libraries. In this case, dilutions of restriction digests were set up as previously described; the appropriate reactions (i.e. in the correct fragment size range) were taken forward by sodium acetate precipitation of fragments, rather than gel extraction. pGADT7 was simultaneously cut with *Cla*I and followed by phosphatase treatment, sodium acetate precipitation and

phosphatase treatment for a second time just before use in ligation reactions. Ligation reactions were set up according to size differences between the vector and average size of insert. A 5.3× concentration difference was used and a reaction was set up using 300 ηg of vector and 60 ηg of insert. This reaction was left overnight, sodium acetate precipitated and resuspended in 5µL of 0.5 × TE buffer, of which 1µL was used in the electroporation reaction into Lucigen electrocompetent *E. coli* cells (Efficiency > 2×10^{10} CFU/mL). This yielded a transformation efficiency of 2.4×10^{5} CFU/mL. Further repeats yielded several libraries with efficiencies of 10^{6} CFU/ mL. A total of 11 separate libraries were made and pooled.

From random libraries, 10 colonies were picked, miniprepped and digested using *Hin*DIII to determine whether an insert/fragment was present.

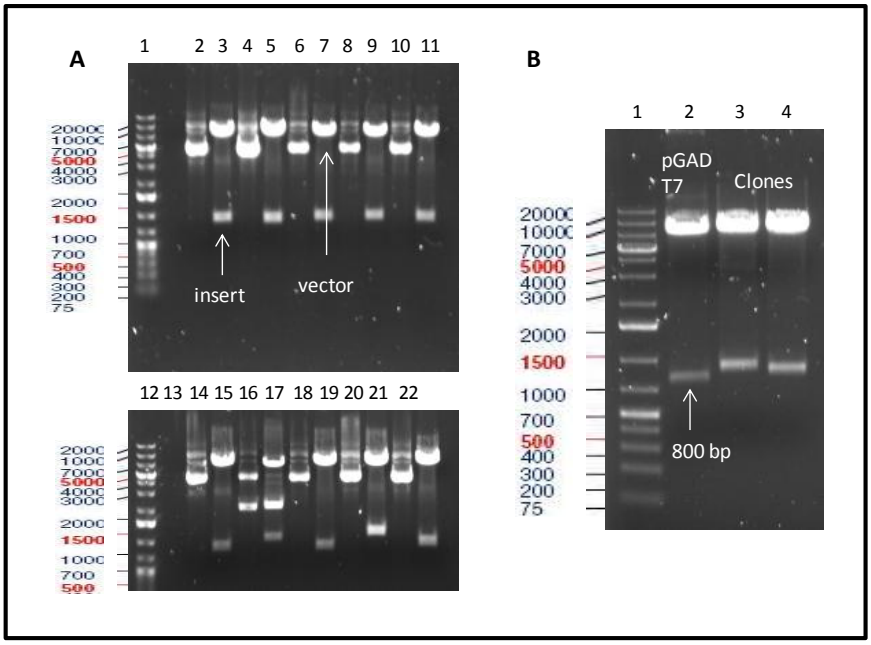


Figure 3.4. Agarose gel of *Hin*DIII digestion of miniprepped clones. **(A)** *Hin*DIII digestion of clones **[Lanes 1, 12]** 1kb generuler; **[Lanes 2, 4, 6, 8, 10, 13, 15, 17, 19, 21]** uncut clones 1-10; **[Lanes 3, 5, 7, 14, 16, 18, 20, 22]** cut clones 1-10. **(B)** *Hin*DIII digestion of pGADT7 compared to clones **[Lane 1]** 1kb generuler; **[Lane 2]** *Hin*DIII digested pGADT7; **[Lanes 3, 4]** *Hin*DIII digested clones 1 & 2.

Digestion of parental pGADT7 with *Hin*DIII will result in an 800 bp fragment. In those clones in the library with *M. smegmatis* genomic DNA fragments inserted into the vector, the 800 bp fragment will increase in size, proportionately to the size of fragment inserted into the

vector. Results of the digest demonstrated the presence of fragments of varying sizes, all bigger than the internal fragment. Figure 3.4B shows a comparison of pGADT7, without any insert, cut with *Hin*DIII with that of some plasmids from the library, which contained bands that were larger. This analysis confirmed the presence of inserts in the library, which together with the number of clones recovered after transformation provided confirmation of a representative of coverage of the library of *M. smegmatis* (~10^6). Freezer stocks of the libraries were made for use in yeast mating experiments.

3.2. Cloning of DD-CPase-encoding genes into yeast bait vectors

Genes were amplified using Phusion DNA polymerase. The initial PCR reactions contained a high amount of non-specific bands of varying intensities. Hence, a gradient PCR was carried out using an annealing gradient between 60 ºC – 70 ºC, the results of which are shown in Figure 3.5.

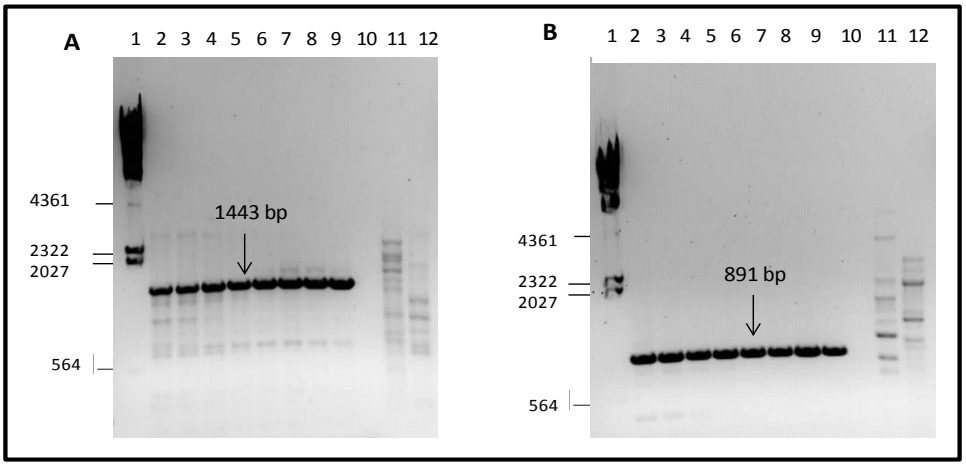


Figure 3.5. Phusion Taq PCR of **(A)** dacB and **(B)** MSMEG_2433 using a temperature gradient. **[Lane 1]** Roche Marker II, **[Lane 2]** 60.0°C, **[Lane 3]** 60.7°C, **[Lane 4]** 61.9°C, **[Lane 5]** 63.7°C, **[Lane 6]** 66.0°C, **[Lane 7]** 68.0°C, **[Lane 8]** 69.2°C, **[Lane 9]** 70.0°C, **[Lane 10]** No template control, **[Lane 11]** Fwd primer only control, **[Lane 12]** Rev primer only control.

All temperatures tested contained the band that corresponded to the correct size for both *dacB*, (1443 bp), and MSMEG_2433 (891 bp), Figure 3.5. However, the 70 ºC reaction was

the cleanest, containing little to no non-specific bands and the resulting fragments were purified by PCR clean up.

3.2.1. Transformation of DD-CPase genes into the yeast bait vector

The bait vector (pGBKT7) was prepared in the same way as pGADT7. All purified products (from PCR) were of the correct sizes and contained no contamination by any other genes, Figure 3.6. The fragments were ligated and transformed and resulting transformants were screened for the correct insert band. One clone of each gene was then chosen and further analyzed by restriction mapping to confirm the genetic integrity of the clone, as demonstrated in Figures 3.7 and 3.8.

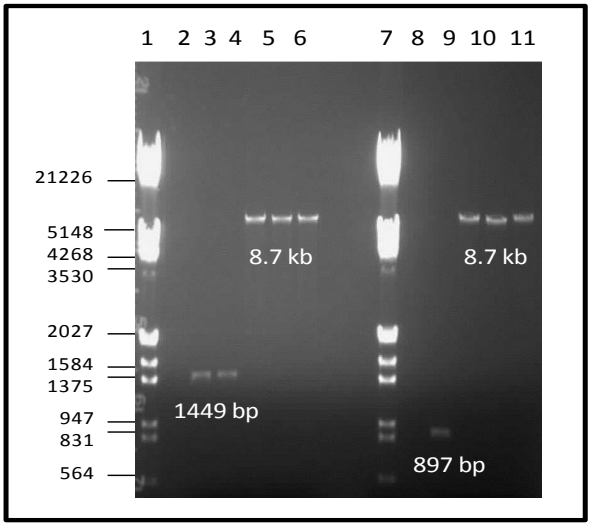
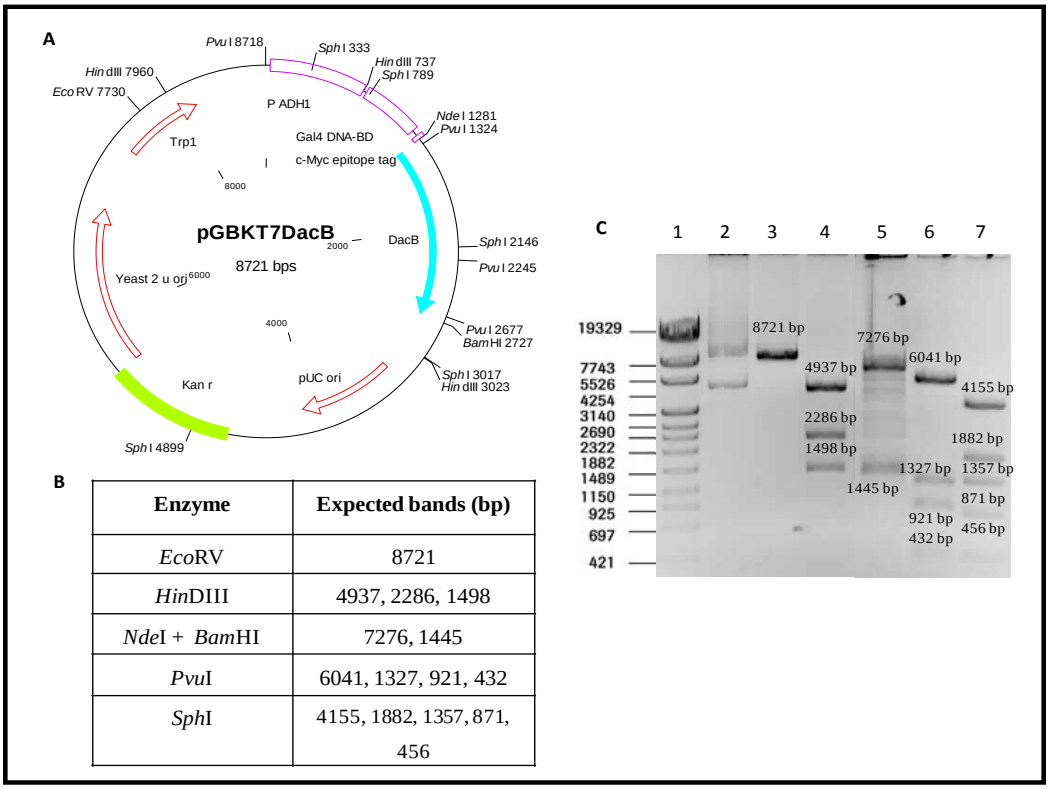


Figure 3.6. Agarose gel of purified products of digested genes and pGBKT7 vector. **[Lanes 1, 7]** Roche Marker III **[Lanes 2, 3]** *dacB*, **[Lanes 4-6]** pGBKT7 restricted with *Nde*I and *Bam*HI, **[Lane 8]** MSMEG_2433, **[Lanes 9-11]** pGBKT7 restricted with *Nde*I and *Pst*I.

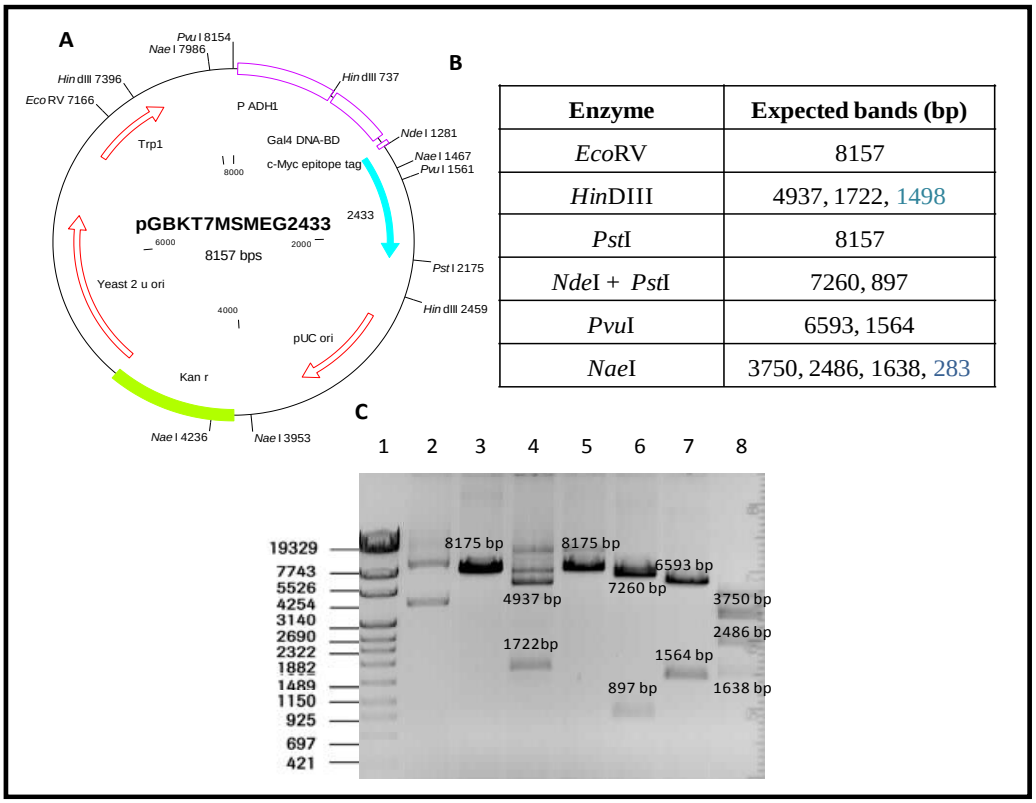


Enzyme	Expected bands (bp)
*Eco*RV	8721
*Hin*DIII	4937, 2286, 1498
*Nde*I + *Bam*HI	7276, 1445
*Pvu*I	6041, 1327, 921, 432
*Sph*I	4155, 1882, 1357, 871, 456

Figure 3.7. Restriction profile of pGBKdacB. **(A)** Plasmid map of *dacB* cloned into yeast vector pGBKT7 (blue arrow). **(B)** Table showing the expected banding profiles of the restriction analysis of the pGBKdacB construct. **(C)** Agarose gel of restriction analysis of pGBKdacB **[Lane 1]** Ladder IV, **[Lane 2]** uncut pGBKT7, **[Lane 3]** *Eco*RV, **[Lane 4]** *Hin*DIII, **[Lane 5]** *Nde*I + *Bam*HI, **[Lane 6]** *Pvu*I, **[Lane 7]** *Sph*I.

The fragments identified during restriction analyses of the clones were consistent with the expected banding patterns. Figures 3.7 and 3.8 shows the various enzymes used with the corresponding bands as expected. In 3.7C, the double digestion with *Nde*I and *Bam*HI displayed extra bands, but this was attributed to the *Bam*HI enzyme being contaminated and once the restriction was repeated with new *Bam*HI, the extra bands disappeared (Appendix F). In Figure 3.8.C there is a single band missing for the *Hin*DIII and *Nae*I digestions, which was attributed to a partial digest in the case of *Hin*DIII. The *Hin*DIII digestion was carried out previously to check the presence of insert though, and this produced the correct banding pattern (Appendix F). The selected clones were also sent for sequencing to Stellenbosch University (Central Analytical Facility – CAF), to further ensure that the genes have been cloned in-frame and there are no mutations from PCR amplification. Sequencing data

confirmed no mutations or deletions (data not shown) confirming the genetic integrity of the clones.



Enzyme	Expected bands (bp)
*Eco*RV	8157
*Hin*DIII	4937, 1722, 1498
*Pst*I	8157
*Nde*I + *Pst*I	7260, 897
*Pvu*I	6593, 1564
*Nae*I	3750, 2486, 1638, 283

Figure 3.8. Restriction profile of pGBK2433. **(A)** Plasmid map of MSMEG_2433 cloned into yeast vector pGBKT7 (blue arrow). **(B)** Table showing the expected banding profiles of the restriction analysis of the pGBK2433 construct. **(C)** Agarose gel of restriction analysis of pGBK2433 **[Lane 1]** Ladder IV, **[Lane 2]** uncut pGBKT7, **[Lane 3]** *Eco*RV, **[Lane 4]** *Hin*DIII, **[Lane 5]** *Pst*I, **[Lane 6]** *Nde*I + *Pst*I, **[Lane 7]** *Pvu*I, **[Lane 8]** *Nae*I.

These clones were then transformed into the yeast strain Y187 as described in section 2.11.2.1 and were taken forward into the yeast system.

3.3. Yeast 2-Hybrid Interactions

3.3.1. Transformation of library into AH109 yeast cells

The library of the multiple electroporations prepared from *E. coli* was combined and sodium acetate precipitated prior to transformation into the yeast AH109 strain. Initially, a large scale transformation was carried out using 15 µg of the library DNA, which produced an efficiency of 10^3-10^4 CFU/mL. This was then up-scaled to a library scale transformation using 0.3 mg

of the library DNA, resulting in an efficiency of 10^6 CFU/mL. This was taken forward into the yeast mating reaction.

3.3.2. DD-CPase autonomous activation

Detection of positive interactions using the Clontech Yeast Two-Hybrid system, which was employed in this study, involved an assessment of growth on various dropout supplemented media that lacked leucine/tryptophan/histidine and adenine, in various combinations. In this system, autonomous activation of the histidine reporter by vectors carrying protein fusions either with the activation or DNA binding domain can lead to the identification of false positive interactions. To prevent this, an inhibitor of autonomous histidine activation, 3-Amino-1,2,4-triazole (3-AT), was added to the plates to reduce the chances of identifying false positive clones. To determine if autonomous histidine activation would occur in our screen, bait vectors were transformed with an empty prey vector and plated on histidine dropout media.

If growth occurs, autonomous activation of the histidine reporter is taking place and the addition of 3-AT is required. For library screening, the concentration of 3-AT to be added was determined by plating yeast strains containing the bait vector only on increasing concentrations of 3-AT to achieve a concentration of 3-AT that gives no growth on histidine with a bait + empty prey vector carrying stain. Hence, vectors carrying bait DD-CPase genes were tested for autonomous activation as described in 2.11.2.2. The pGADT7 vector carries a leucine marker, while the pGBKT7 vector carries a tryptophan marker – these serve as selectable markers for the plasmids. Hence the strains were initially plated on the lowest stringency plates, i.e. lacking one amino acid, in order to select for either pGADT7 (SD/-Leu) or pGBKT7 (SD/-Trp). Thereafter, plating was carried out on higher stringency plates, i.e. lacking two amino acids (SD/-Leu/-Trp) in order to select for clones containing both vectors.

Table 3.1. Growth on SD plates lacking specific amino acids

	SD/-Leu	SD/-Trp	SD/-Leu/-Trp
pGADT7 only	+	-	-
pGBKdacB only	-	+	-
pGBKdacB + pGADT7	+	+	+
pGBK2433 only	-	+	-
pGBK2433 + pGADT7	+	+	+

+ = growth, - = no growth

Results, shown in Table 3.1, revealed that the pGADT7 control only grew on SD/-Leu, while the controls containing no pGADT7 grew only on SD/-Trp. This was expected as these vectors can only grow in the absence of Leu for pGADT7, and Trp for pGBKT7. Transformants containing both vectors would grow on both these plates as both markers would be present, but only vectors which carry interacting partners would grow on higher stringency – Leu/Trp/His and Leu/Trp/His/Ade media. Two colonies of each of the bait – empty vector combinations on the SD/-Leu/-Trp were picked and plated as described in section 2.11.2.2.

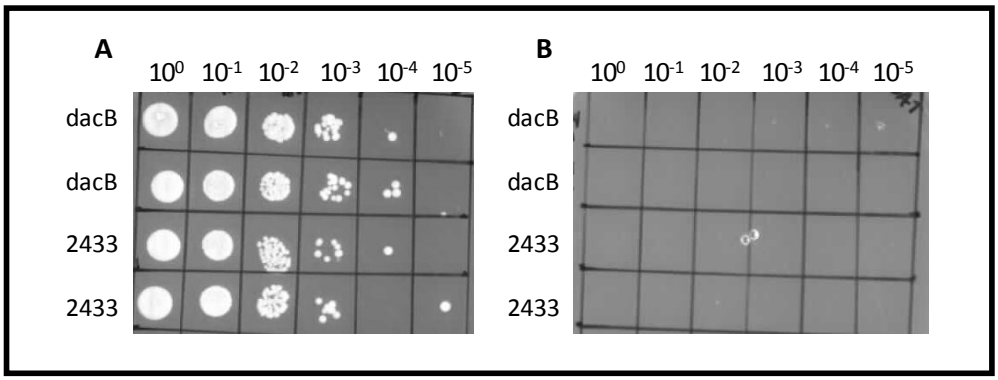


Figure 3.9. Spotting of DD-CPase transformants testing for autoactivation. **(A)** Serial dilutions of pGBK2433 + pGADT7 and pGBKdacB + pGADT7 on **SD/-Leu/-Trp**. **(B)** Serial dilutions of pGBK2433 + pGADT7 and pGBKdacB + pGADT7 on **SD/-Leu/-Trp/-His with no (0 mM) 3AT**.

Results showed growth on SD/-Leu/-Trp plates and no growth on SD/-Leu/-Trp/-His plates, Figure 3.9. Hence, autonomous activation of the His marker was not occurring with either of the clones and 3AT supplementation was not required for our screen.

3.3.3. Yeast Mating

Mating was carried out according to the manufacturer's protocol for the Matchmaker™ Gold Yeast 2-Hybrid system. Cells were counted using a hemocytometer. Bait was used at a cell density of approximately 2×10^8 CFU and prey (library) at approximately 3×10^7 CFU. Zygote formation was checked using 40 × magnification on the light microscope (Appendix D).

Initial mating efficiencies were approximately 0.5 %. The optimum efficiency according to the Matchmaker Gold Yeast Two Hybrid System User Manual, 2012, was 5 %. After numerous attempts and trouble shooting, mating efficiencies increased to 1 % (calculations in Appendix D), these conditions were used for screening. Once plated, a total of 100 and 160 putative interacting colonies were identified for *dacB* and MSMEG_2433, respectively, on SD/-Leu/-Trp/-His/-Ade. These were picked and replica plated in order to rule out false positives, shown in Figure 3.10.

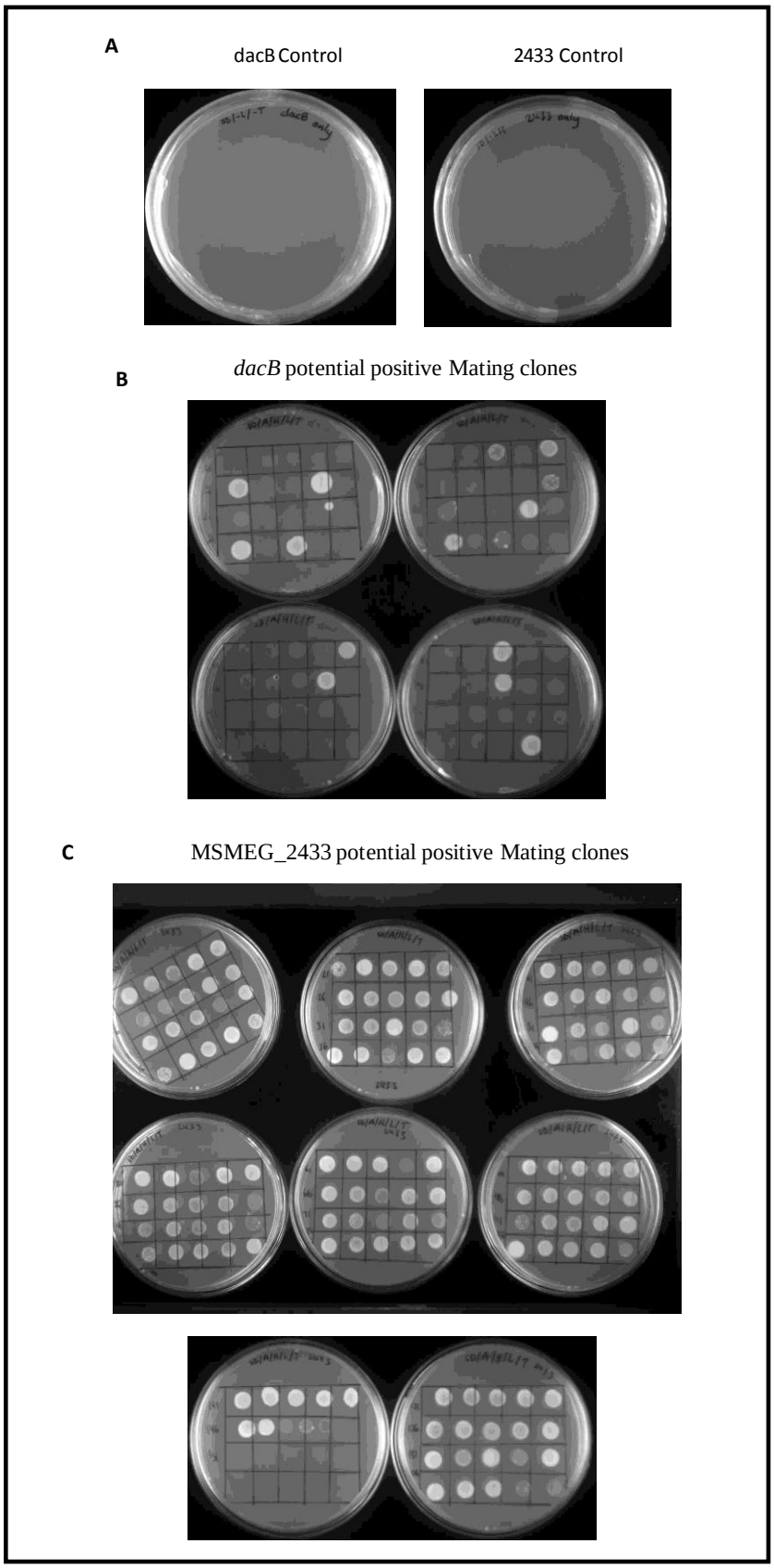


Figure 3.10. Mating clones. **(A)** Control reactions plated on SD/-Leu/-Trp. **(B)** *dacB* mating clones plated on SD/-Leu/-Trp/-His/-Ade. **(C)** MSMEG_2433 mating clones plated on SD/-Leu/-Trp/-His/-Ade.

X-α-Gal is included as a further indication of possible positive interactions. It works as a chromogenic substrate for α-galactosidase produced by some yeast strains and encoded by the *mel1* gene in *S. cerevisiae* (Aho et al., 1997) Colonies which were blue on SD/-Leu/-Trp/-His/X-α-Gal and displayed growth on SD/-Leu/-Trp/-His/-Ade, shown in Figure 3.10, were then picked, the cell density adjusted to OD_{600} = 1 and 10 ul spotted on plates to reconfirm the result. The controls, the bait only, contained no colonies, Figure 3.10.A.

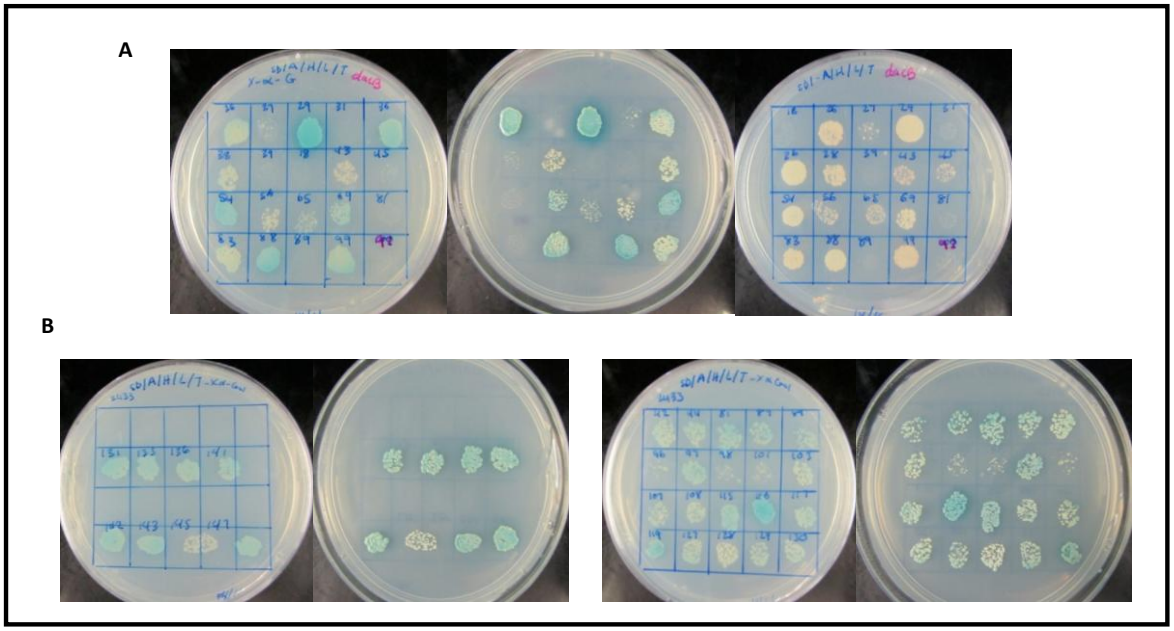


Figure 3.11. Potential positive mating clones. **(A)** *dacB* mating clones plated on SD/-Leu/-Trp/-His/-Ade/X-α-Gal. **(B)** MSMEG_2433 mating clones plated on SD/-Leu/-Trp/-His/-Ade/X-α-Gal.

The results of this analysis revealed that 10 of the putative clones for *dacB* grew and remained blue, Figure 3.11A, and 24 of the putative clones for MSMEG_2433 remained blue, Figure 3.11B. The above-mentioned clones were taken forward by streaking each to single colonies and a blue colony of each was propagated, the plasmid isolated and the insert sequenced to determine the identity of the interacting partner.

3.3.4. DacB and MSMEG_2433 have a number of possible interacting partners

Plasmid isolation from yeast was carried out using the Zyppy™ miniprep kit which produced pure preparations for sequencing (data not shown). A few clones were subsequently digested

with *Hin*DIII prior to sending for sequencing to ensure the presence of the insert. The digests are shown in Figure 3.12.

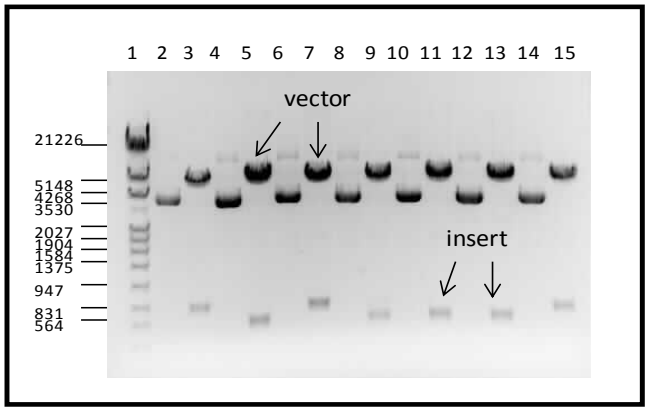
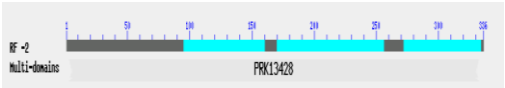
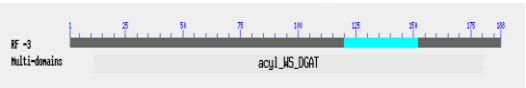
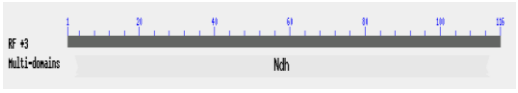
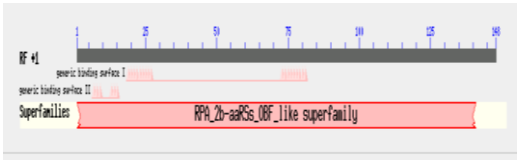
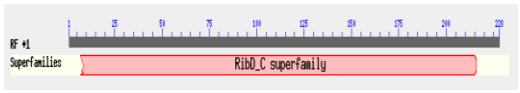
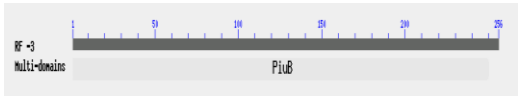
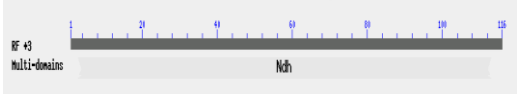


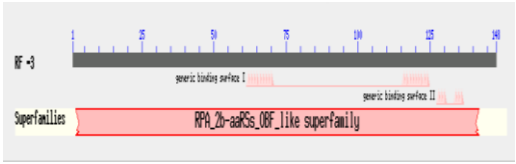
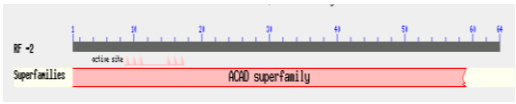
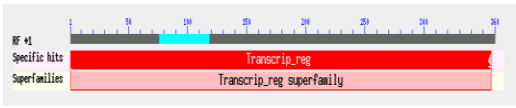
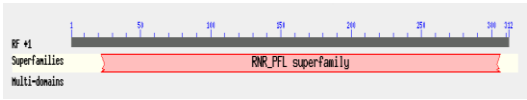
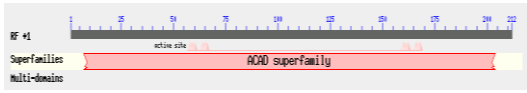
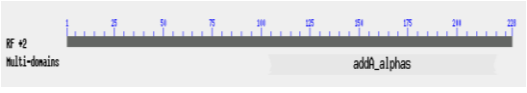
Figure 3.12. Agarose gel of Zyppy plasmid miniprep and *Hin*DIII digestion. **[Lane 1]** Roche marker III, **[Lane 2]** miniprepped dacB_29, **[Lane 3]** *Hin*DIII digested dacB_29, **[Lane 4]** miniprepped dacB_54, **[Lane 5]** *Hin*DIII digested dacB_54, **[Lane 6]** miniprepped *dacB*_38, **[Lane 7]** *Hin*DIII digested *dacB*_38 , **[Lane 8]** miniprepped 2433_127, **[Lane 9]** *Hin*DIII digested 2433_127, **[Lane 10]** miniprepped 2433_116, **[Lane 11]** *Hin*DIII digested 2433_116, **[Lane 12]** miniprepped 2433_135, **[Lane 13]** *Hin*DIII digested 2433_135, **[Lane 14]** miniprepped 2433_115, **[Lane 15]** *Hin*DIII digested 2433_115.

*Hin*DIII digestion confirmed the presence of varying sizes of insert fragments as shown in Figure 3.12, which was quite promising in terms of finding interacting proteins. All the clones selected for plasmid isolation were sent for sequencing using primers specific for the T7 promoter and terminator sequences.

Table 3.2. Sequencing results of potential positive mating clones using Blastx

Clone	Blastx Hits (mc^2155)	Putative conserved Domain
DacB_29	F0F1 ATP synthase subunit delta	PRK13428 
DacB_26	Acyltransferase	
DacB_38	Acyltransferase	Acyl_WS_DGAT 
DacB_83	Acyltransferase	None identified

DacB_54	hypothetical protein MSMEG_0738	None identified
DacB_88	hypothetical protein MSMEG_0738	None identified
DacB_36	Transcriptional regulator, TetR family protein	None identified
DacB_38	NADH dehydrogenase	Ndh 
2433_19	Chain A (single-stranded binding)	
2433_44	bifunctional membrane-associated penicillin-binding protein 1A/1B ponA2 : penicillin-insensitive transglycosylase + penicillin-sensitive transpeptidase	None identified
2433_81	Hypothetical protein MSMEG_6786	RibD_C 
2433_96	HAD-superfamily hydrolase subfamily IA, variant 3:Beta-phosphoglucomutase hydrolase	PRK 
2433_97	Integral membrane protein	PiuB 
2433_103	GntR family transcriptional regulator	None identified
2433_107	beta-lactamase	None identified
2433_115	NADH dehydrogenase	Ndh 

2433_116	Chain A (single-stranded binding)	
2433_117	acyl-CoA dehydrogenase	ACAD Superfamily 
2433_127	hypothetical protein MSMEG_2940	Transcriptional Regulator 
2433_129	Transcriptional regulator	TetR 
2433_130	bifunctional membrane-associated penicillin-binding protein 1A/1B ponA2 : penicillin-insensitive transglycosylase + penicillin-sensitive transpeptidase	None identified
2433_135	Ribonucleotide-diphosphate reductase subunit alpha	
2433_136	acyl-CoA dehydrogenase	ACAD Superfamily 
2433_147	UvrD/REP helicase	addA_alphas 

The resulting sequencing data was analyzed using NCBI BLASTn to obtain the mycobacterial specific sequences, which were then run through NCBI BLASTx to determine the corresponding protein in order to identify the putative interacting proteins. The hits shown in Table 3.2 are those which produced 100 % identity in BLASTx. DacB was shown to

potentially interact with an acyltransferase and both DacB and MSMEG_2433 seem to interact with a common Tet regulator, which points to the possibility that both genes are under coordinated regulation. The acyltransferase could point to a DacB playing a more direct role in cross linking of the PG.

MSMEG_2433-interacting proteins include a number of proteins involved in DNA replication such as helicases and ss-DNA binding proteins. This could point to a role for MSMEG_2433 in co-ordinating initiation of DNA replication and cell division. The most interesting hit was a PBP, specifically PonA2, which could point to the formation of a complex as PBP1 (PonA1) has been demonstrated to interact with and antagonistically affect the synergistic RpfB and RipA interaction (Hett et al, 2008; Hett et al, 2010). The most promising hits were then taken forward for further confirmation.

3.3.5. Confirmation of interaction in putative clones isolated from yeast mating

Confirmation was carried out as described in section 2.11.7. Initially, confirmation was carried on all potential positive interactions but due to the increased workload of multiple plating, we decided to focus on the PBP1A/1B hit only for further confirmation, since this protein is a PG synthetic protein. Confirmation studies in this case revealed reduced growth in low, as well as high stringency plates. Very few colonies were obtained from numerous experiments, Figure 3.13. This did not improve and precluded further confirmation of the PonA2 hit. Other putative interacting partners identified in this study await further confirmation.

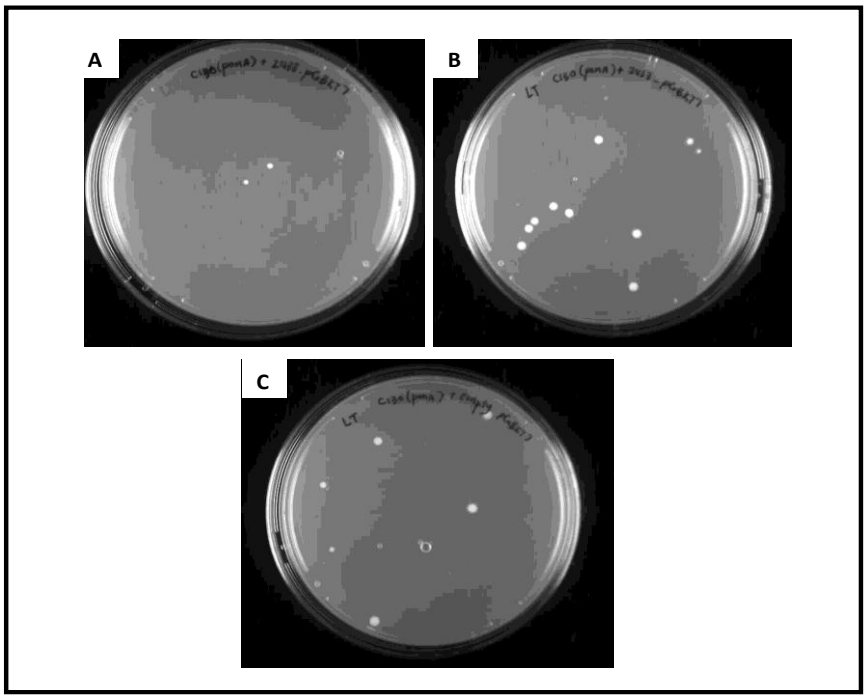


Figure 3.13. Plates of confirmation reaction of clone 2433_130. **(A)** 2433_130 + pGBKT7::MSMEG2433 plated on SD/-Leu/-Trp, **(B)** 2433_130 + pGBKT7::MSMEG2433 plated on SD/-Leu/-Trp/-His, **(C)** 2433_130 + pGBKT7 (empty) plated on SD/-Leu/-Trp.

3.4. Localization of DacB

3.4.1. Cloning of DacB-fluorescent protein fusions using crossover PCR

The crossover (or stitch) PCR strategy that was initially used to obtain a fusion of the DD-CPase gene/s (*dacB* in this case) to the fluorescent proteins is shown in Figure 3.14. The product of this reaction, would subsequently be cloned into pSE100 and localization patterns determined by microscopy. Stitch PCR of *dacB* with the 3 fluorescent genes was attempted. The first step, amplification of the *dacB* gene using PCR, resulted in single, clear bands of the desirable size (data not shown) which were purified for use as the mega-primer in the second step of the stitch PCR. However, during the second step, fusion of *dacB* and fluorescent gene, proved to be problematic. A number of optimization steps were attempted with no success and thus it was decided to try an alternative method.

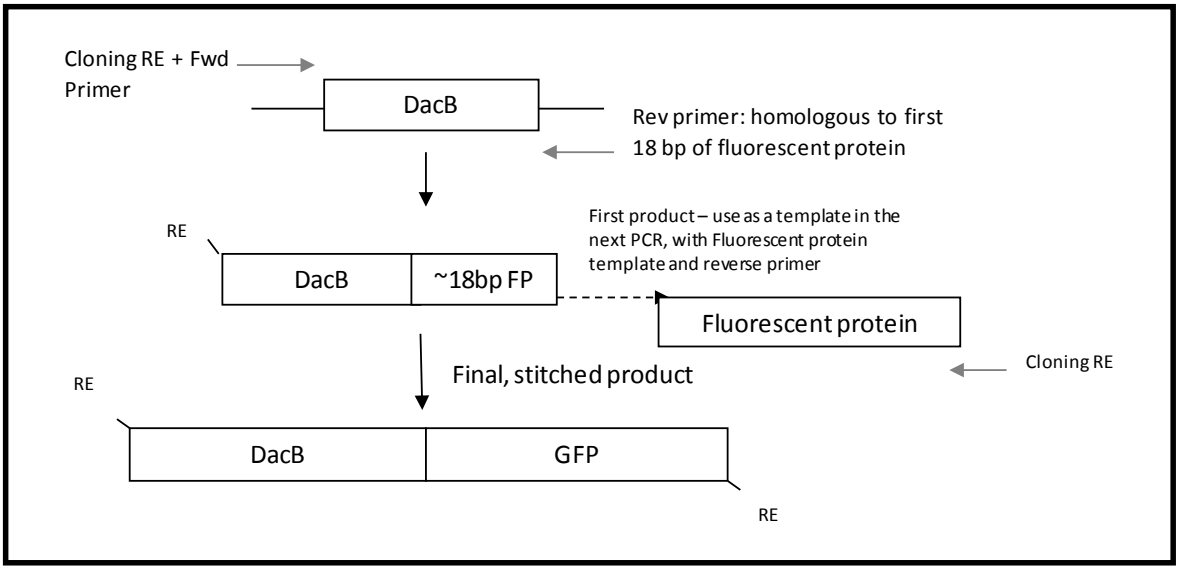


Figure 3.14. Stitch PCR strategy (DacB and GFP). Initially DacB is amplified with the incorporation of a restriction site in the forward primer and the reverse primer containing sequence that is homologous to the first ˜18bp of the GFP gene. This product is then used as a "primer" with another reverse primer and the gene encoding a fluorescent protein as a template (another restriction site is introduced at the C terminus of the GFP). This results in a C-terminal fusion of the DacB to the GFP. Restriction sites are required for subsequent cloning steps

3.4.2. 3-way cloning

This method involved amplifying the DD-CPase gene and fluorescent gene separately and thereafter using a 3 way ligation to clone these genes into the desired vector, in this case pSE100.

3.4.2.1. DacB-mCherry

Using this approach, the *dacB* and *mCherry* genes were successfully amplified (1458 bp for *dacB* and 720 bp for *mCherry*), Figure 3.15. Ligation reactions into pSE100 were successful and 24 test colonies were picked, miniprepped, and double digested using *Pac*I and *Pst*I to check for the presence of the correct insert (*dacB* + *mCherry*). All clones except one were positive (data not shown) and a single clone was then selected and further analysed by extensive restriction mapping, Figure 3.16.

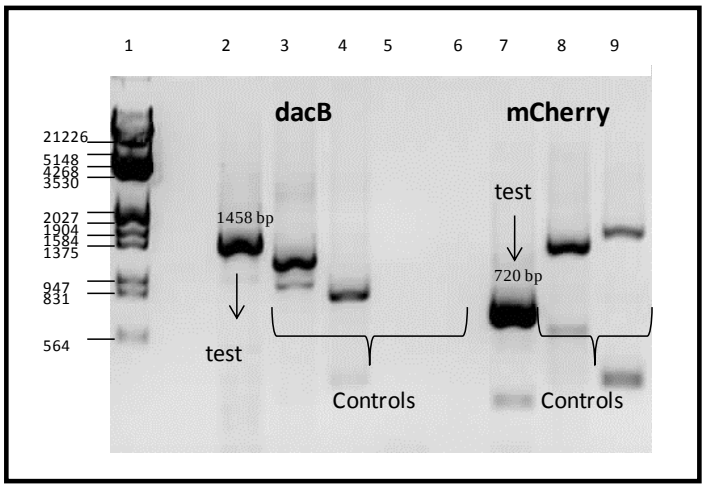
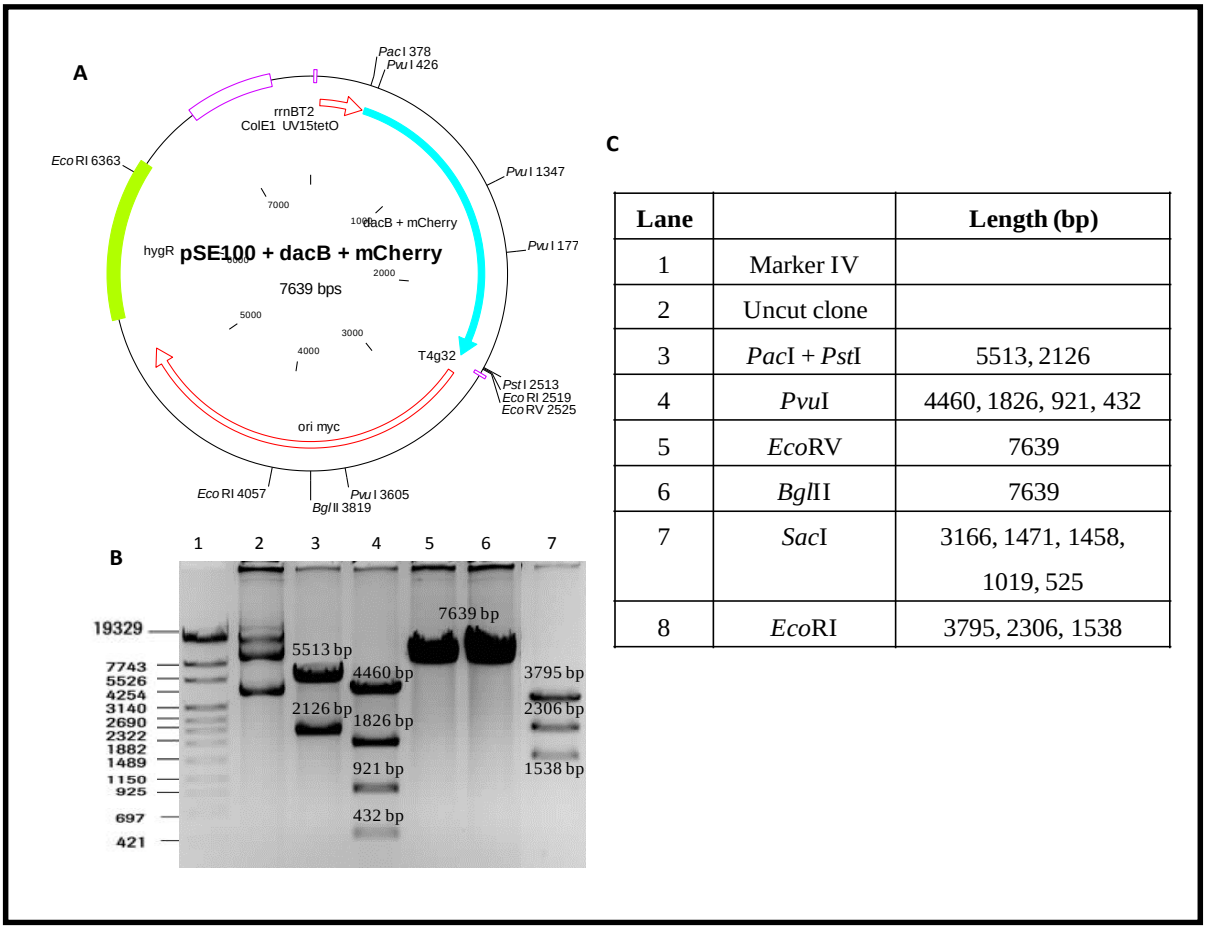


Figure 3.15. Agarose gel of Phusion PCR of dacB and mCherry. **[Lane 1]** Roche Marker III, **[Lane 2]** *dacB* PCR, **[Lane 3]** No *dacB* forward primer control **[Lane 4]** No *dacB* reverse primer control, **[Lane 5]** No DNA control (*dacB*), **[Lane 6]** No DNA control (mCherry), **[Lane 7]** mCherry PCR, **[Lane 8]** No mCherry forward primer control, **[Lane 9]** No mCherry reverse primer control.



Lane		Length (bp)
1	Marker IV	
2	Uncut clone	
3	*Pac*I + *Pst*I	5513, 2126
4	*Pvu*I	4460, 1826, 921, 432
5	*Eco*RV	7639
6	*Bgl*II	7639
7	*Sac*I	3166, 1471, 1458, 1019, 525
8	*Eco*RI	3795, 2306, 1538

Figure 3.16. Restriction profile of dacB and mCherry cloned into pSE100. **(A)** Plasmid map of *dacB* and mCherry cloned into pSE100 (blue arrow). **(B)** Agarose gel of restriction analysis of pSEdacB-mCherry **[Lane 1]** Roche Marker IV, **[Lane 2]** uncut pSEdacB-mCherry, **[Lane 3]** *Pac*I + *Pst*I, **[Lane 4]** *Pvu*I, **[Lane 5]** *Eco*RV, **[Lane 6]** *Bgl*II, **[Lane 7]** *Eco*RI. **(C)** Table showing the expected banding profiles of the restriction analysis of the pSEdacB-mCherry construct.

Restriction mapping analysis of pSEdacB-mCherry, revealed the presence of the correct expected patterns for all enzymes tested, Figure 3.16B. The clone was then sequenced to confirm that PCR amplification did not introduce mutations. Sequence analysis revealed no mutations or deletions and confirmed the fusion junction between *dacB* and *mCherry* (data not shown). Following mapping, clones were electropolated into *M. smegmatis*, a single colony was picked from each test plate, DNA was extracted as per section 2.2.1.2, followed by PCR using *dacB* forward primer and *mCherry* reverse primer to ensure the cell contains the vector with the insert. PCR resulted in the expected band of 2126 bp (Appendix E). This clone was taken forward to determine localization pattern of DacB by microscopy.

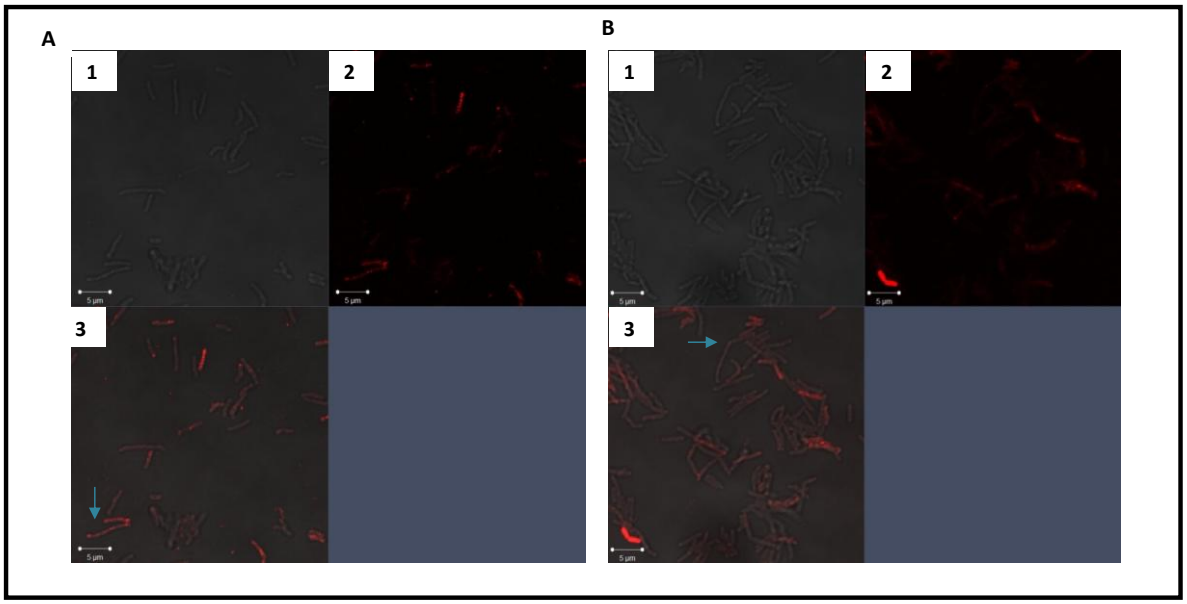


Figure 3.17. Confocal microscopy of pSEdacB-mCherry construct. **(A)** and **(B)** pSEdacB-mCherry construct. **[1]** DIC, **[2]** mCherry, **[3]** Merged channels. Blue arrows indicate diffused localization. Scale bar: 5µm for all images.

Fluorescence microscopy to detect mCherry, with Differential Interference Contrast (DIC) to identify cells, revealed dispersed localization of the DacB-mCherry fusion, without any specific localization patterns, Figure 3.17. Analyses with different preparation of cells yielded the same result. The lack of any observable localization patterns may be due to folding problems with the fusion protein (Stiel et al., 2008, Lukyanov et al., 2005). Analysis using

the SignalP algorithm indicates that DacB has a signal sequence (Ealand and Kana, unpublished) suggesting that it is transported to the periplasmic compartment. In this case, the folding and processing of the fusion protein in the periplasm may be affected, leading to diffused localization. To further study DacB localization in mycobacteria, we decided to change the fluorescent protein tag on DacB and opted to use the Venus fluorescent protein.

3.4.2.2. DacB-Venus

A fusion of DacB to the Venus fluorescent protein was obtained by three-way cloning of the genes generated through PCR. PCR amplification of the desired genes was successful, as indicated by presence of the expected band sizes of ~1458 bp for *dacB* and ~710 bp for Venus, Figure 3.18. The controls, including the no DNA controls, were clean and indicated no cross-contamination. The non-specific bands in the forward primer and reverse primer controls in Figure 3.18A were of a much lower intensity than the specific band and were attributed to by-products of mis-priming on wild type genomic DNA. Following three-way ligation, 10 putative colonies were digested with *Pac*I + *Hin*DIII to assess the presence the insert. One positive clone was selected and analysed by extensive restriction mapping, Figure 3.19.

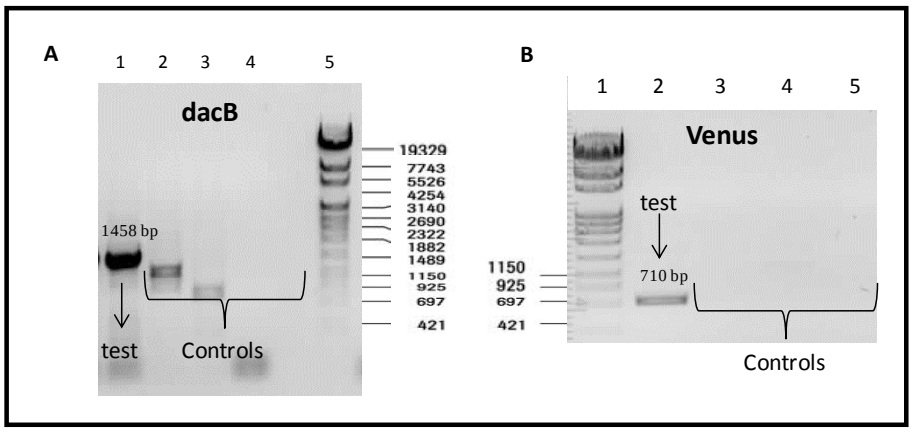
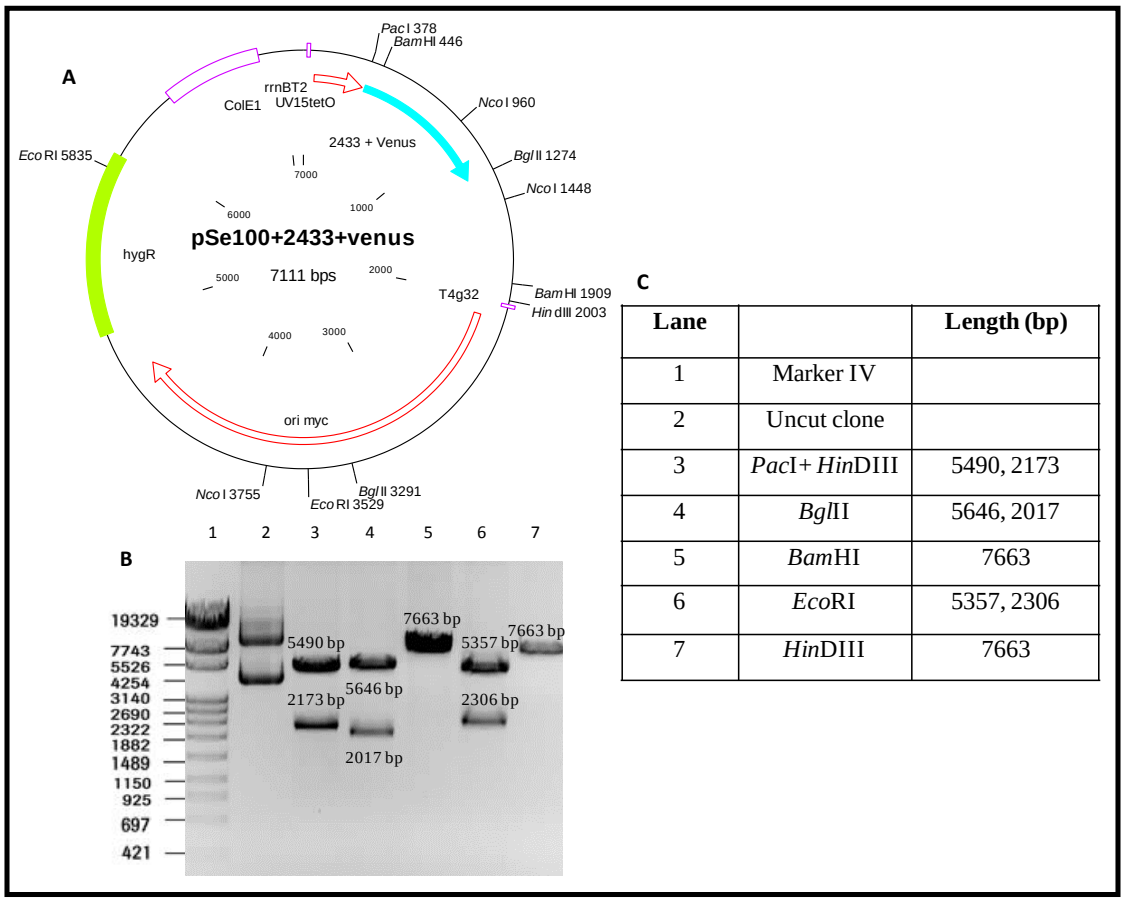


Figure 3.18. Agarose gels of Phusion PCR of dacB and Venus. **(A)** *dacB* phusion PCR **[Lane 1]** *dacB* PCR, **[Lane 2]** No *dacB* forward primer control, **[Lane 3]** No *dacB* reverse primer control, **[Lane 4]** No DNA control (*dacB*), **[Lane 5]** Roche marker IV. **(B)** Venus phusion PCR **[Lane 1]** Roche marker IV, **[Lane 2]** Venus PCR, **[Lane 3]** No Venus forward primer control **[Lane 4]** No Venus reverse primer control, **[Lane 5]** No DNA control (Venus).



C

Lane		Length (bp)
1	Marker IV	
2	Uncut clone	
3	*Pac*I+ *Hin*DIII	5490, 2173
4	*Bgl*II	5646, 2017
5	*Bam*HI	7663
6	*Eco*RI	5357, 2306
7	*Hin*DIII	7663

Figure 3.19. Restriction profile of dacB and Venus cloned into pSE100. **(A)** Plasmid map of *dacB* and Venus cloned into pSE100 (blue arrow). **(B)** Agarose gel of restriction analysis of pSEdacB-Venus **[Lane 1]** Roche Marker IV, **[Lane 2]** uncut pSEdacB-Venus, **[Lane 3]** *Pac*I + *Hin*DIII, **[Lane 4]** *Bgl*II, **[Lane 5]** *Bam*HI, **[Lane 6]** *Eco*RI, **[Lane 7]** *Hin*DIII. **(C)** Table showing the expected banding profiles of the restriction analysis of the pSEdacB-Venus construct.

Restriction analysis of the putative clone revealed the correct banding patterns for all enzymes tested, as shown in Figure 3.19B. This is indicative of the genes being cloned in the correct orientation, in-frame, a result that was confirmed by sequencing, which revealed no mutations or deletions (data not shown). Following mapping, the plasmid was electroplated into *M. smegmatis* and PCR was carried out using *dacB* forward primer and Venus reverse primer to ensure the cell contains the vector with the insert. PCR showed a sharp band of the correct size (2172 bp) (Appendix E). Freezer stocks were made of *M. smegmatis* clones and microscopy was then carried out.

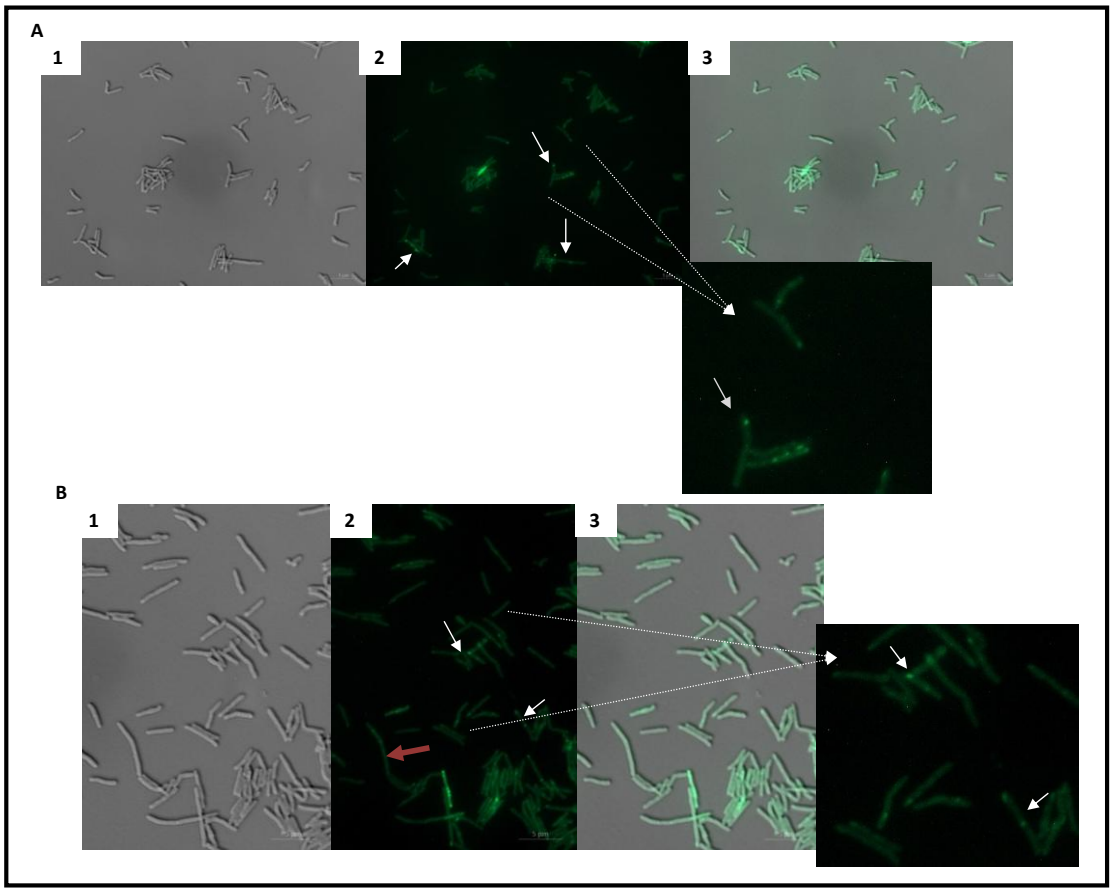


Figure 3.20. Fluorescent microscopy of pSEdacB-Venus construct. **(A)** and **(B)** pSEdacB-Venus construct. **[1]** DIC, **[2]** Fluorescence, **[3]** Merge. Red arrow indicates longer cells, White arrows indicate polar and septal localizations and variations thereof. Dotted arrows lead to zoomed image. Scale bar: 5 µm for (A) and (B), 2 µm for zoomed images.

The results of confocal microscopy to detect the DacB-Venus fusion protein is shown in Figure 3.20. The majority of DacB detected seemed to have dispersed localization along the entire cell. However, there was a minority of the fusion protein that was found in punctate localization either at the pole or along the lateral axis of the cell, Figure 3.20. In some cases, localization of DacB at the septum was also observed. With regards to polar localization, we noted a significant proportion of monopolar, as well as monopolar plus septal localization, with lower occurrences of bipolar, septal only and bipolar with septal localization, Figure 3.20. Venus, with range of 510 – 530 nm, is characterized as a yellow fluorescent protein (YFP) and has the disadvantage of having very low photostability, i.e. it bleaches at a rapid rate. It is approximately 75 % less photostable than other YFPs and thus very few images can

be captured before bleaching occurs (Shaner et al., 2005). This could explain why initially localization patterns were observed (such as a high occurrence of polar localization), but thereafter, only diffused localization was observable. After numerous attempts, the signal from the DacB-Venus fusion protein could not be improved and it was opted to search for a more stable fluorescent protein. In this regard, our collaborator, Dr Musa Mhalanga provided us with a photo-switchable GFP - rsEGFP.

3.4.2.3. DacB-rsEGFP

The fusion of DacB to rsEGFP was done through three-way cloning. PCR amplification of the *dacB* gene yielded a fragment of the correct size, but with a number of non-specific bands. Due to the high concentration of the desired band present, Figure 3.21A, it was possible to gel extract the *dacB* gene. PCR for the *rsEGFP* yielded the desired band and the no DNA controls in both cases were clean, Figure 3.21. Double digests and 3 way ligations were carried out as previously described. Twelve colonies were picked and screened by double digestion using *Hin*DIII and *Bam*HI to check for the presence of the insert (*dacB* and rsEGFP). All colonies were positive clones, with the expected bands of 5508 bp and 2172 bp (data not shown). One clone was then taken forward and analysed by restriction digest, Figure 3.22.

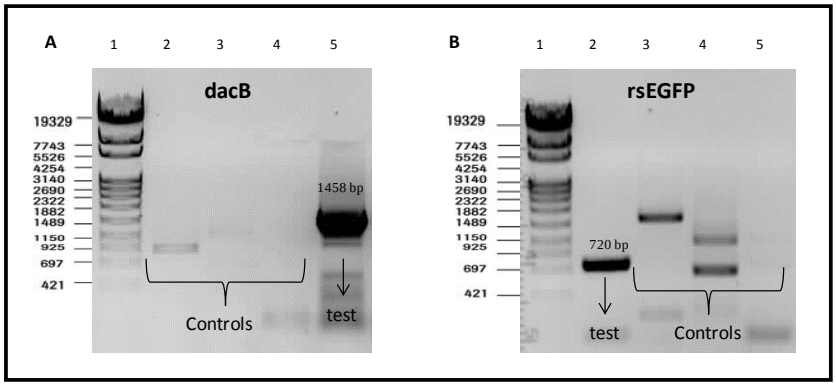
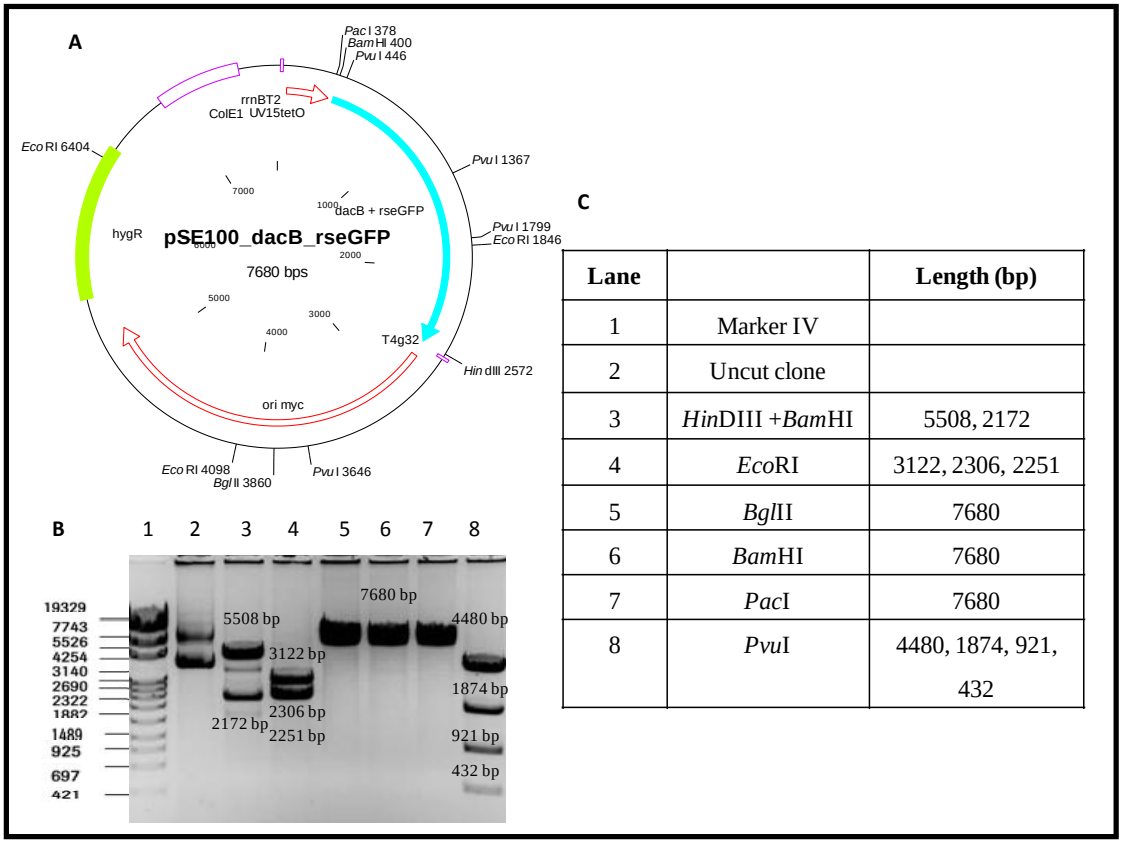


Figure 3.21. Agarose gels of Phusion PCR of *dacB* and *rsEGFP*. **(A)** *dacB* phusion PCR **[Lane 1]** Roche marker IV, **[Lane 2]** No *dacB* forward primer control, **[Lane 3]** No *dacB* reverse primer control, **[Lane 4]** No DNA control (*dacB*), **[Lane 5]** *dacB* PCR. **(B)** *rsEGFP* phusion PCR **[Lane 1]** Roche marker IV, **[Lane 2]** *rsEGFP* PCR, **[Lane 3]** No *rsEGFP* forward primer control **[Lane 4]** No *rsEGFP* reverse primer control, **[Lane 5]** No DNA control (*rsEGFP*).



C

Lane		Length (bp)
1	Marker IV	
2	Uncut clone	
3	*Hin*DIII +*Bam*HI	5508, 2172
4	*Eco*RI	3122, 2306, 2251
5	*Bgl*II	7680
6	*Bam*HI	7680
7	*Pac*I	7680
8	*Pvu*I	4480, 1874, 921, 432

Figure 3.22. Restriction profile of dacB and rsEGFP cloned into pSE100. **(A)** Plasmid map of *dacB* and rsEGFP cloned into pSE100 (blue arrow). **(B)** Agarose gel of restriction analysis of pSEdacB-rsEGFP **[Lane 1]** Roche Marker IV, **[Lane 2]** uncut pSEdacB-rsEGFP, **[Lane 3]** *Hin*DIII + *Bam*HI, **[Lane 4]** *Eco*RI, **[Lane 5]** *Bgl*II, **[Lane 6]** *Bam*HI, **[Lane 7]** *Pac*I, **[Lane 8]** *Pvu*I. **(C)** Table showing the expected banding profiles of the restriction analysis of the pSEdacB-rsEGFP construct.

Restriction analysis of the pSEdacB-rsEGFP construct was indicative of in-frame cloning of the genes since the restriction profiles were all correct, Figure 3.22B. The *Eco*RI restriction seemed to produce two bands instead of three, but this was attributed to the 2306 bp and 2251 bp being of similar size, such that they appear as one band of bright intensity. Sequencing of this construct revealed no mutations or deletions and confirmed in-frame cloning. Electroporation into *M. smegmatis* was carried out, followed by PCR using *dacB* forward primer and *rsEGFP* reverse primer as confirmation for the presence of the correct vector. PCR showed a sharp band of 2172 bp, which was the expected size (data not shown). Microscopy of this strain was carried out simultaneously with the strain including the tetracycline repressor to allow for regulation of expression for the fusion protein. TEM using

the immunogold strategy was also carried out on the strain, which lacked the tetracycline repressor and is expected to over-express the DacB-rsEGFP fusion protein. Immunogold is an antibody based strategy which utilizes rabbit anti-EGFP and gold-labeled goat anti-rabbit as the primary and secondary antibodies, with the primary antibody recognizing GFP/EGFP epitope, and the secondary antibody recognizing the complex of the primary antibody and the epitope, resulting in the ability to view the gold nanoparticles as black spots on TEM, Figure 3.23 (Hainfeld et al., 1991).

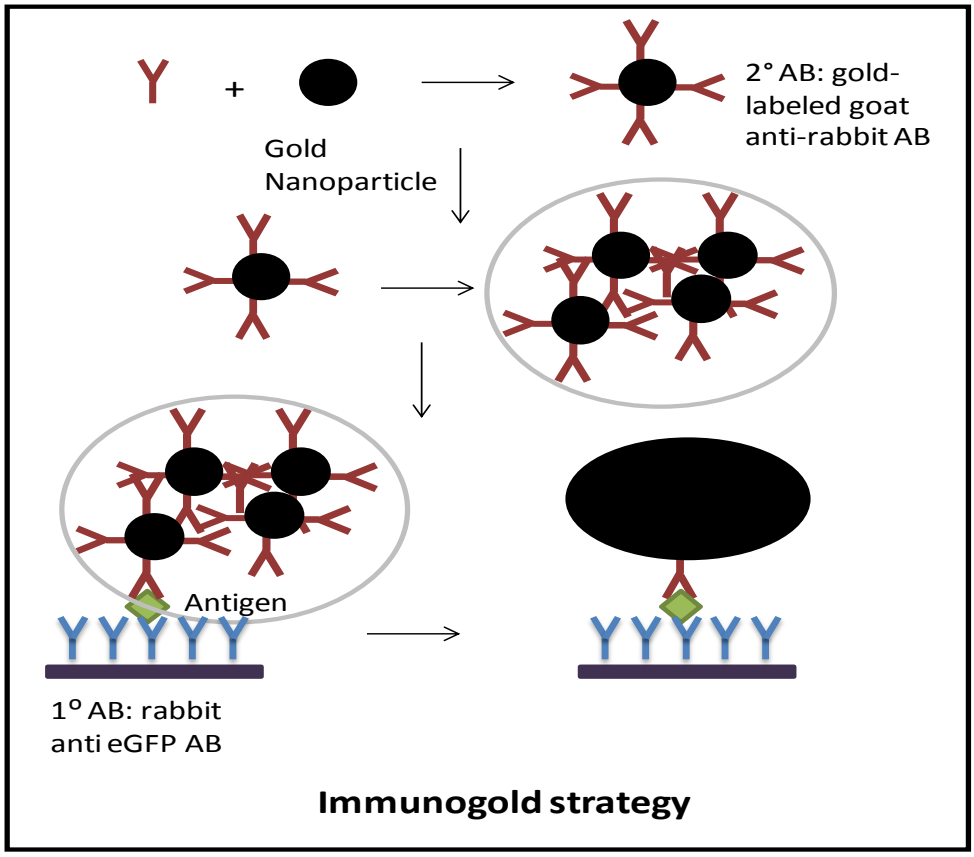


Figure 3.23. Immunogold strategy. The primary antibody with the antigen (eGFP epitope), is recognised by the secondary antibody to which gold nanoparticles are attached. This results in aggregation of the gold particles, which is viewed as black dots during TEM. Adapted from (Hwang et al., 2008)

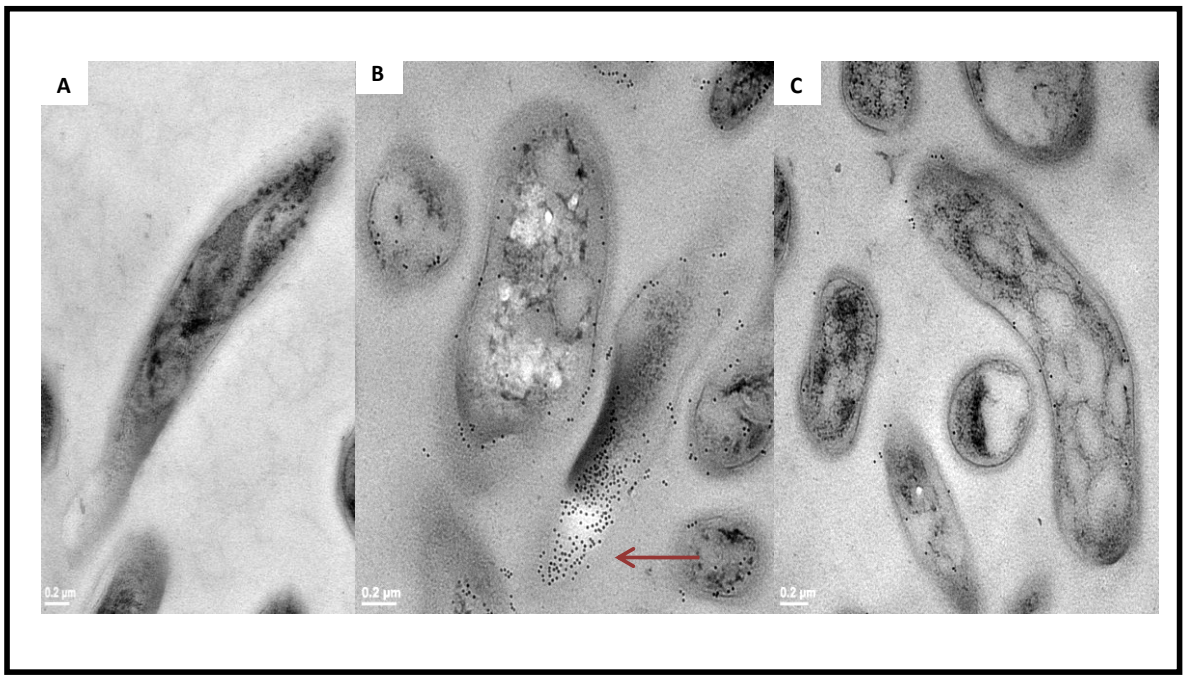


Figure 3.24. TEM of pSEdacB-rseGFP construct using Immunogold. **(A)** Negative control (No 1º AB), **(B)** Construct- 1:100 dilution of 1º AB, **(C)** Construct- 1:500 dilution of 1º AB. Scale bar: 0.2 µm. Black dots indicate positive immunogold localization.

The results of the Immunogold method using an antibody directed to the GFP is shown in Figure 3.24, which revealed that DacB localized along the entire cell wall, however in some cells, protein seemed to concentrate at one pole. Due to the way cells were prepared for TEM, i.e. through embedding in resin, the cells get cut in varying planes either along the lateral axis of the cell or perpendicular to it (these are the cells that display a spherical morphology in Figure 3.24). Thus it is difficult to definitively comment on polarity at a specific site. The only pattern that can be concluded is that *dacB* is present along the entire cell wall and may concentrate at a single pole. The aberrant shapes observed were not due to the over-expression of the gene, but as a result of the immunogold treatment. The structural integrity of the cells were affected when treated with lead citrate, thus any phenotypic changes due to over-expression would not be able to be observed using this methodology.

3.4.3. Growth kinetics and Repression of *dacB*

The localization patterns of *dacB* were further analyzed by the addition of the tetracycline repressor (carried on vector pMC1s) in order to determine whether the localization pattern changes when the gene dosage is reduced. PCR was used to confirm pMC1s integration. The basic principle of this method relies on 2 sets of primers, with one set binding the $tRNA^{glycine}$ flanking locus on the genomic DNA and the other binding the plasmid integration site (AP site) flanking the plasmid DNA (Guo et al., 2007). Hence if amplification occurs, integration was successful and occurred at the correct site. This analysis was only carried out only with the DacB-rsEGFP fusion. The repressor was electroporated into the *M. smegmatis* clone already containing pSEdacB-rsEGFP. Confirmation was performed by PCR.

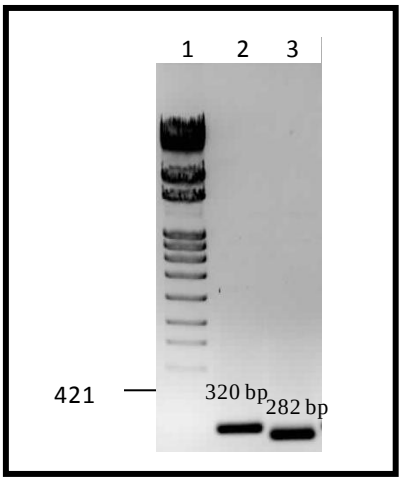


Figure 3.25. PCR screen for integration of pMC1s. **[Lane 1]** Roche Marker IV, **[Lane 2]** *attBS2, attL4* PCR, **[Lane 3]** *attL2, attBS1* PCR.

PCR analysis confirmed that pMC1s integrated in the correct position - at the *attB* site - since both sets of *att* primers amplified the correct amplicons, Figure 3.25. Expression of *dacB* could now theoretically be controlled by the addition of anhydrous tetracycline (AHT). With this method, the addition of AHT will increase gene expression.

3.4.3.1. Altered levels of *dacB* has no effect on growth kinetics of *M. smegmatis*

We hypothesized that introduction of the fusion DacB-rsEGFP protein may affect cell growth since over-expression of PG remodelling enzymes has been known to affect cell wall stability. To test for this, growth was determined by taking OD_{600nm} readings at 6, 9 and 18 hours after inoculation of the pSEdacB-rsEGFP with the repressor (pMC1s) construct alongside *M. smegmatis* mc^2155 (as described in section 2.9.1.). All experiments were set up in triplicate to ensure results were consistent and unbiased. The growth curve did not show any significant differences in growth rates of the strains (data not shown).

3.4.3.2. Regulated expression of the fusion protein.

To determine if addition of AHT would result in an increase in gene expression of the *dacB-rsEGFP* fusion, qPCR was carried out with the repressor and without against wild type *M. smegmatis* mc^2155.

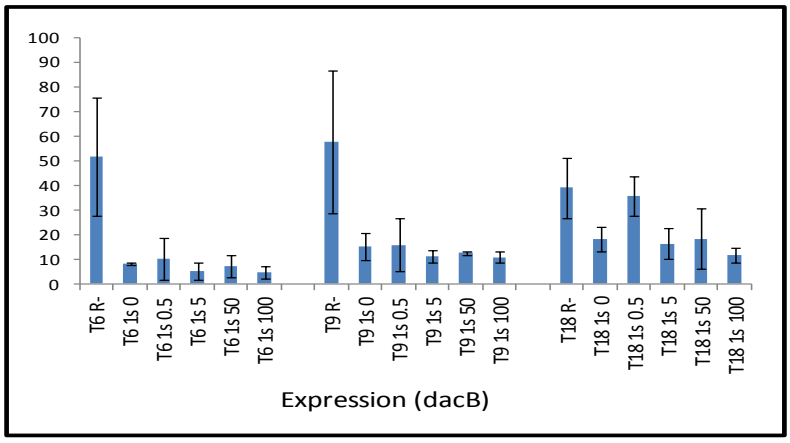


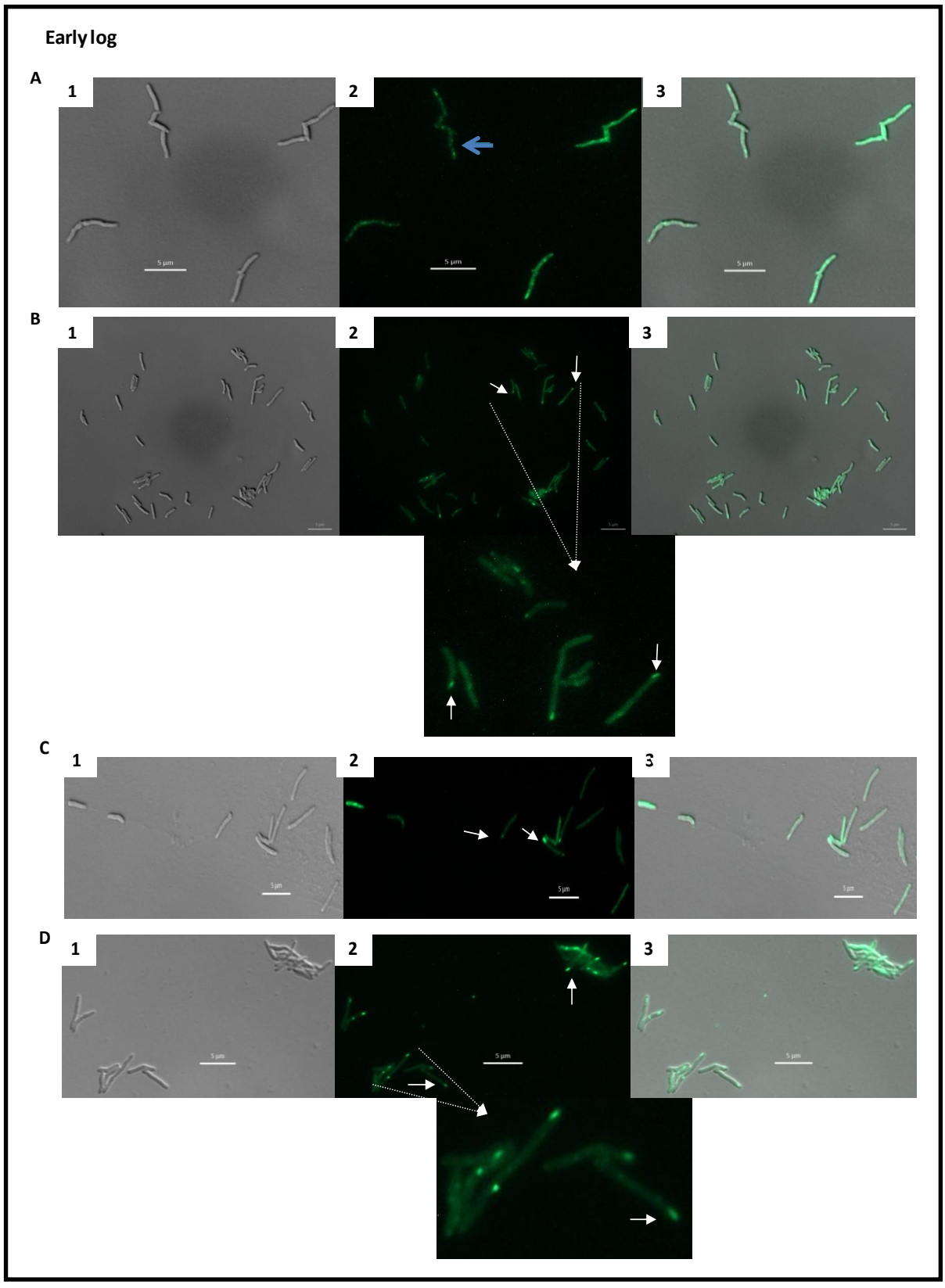
Figure 3.26. Expression data of wild type *M. smegmatis* against the pSEdacB-rsEGFP construct with the pMC1s repressor. Data shown are representative of three independent experiments.

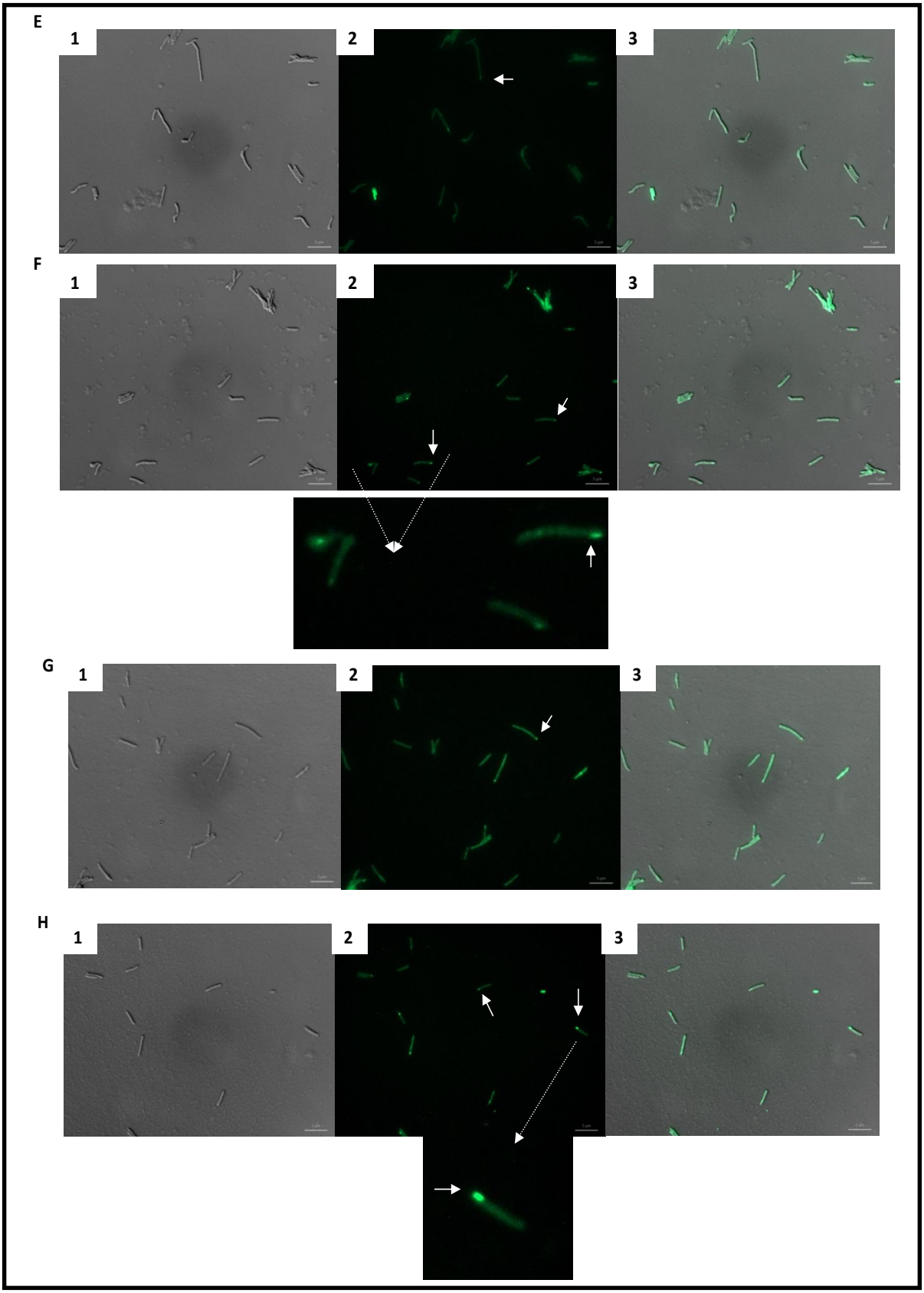
As expected, gene expression in the repressor-less strain was higher than in the strain carrying the repressor, Figure 3.26. All strains were normalized against wild type and plotted. There were no significant differences in expression between the different concentrations of AHT inducer. Considering this, we hypothesized that the inability to control expression could be attributed to the pSE100 that was used as an episomal instead of integrative format, and

thus multiple copies of the gene (and the *tetO* operator) were present and the repressor cannot effectively control the expression of the *dacB* gene, i.e. it partially represses the gene, but not to the level required. Hence under all conditions tested, the DacB fusion protein was over-expressed relative to wild type levels. Despite these limitations, microscopy was carried out at the following time points during a growth curve: (I) 6 hours post inoculation – corresponding to early log phase and (II) 18 hours post inoculation – corresponding to mid – log phage.

3.4.3.3. Over-expression of DacB causes increased monopolar localization

Confocal microscopy at early- and mid- log phase are shown in Figure 3.27 and Figure 3.28, with a graph quantifying the occurrence of the different patterns shown in Figure 3.29. The results showed that most strains contained increased monopolar localization, with the repressor-less strain containing the highest frequency of monopolar localization, Figures 3.27B and C, 3.28B, 3.29. The addition of 50 ηg/mL AHT, in the strain containing the repressor, yielded similar percentages of localization between strains, with the highest percentage still being the monopolar localization. Cells with the repressor seemed to also have a higher percentage of monopolar localization, but also consistent (albeit lower) occurrences of the other patterns, Figures 3.27C-L, 3.28B-H and 3.29. At lower AHT concentrations, a very high number of cells contain dispersed localization, Figures 3.27C-F, 3.28B and 3.28C. At 5 ηg/mL AHT, occurrence of dispersed localization seemed to decrease, Figures 3.27G, 3.27H and 3.28D, and at 50 ηg/mL and 100 ηg/mL, there was a higher occurrence of localization concentrated to specific locations of the cell compared to dispersed fluorescence, Figures 3.27I-L and 3.28E-H. The lack of any significant differences in localization patterns between strains with different levels of AHT inducer is consistent with the expression data viewed in Figure 3.26, where levels of gene expression are similar for these strains.


Early log
A
1
2
3
B
1
2
3
C
1
2
3
D
1
2
3


E
1
2
3
F
1
2
3
G
1
2
3
H
1
2
3

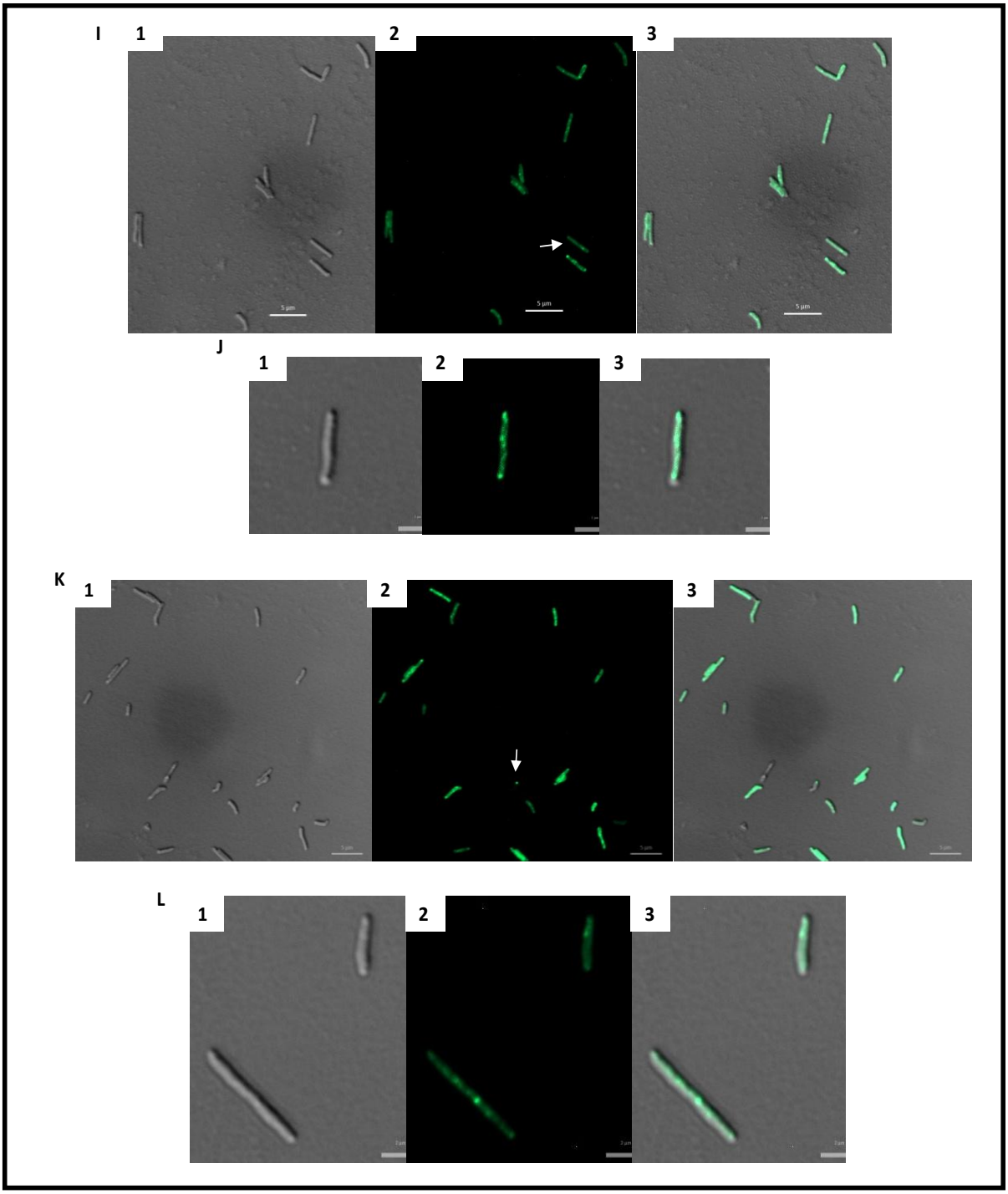
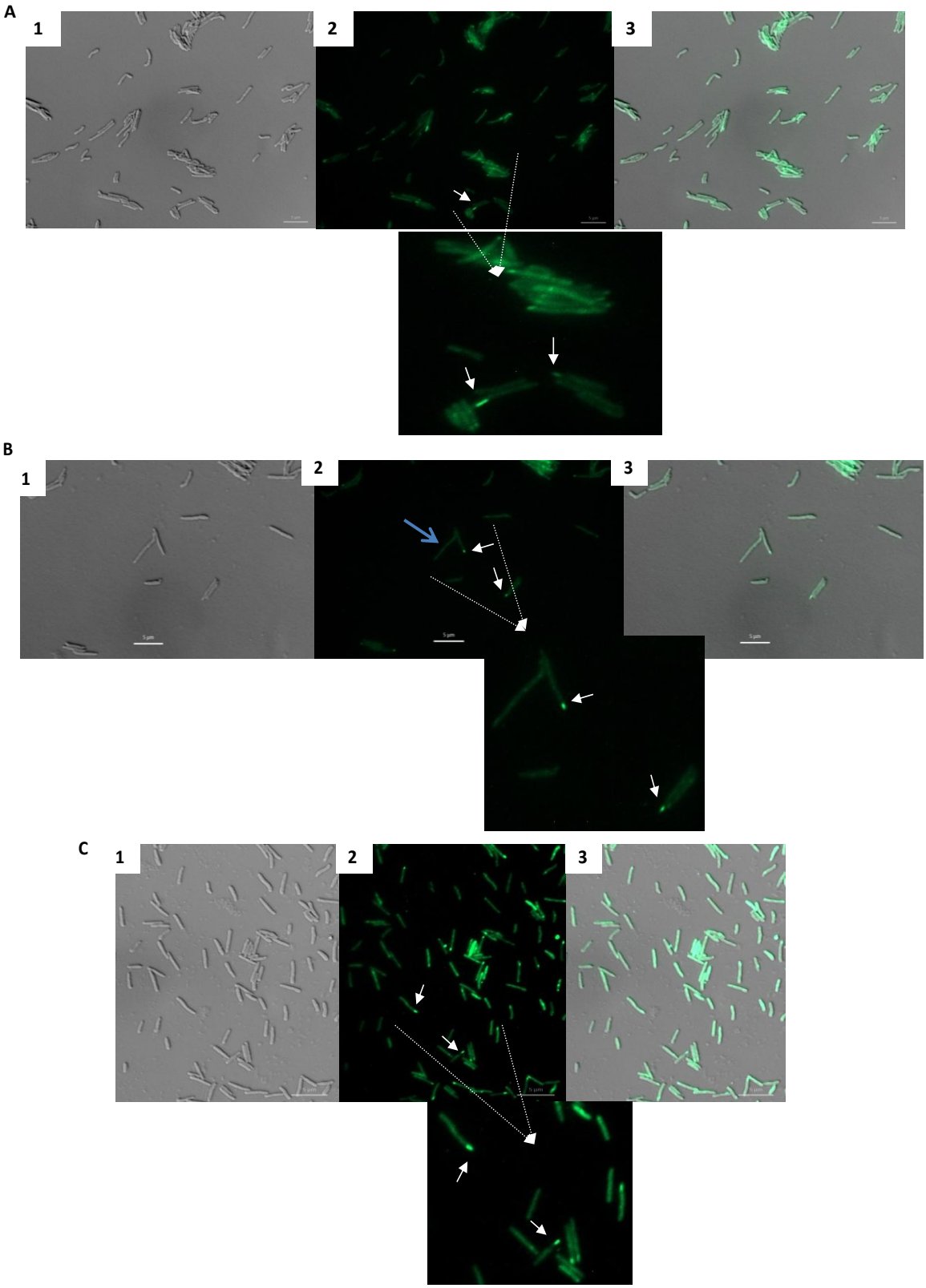


Figure 3.27. Confocal microscopy at early log phase. **(A)** and **(B)** pSEdacB-rseGFP (R-), **(C)** and **(D)** pSEdacB-rsEGFP + pMC1s 0 AHT, **(E)** and **(F)** pSEdacB-rsEGFP + pMC1s 0.5 AHT, **(G)** and **(H)** pSEdacB-rsEGFP + pMC1s 5 AHT, **(I)** and **(J)** pSEdacB-rsEGFP + pMC1s 50 AHT, **(K)** and **(L)** pSEdacB-rsEGFP + pMC1s 100 AHT. **[1]** DIC, **[2]** Fluorescence, **[3]** Merge. Blue arrows indicate punctate localization along the cell, White arrows indicate monopolar localization. Dotted arrows lead to zoomed image. Scales bars: 5 µm for (A) – (I) and (K), and 2 µm for zoomed images, (J) and (L).

Mid log



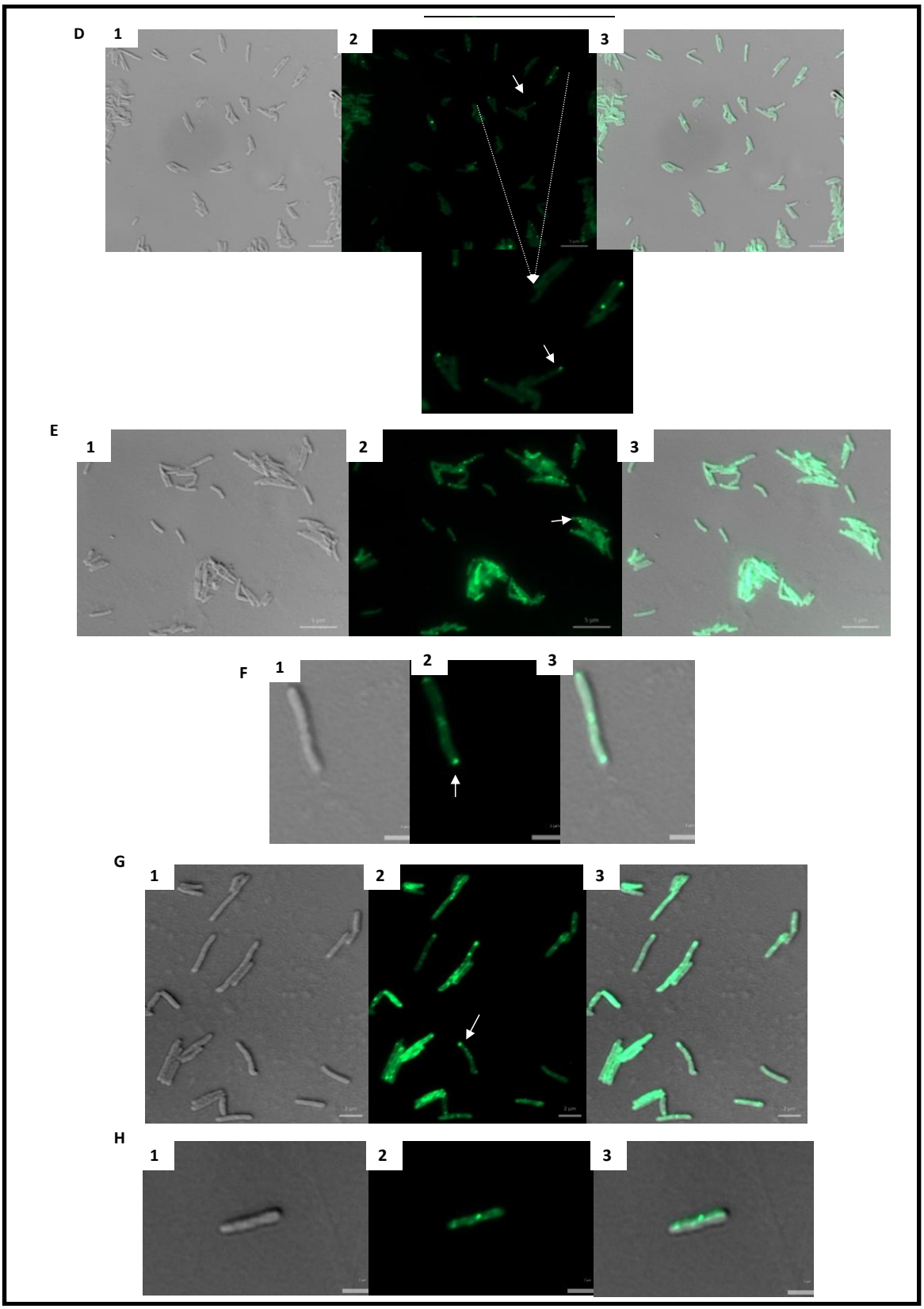


Figure 3.28. Confocal microscopy during mid-log phase of growth. **(A)** pSEdacB-rsEGFP (R-), **(B)** pSEdacB-rsEGFP + pMC1s 0 AHT, **(C)** pSEdacB-rseGFP + pMC1s 0.5 AHT, **(D)** pSEdacB-rsEGFP + pMC1s 5 AHT, **(E)** and **(F)** pSEdacB-rsEGFP + pMC1s 50 AHT, **(G)** and **(H)** pSEdacB-rsEGFP + pMC1s 100 AHT. **[1]** DIC, **[2]** Fluorescence, **[3]** Merge. Blue arrows indicate punctate localization along the cell, White arrows indicate monopolar localization. Dotted arrows lead to zoomed image. Scales bars: 5 µm for (A) – (E) and (G), and 2 µm for zoomed images, (F) and (H).

Cell localization patterns from all microscopy were quantified by counting each type of pattern viewed, results are shown in Fig. 3. 29.

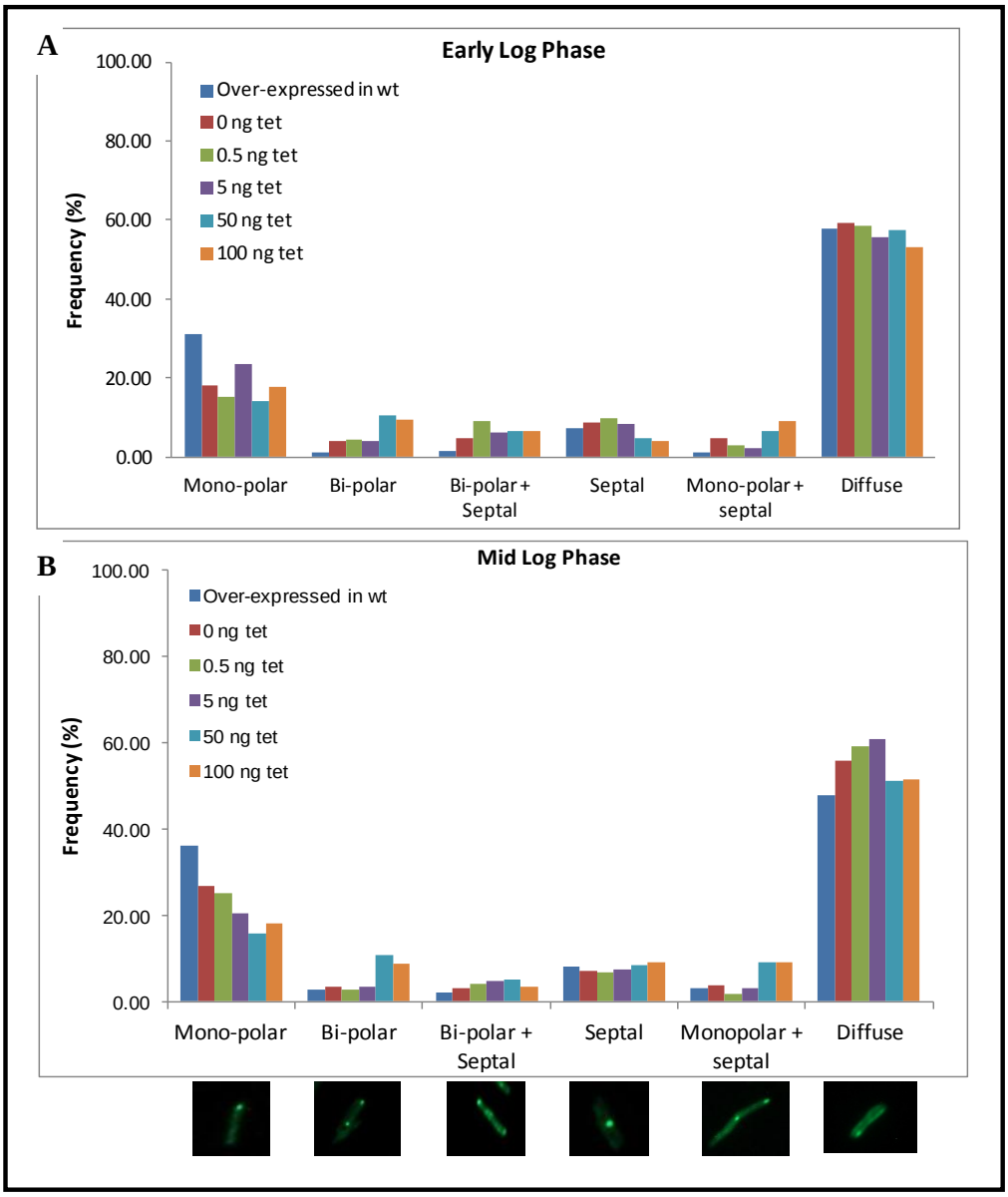


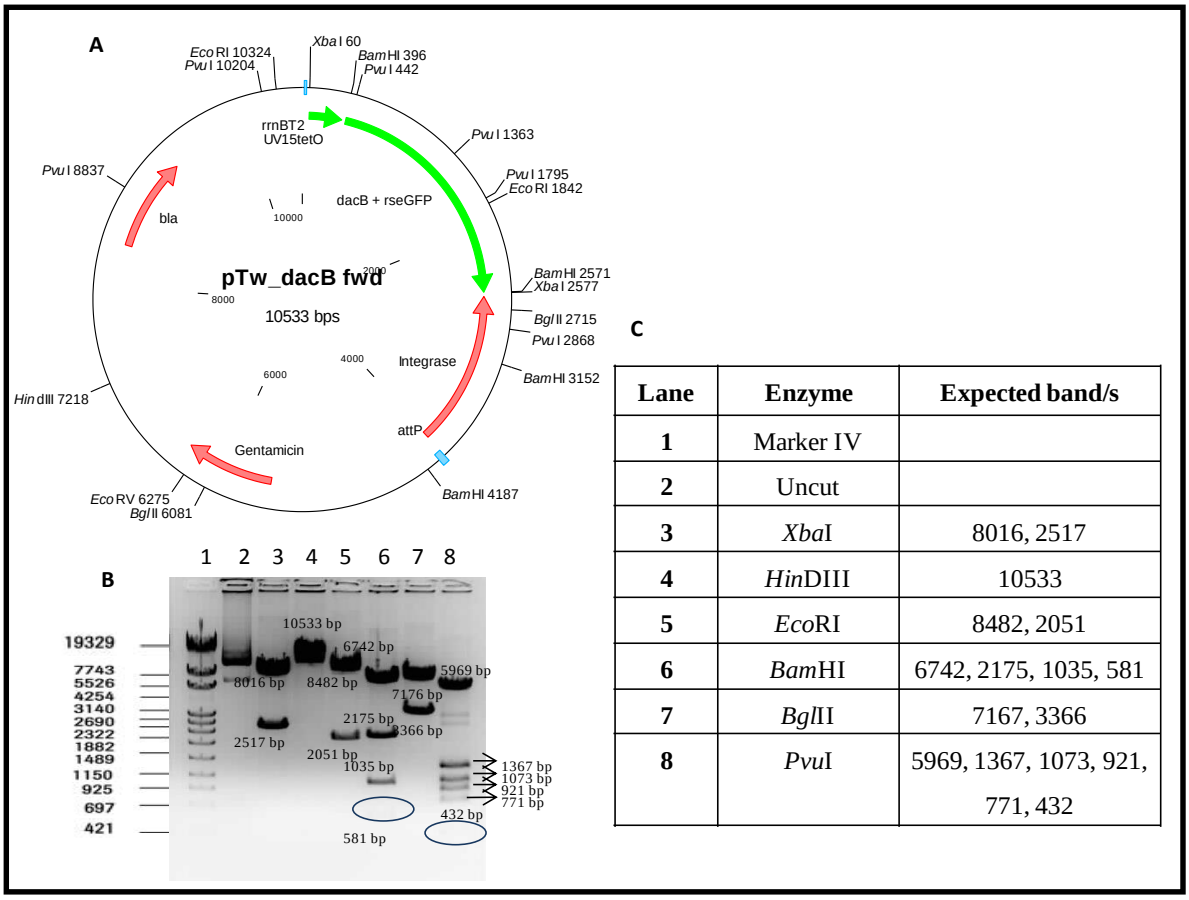
Figure 3.29. Graph of localization patterns observed during microscopy. **(A)** Localization patterns during early log-phase. **(B)** Localization patterns during mid-log phase.

3.4.3.4. Cloning of *dacB-rsEGFP* into integrating vector pTweety

A modified pTweety integrating vector with a gentamycin resistance cassette was created in our lab by Nicole C. Narrandes (unpublished) which was used to clone the *dacB-rsEGFP* gene (including the *tetO*). This vector was integrated at the Tweety site in the mycobacterial genome and the pMC1s vector was integrated at the *attB* site (Pham et al., 2007). We

hypothesized this strategy would reduce the gene dosage for the fusion protein and allow for better regulation of expression of the *dacB* gene.

The cloning was carried out as described in section 2.6.2, where 20 potential clones were digested using *Xba*I. Two orientations of the insert were possible, with expected band sizes of 8016bp and 2517bp or 10269bp and 264bp, respectively. All clones seemed to be in one orientation only (data not shown) and a single clone was chosen for further restriction analysis, Figure 3.30.



Lane	Enzyme	Expected band/s
1	Marker IV	
2	Uncut	
3	*Xba*I	8016, 2517
4	*Hin*DIII	10533
5	*Eco*RI	8482, 2051
6	*Bam*HI	6742, 2175, 1035, 581
7	*Bgl*II	7167, 3366
8	*Pvu*I	5969, 1367, 1073, 921, 771, 432

Figure 3.30. Restriction profile of tetO-*dacB*-rsEGFP cloned into pTweety. **(A)** Plasmid map of tetO-*dacB*-rsEGFP cloned into pTeety (blue arrow). **(B)** Agarose gel of restriction analysis of pTw::dacB-rsEGFP **[Lane 1]** Roche Marker IV, **[Lane 2]** uncut pTw::dacB-rsEGFP, **[Lane 3]** *Xba*I, **[Lane 4]** *Hin*DIII, **[Lane 5]** *Eco*RI, **[Lane 6]** *Bam*HI, **[Lane 7]** *Bgl*II, **[Lane 8]** *Pvu*I. **(C)** Table showing the expected banding profiles of the restriction analysis of the pTw::dacB-rsEGFP construct. Circles indicate the position of the faint bands.

All enzymes used to digest the plasmid yielded the expected banding patterns, Figure 3.30. This is indicative of the insert being cloned correctly into the pTweety vector. In order to control expression, the strain was transformed with pMC1s, as previously described.

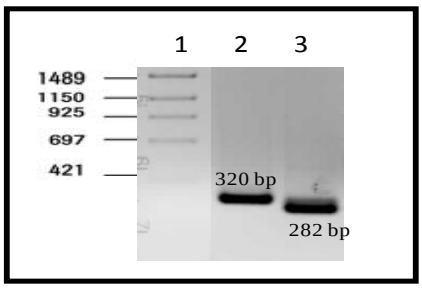
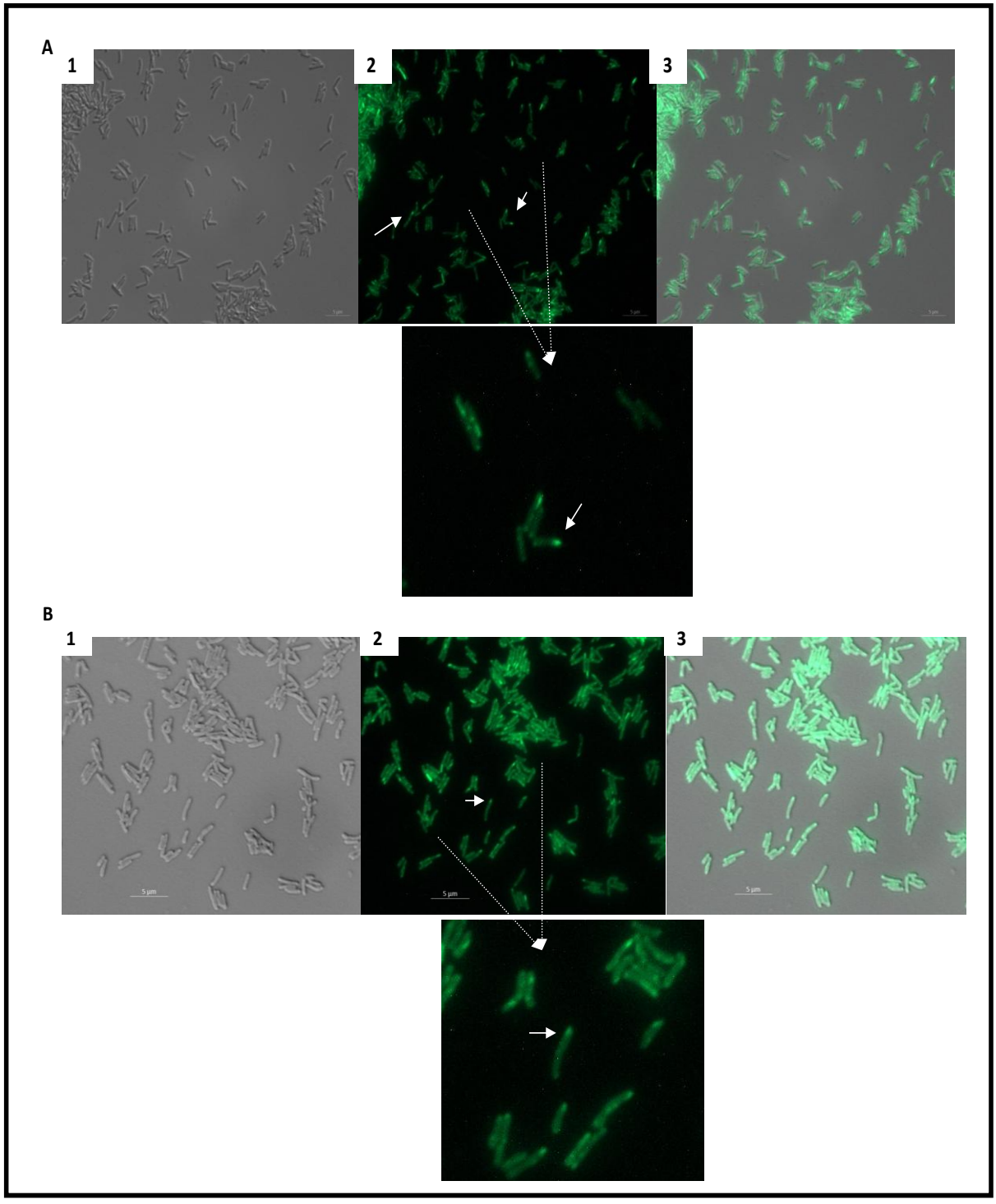
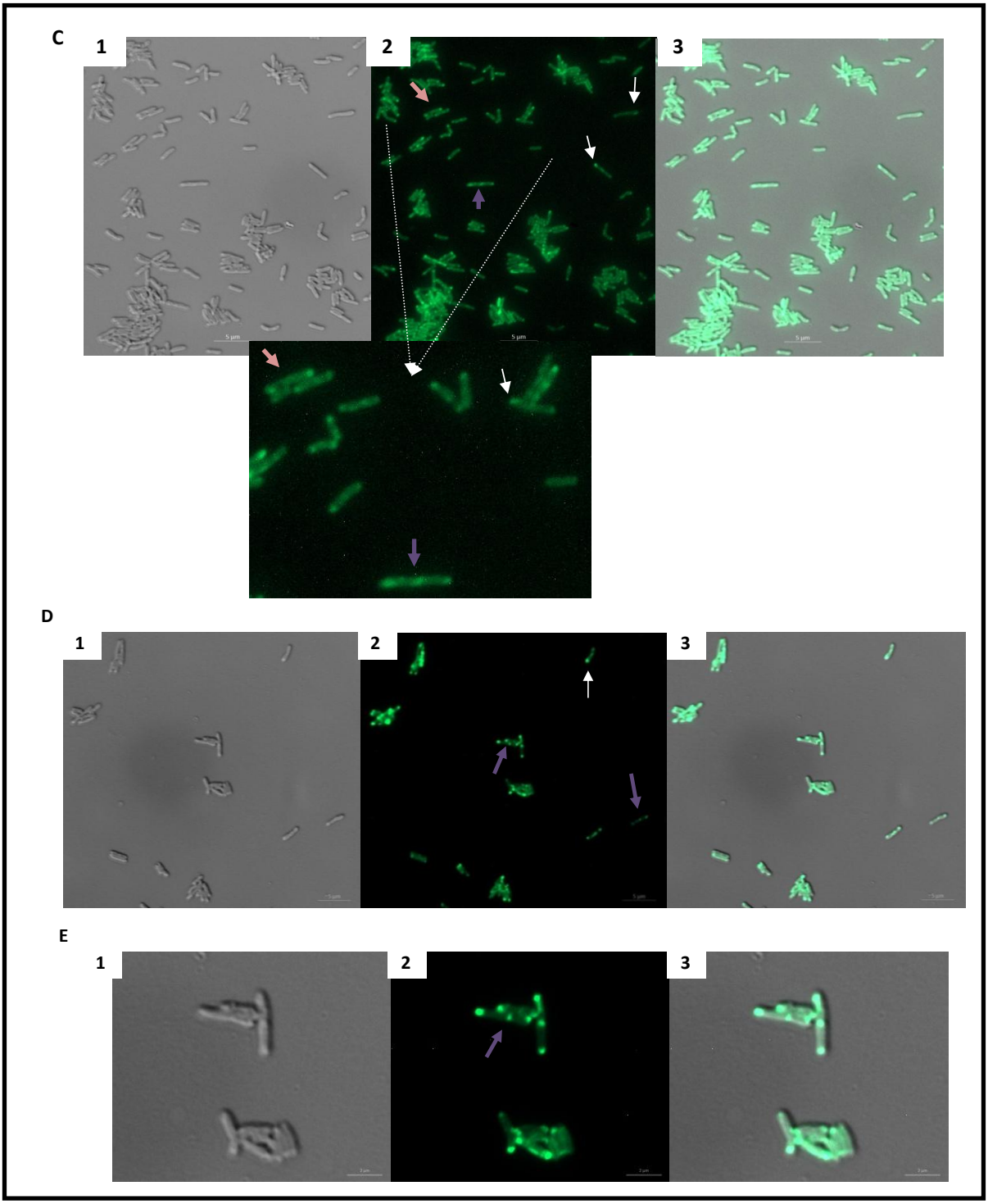


Figure 3.31. PCR screen for integration of pMC1s. **[Lane 1]** Roche Marker IV, **[Lane 2]** *attBS2, attL4* PCR, **[Lane 3]** *attL2, attBS1* PCR.

PCR screen for the pMC1s repressor-encoding gene yielded the correct bands (screen explained in section 3.4.3), confirming that the repressor integrated at the correct site, Figure 3.31. A PCR screen was also carried out on the repressor-less strain to determine the presence of *dacB*-rsEGFP, which produced the desired band of 2165 bp (data not shown).

We then attempted to grow pTw::dacB-rsEGFP, lacking the repressor; however a poor biomass was obtained during log phase. Different approaches, including growing the strain in 7H9 with OADC (Oleic acid-albumin-dextrose-catalase) instead of glycerol; growing at 30 ºC instead of 37 ºC; shaking at a higher speed and growing in LB instead of 7H9 did not improve this. The strain was taken forward by growing in the selective media and thereafter in varying concentrations of AHT. There was notable variability in the biological replicates, which precluded expression analysis however, microscopy was still carried out.


A
1
2
3
B
1
2
3


C
1
2
3
D
1
2
3
E
1
2
3

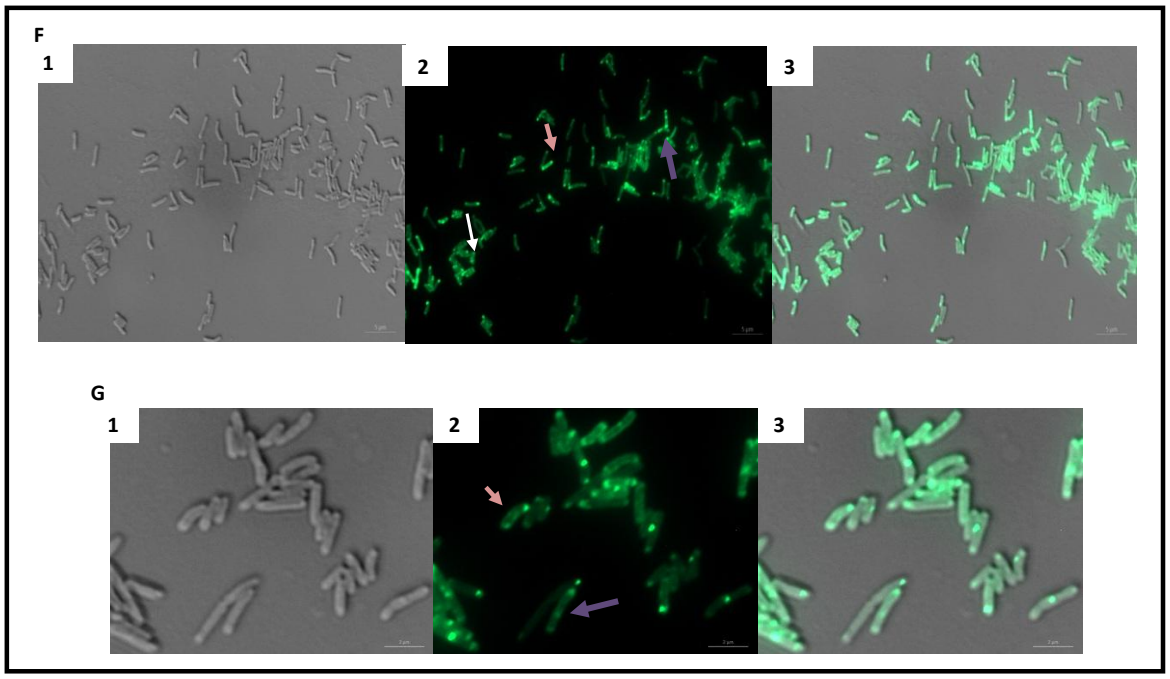


Figure 3.32. Confocal microscopy of pTw::dacB-rsEGFP with pMC1s construct, at varying concentrations of AHT during log phase. **(A)** pTw::dacB-rseGFP + pMC1s 0 AHT, **(B)** pTw::dacB-rsEGFP + pMC1s 0.5 AHT, **(C)** pTw::dacB-rsEGFP + pMC1s 5 AHT, **(D)** and **(E)** pTw::dacB-rsEGFP + pMC1s 50 AHT, **(F)** and **(G)** pTw::dacB-rsEGFP + pMC1s 100 AHT. **[1]** DIC; **[2]** Fluorescence; **[3]** Merged. White arrows indicate monopolar and/or septal localization, Pink arrows indicate bipolar localization, and Purple arrows indicate bipolar and septal localization. Dotted arrows lead to zoomed image. Scales bars: 5 µm for (A) – (D) and (F), and 2 µm for zoomed images, (E) and (G).

Microscopy results revealed localization patterns at lower concentrations of AHT to be very similar to those observed previously, i.e. a high proportion of monopolar localization, Figure 3.32A and 3.32B. However, supplementation with 5 ηg/mL AHT yielded increased bipolar and bipolar with septal localization, with monopolar staining still being the in the highest proportion, Figures 3.32C and 3.33. At 50 ηg/mL and 100 ηg/mL AHT, the bipolar and bipolar plus septal localization increased, with a decrease in monopolar localization, Figures 3.32D-3.32G, 3.33. An interesting observation was that at the higher concentrations of AHT (50 ηg/mL and 100 ηg/mL), diffused localization seemed to decrease drastically, with an increase in the concentration of fluorescent accumulation at specific locations, Figures 3.32D-3.32G, 3.33. This was consistent in all experiments carried out using AHT as described in the previous section. This could point to one of two scenarios, either higher AHT

concentrations aids in localization when using fluorescent tags or the AHT itself is affecting the fluorescent protein. It is difficult to determine which is occurring, and the mechanism could be related to the expression of the fusion protein.

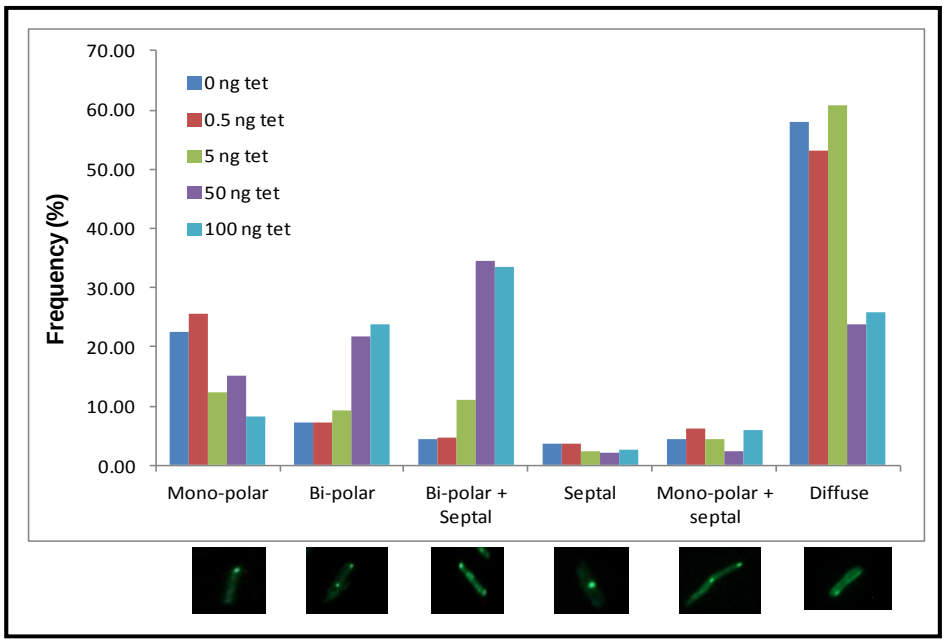
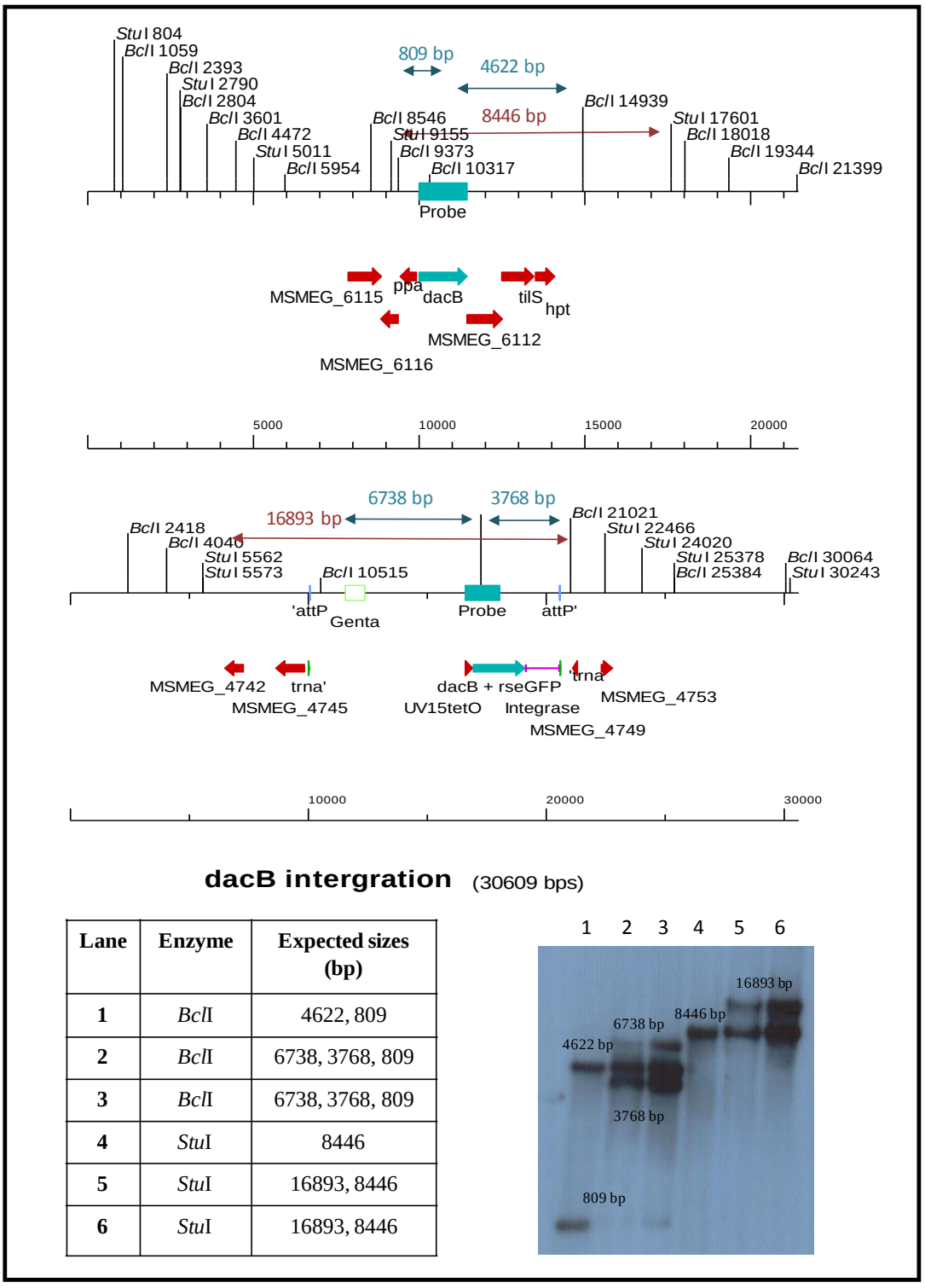


Figure 3. 33. Graph of localization patterns observed during microscopy of pTw::dacB-rsEGFP.

Due to the above-mentioned difficulty of growing the strain under standard conditions, we decided to confirm that integration of the pTw::dacB-rsEGFP construct had occurred in a site specific manner. For this, Southern Blot analysis was carried out using the enzymes *Bcl*I and *Stu*I with the *dacB* opening reading frame serving as the probe. The integration site of the pTweety vector is the $tRNA^{lys}$ (MSMEG_4746).



Lane	Enzyme	Expected sizes (bp)
1	*Bcl*I	4622, 809
2	*Bcl*I	6738, 3768, 809
3	*Bcl*I	6738, 3768, 809
4	*Stu*I	8446
5	*Stu*I	16893, 8446
6	*Stu*I	16893, 8446

Figure 3. 34. Southern Blot analysis of pTw::dacB-rsEGFP construct. (A) Genome map of mc^{2}155 dacB region, (B) Genome map of integrated construct, (C) Southern blot of mc2155 and construct [Lane 1] BclI restriction of mc2155, [Lane 2] BclI restriction of pTw::dacB-rsEGFP construct, **[Lane 3]** *Bcl*I restriction of pTw::dacB-rsEGFP construct with pMC1s, **[Lane 4]** *Stu*I restriction of mc^{2}155, **[Lane 5]** *Stu*I restriction of pTw::dacB-rsEGFP construct, **[Lane 6]** *Stu*I restriction of pTw::dacB-rsEGFP construct with pMC1s. Blue arrows indicate required gene (dacB or dacB-rsEGFP), red arrows indicate genes flanking required gene (dacB or dacB-rsEGFP)

Southern blot analysis yielded the correct, expected band sizes for mc^2155, for both restriction enzymes used (4622 bp and 809 bp for *Bcl*I and 8446 bp for *Stu*I). *Bcl*I digestion of mc^2155 produces two bands due to the presence of a *Bcl*I site in the *dacB* gene, Figure 3.34A and C. The pTw::dacB-rsEGFP construct contained both the wild type bands (4622 bp and 809 bp), as well as two other bands, of 6738 bp and 3768 bp, as expected, Figure 3.34B and C. *Stu*I digest of pTw::dacB-rsEGFP also contained the wild type band (8446 bp), Figure 3.34A and C, and one other band of 16893 bp, which was expected, Figure 3.34B and C. Both these results indicate that integration occurred at the correct site. Thus, the inability to grow this strain is not due to a defect in integration. Considering this, the growth defect may be attributed to the deregulated expression of DacB, which would explain the inability of the repressor-less strain to grow, and the very slow growth of the strain with the repressor. To circumvent this, the construct may need to be cloned into a different backbone - or the native *dacB* gene could be replaced by one carrying the rsEGFP fusion.

3.5. Localization of MSMEG_2433

3.5.1. MSMEG_2433-Venus

Localization of MSMEG_2433 was carried out in a manner similar to DacB where the gene encoding this protein was fused to that encoding the Venus protein using cloning. PCR amplification of the genes was successful, Figure 3.35. The MSMEG_2433 no DNA control contained a faint band at 852 bp, this was repeated again and the band disappeared, indicating that this band was due to cross-contamination (data not shown). Products were ligated as previously described. And following transformation 12 colonies were selected and the DNA digested using *Pac*I and *Hin*DIII (data not shown). One positive clone was selected and mapped through restriction analysis.

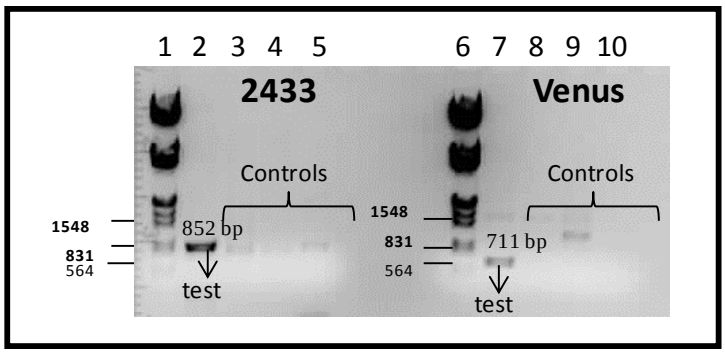
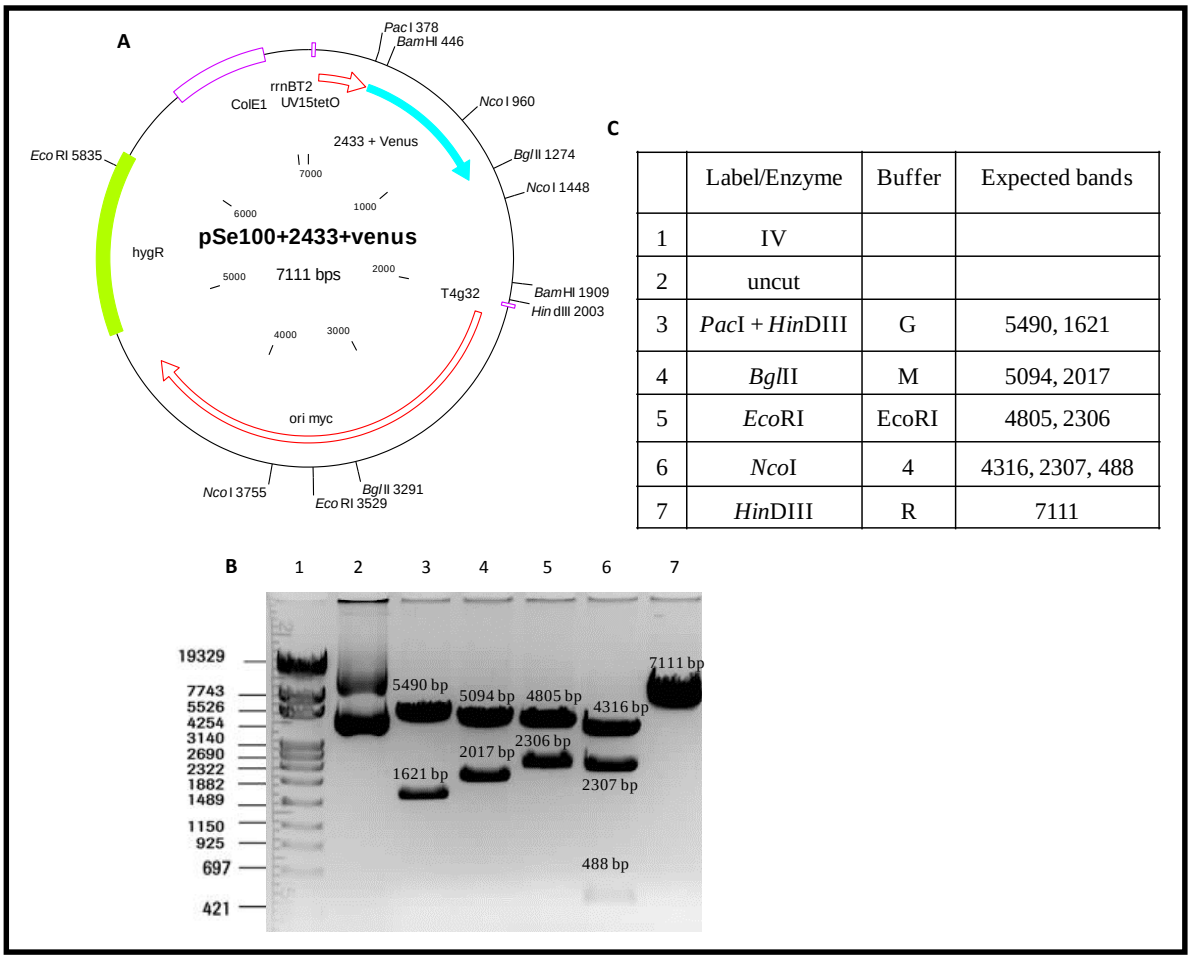


Figure 3. 35. Agarose gels of Phusion PCR of MSMEG_2433 and Venus. **[Lane 1]** Roche marker IV, **[Lane 2]** MSMEG_2433 PCR, **[Lane 3]** No MSMEG_2433 forward primer control, **[Lane 4]** No MSMEG_2433 reverse primer control, **[Lane 5]** No DNA control (MSMEG_2433), **[Lane 6]** Roche marker IV, **[Lane 7]** Venus PCR, **[Lane 8]** No Venus forward primer control, **[Lane 9]** No Venus reverse primer control, **[Lane 10]** No DNA control (Venus).



C

	Label/Enzyme	Buffer	Expected bands
1	IV		
2	uncut		
3	*Pac*I + *Hin*DIII	G	5490, 1621
4	*Bgl*II	M	5094, 2017
5	*Eco*RI	EcoRI	4805, 2306
6	*Nco*I	4	4316, 2307, 488
7	*Hin*DIII	R	7111

Figure 3. 36. Restriction profile of MSMEG_2433 and Venus cloned into pSE100. **(A)** Plasmid map of MSMEG_2433 and Venus cloned into pSE100 (blue arrow). **(B)** Agarose gel of restriction analysis of pSE2433 -Venus **[Lane 1]** Roche Marker IV**, [Lane 2]** uncut pSE2433 -Venus, **[Lane 3]** *Pac*I + *Hin*DIII, **[Lane 4]** *Bgl*II, **[Lane 5]** *Eco*RI, **[Lane 6]** *Nco*I, **[Lane 7]** *Hin*DIII. **(C)** Table showing the expected banding profiles of the restriction analysis of the pSE2433 -Venus construct.

The restriction profile of the pSE2433-Venus yielded the correct banding patterns for the enzymes tested, Figure 3.36. - indicating that the cloning was successful. Sequencing further confirmed this and revealed no mutations or deletions. Following electroporation into *M. smegmatis*, PCR was carried out using the MSMEG_2433 forward primer and Venus reverse primer, which resulted in a clear band at 1607 bp, as expected (data not shown). Confocal microscopy was carried out in order to determine the localization patterns of this protein, Figure 3.37.

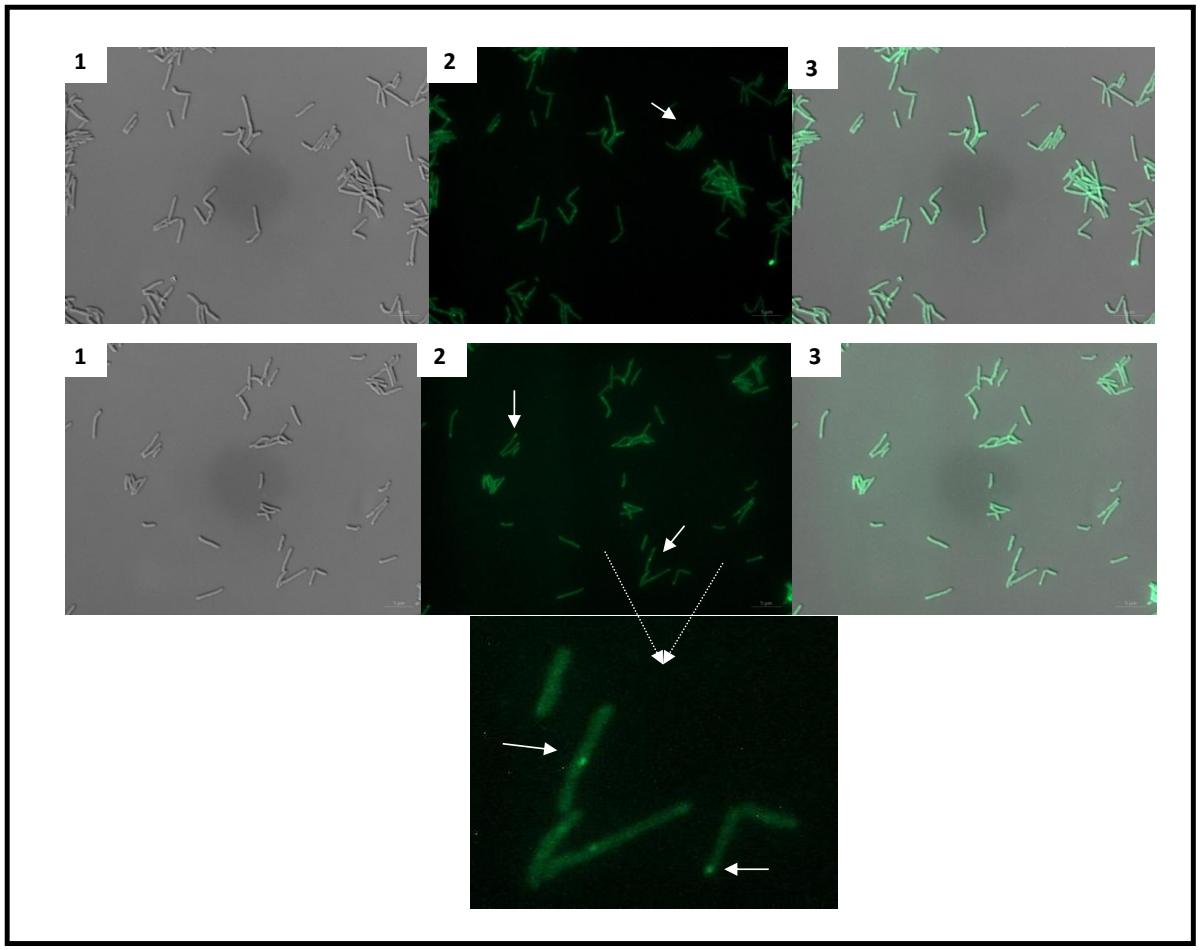


Figure 3. 37. Fluorescence microscopy of pSE2433-Venus. **[1]** DIC; **[2]** Fluorescence; **[3]** Merged. White arrows indicate polar or septal localization. Dotted arrows lead to zoomed image. Scale bar: 5µm, 2 µm for zoomed images.

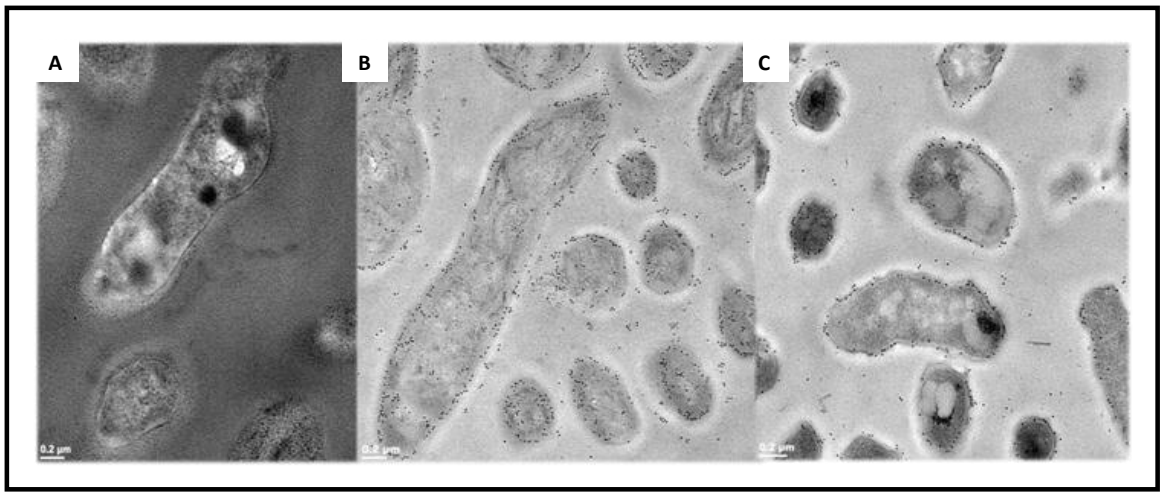


Figure 3. 38. TEM of Immunogold pSE2433-rsEGFP construct. **(A)** Negative control (No 1º AB), **(B)** Construct- 1:100 dilution of 1º AB, **(C)** Construct- 1:500 dilution of 1º AB. Scale bar: 0.2 µm.

MSMEG_2433 is constituently over-expressed and would be expected to localize at sites of new peptidoglycan incorporation due to the action of DD-CPase genes in general. However, most cells indicated dispersed localization, with a small percentage of cells showing monopolar or septal localization, Figure 3.37, white arrows. In addition to confocal microscopy, TEM was carried out using the Immunogold strategy, Figure 3.38, which showed MSMEG_2433 to be localized/dispersed along the cell wall.

3.5.2 MSMEG_2433-rsEGFP

Construction of an MSMEG_2433-rsEGFP fusion required PCR amplification and three-way cloning. In this case, PCR amplification, yielded fragments of the correct size indicated by the bands of 852 bp and 721 bp, Figure 3.39. The faint band present in the no DNA control was again due to cross-contamination, as the PCR reactions for the Venus construct and the rsEGFP construct were carried out at the same time. Following ligation, 12 putative clones were digested using *Pst*I and *Hin*DIII. Only one clone produced the expected banding pattern of 5508bp and 2172bp (data not shown), which was then mapped further.

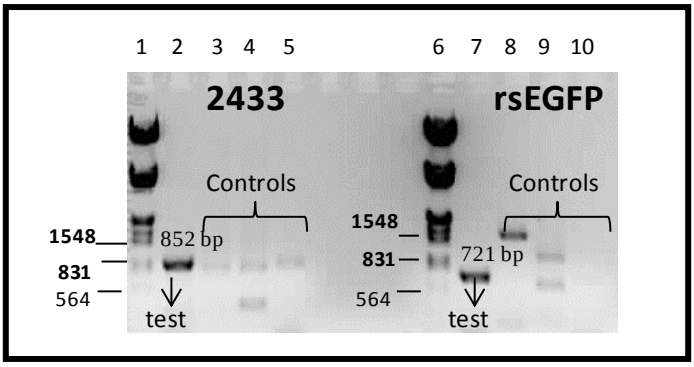
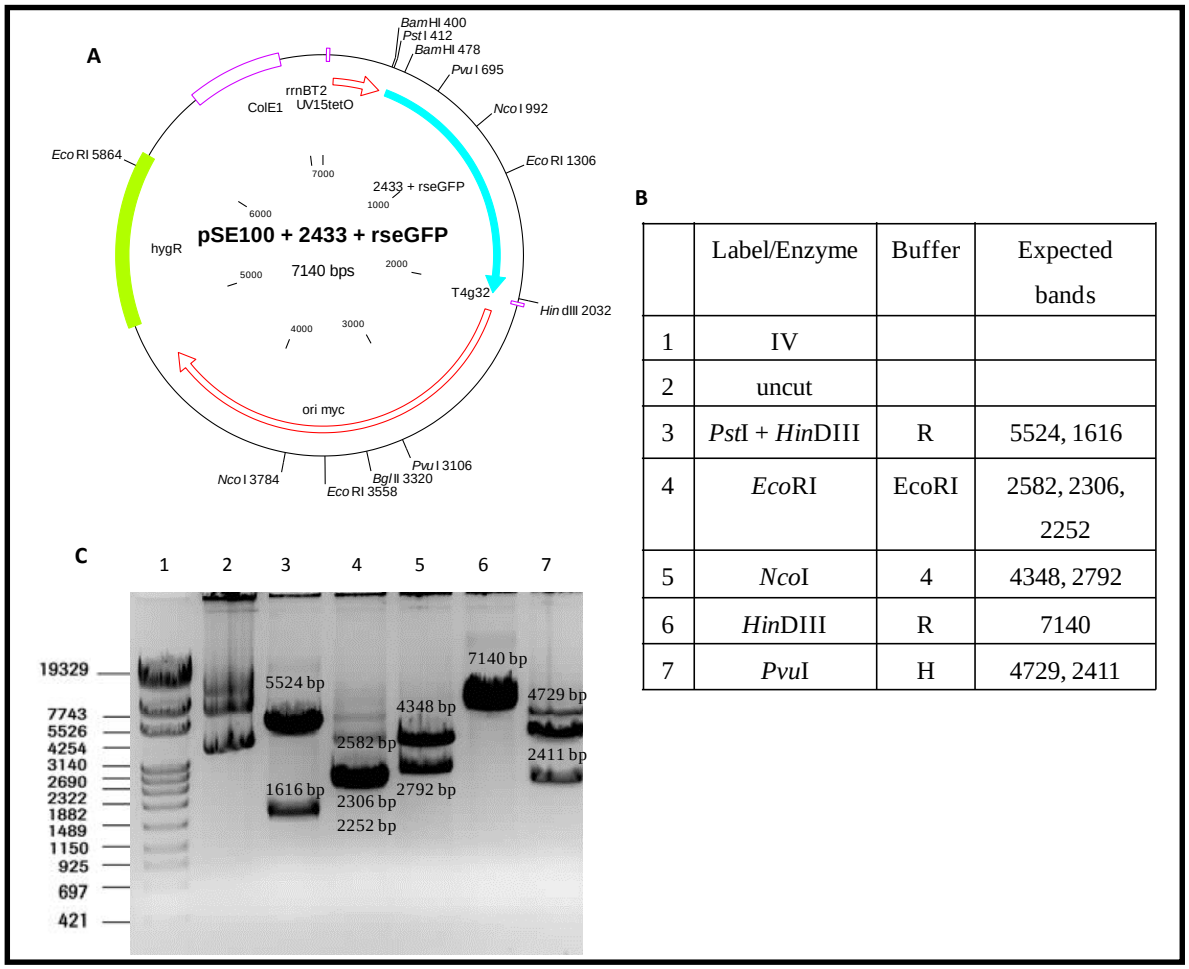


Figure 3. 39. Agarose gels of Phusion PCR of MSMEG_2433 and rsEGFP. **[Lane 1]** Roche marker IV, **[Lane 2]** MSMEG_2433 PCR, **[Lane 3]** No MSMEG_2433 forward primer control, **[Lane 4]** No MSMEG_2433 reverse primer control, **[Lane 5]** No DNA control (MSMEG_2433), **[Lane 6]** Roche marker IV, **[Lane 7]** rsEGFP PCR, **[Lane 8]** No rsEGFP forward primer control **[Lane 9]** No rsEGFP reverse primer control, **[Lane 10]** No DNA control (rsEGFP).



	Label/Enzyme	Buffer	Expected bands
1	IV		
2	uncut		
3	*Pst*I + *Hin*DIII	R	5524, 1616
4	*Eco*RI	EcoRI	2582, 2306, 2252
5	*Nco*I	4	4348, 2792
6	*Hin*DIII	R	7140
7	*Pvu*I	H	4729, 2411

Figure 3. 40. Restriction profile of MSMEG_2433 and rsEGFP cloned into pSE100. **(A)** Plasmid map of MSMEG_2433 and rsEGFP cloned into pSE100 (blue arrow). **(B)** Agarose gel of restriction analysis of pSE2433-rsEGFP **[Lane 1]** Roche Marker IV, **[Lane 2]** uncut pSE2433-rsEGFP, **[Lane 3]** *Pst*I + *Hin*DIII**, [Lane 4]** *Eco*RI, **[Lane 5]** *Nco*I, **[Lane 6]** *Hin*DIII, **[Lane 7]** *Pvu*I. **(C)** Table showing the expected banding profiles of the restriction analysis of the pSE2433-rsEGFP construct.

The restriction profile of the pSE2433-rsEGFP vector yielded the correct sizes for the enzymes tested, Figure 3.40. An extra band was observed for the *Pvu*I digest which was attributed to partial digestion. Following electroporation into *M. smegmatis*, PCR using the MSMEG_2433 forward primer and rsEGFP reverse primer was carried out, which resulted in a sharp band at 1616 bp, as expected (Appendix E). Confocal microscopy was carried out, Figure 3.41.

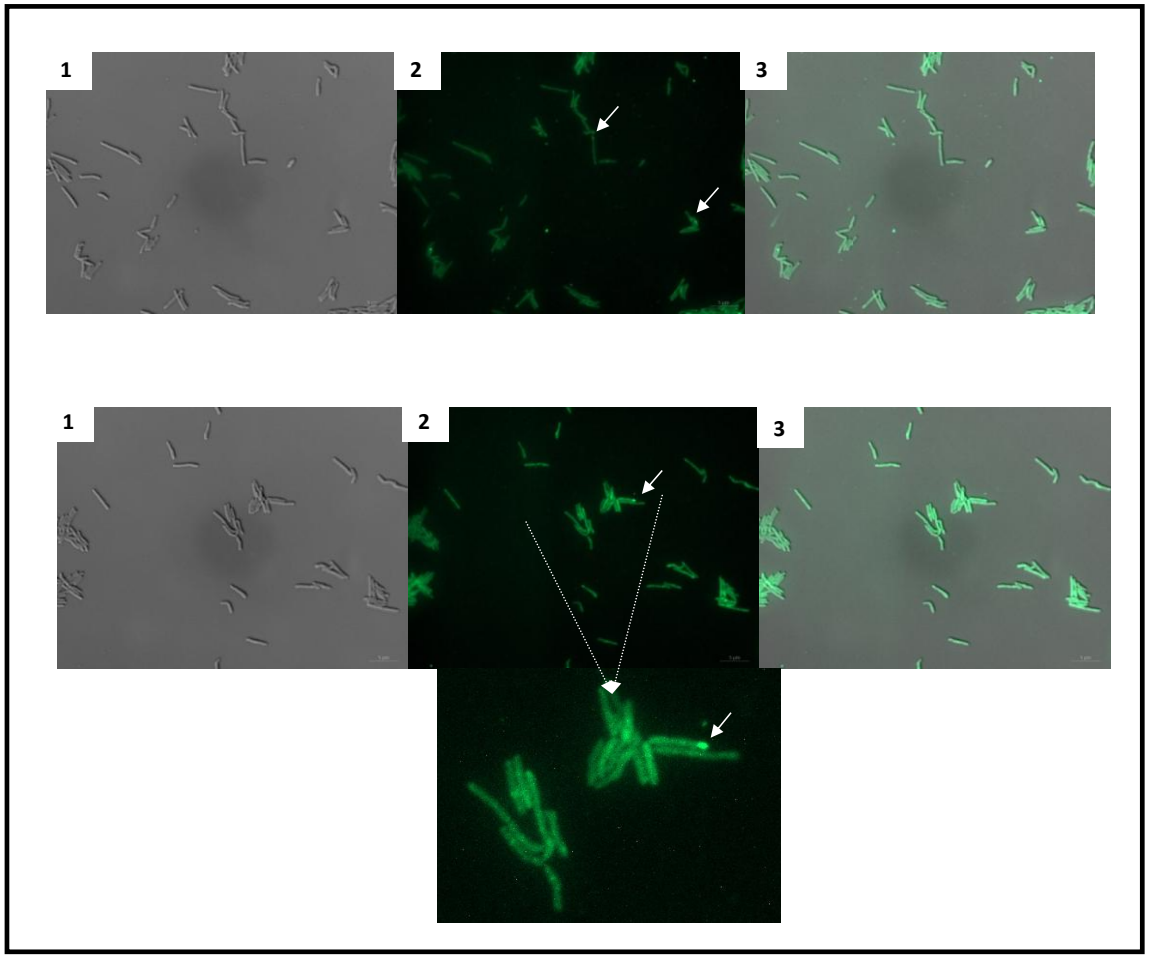


Figure 3. 41. Fluorescence microscopy of pSE2433-rsEGFP constructs. **[1]** DIC; **[2]** Fluorescence; **[3]** Merged. White arrows indicate polar or septal localization. Dotted arrows lead to zoomed image. Scale bar: 5µm, 2 µm for zoomed images.

Microscopy of pSE2433-rsEGFP resulted in similar patterns as the Venus microscopy, i.e. majority dispersed localization with a small percentage of monopolar or septal localization, Figure 3.41. No quantification or further analysis could be carried out.

3.6. Single DD-CPase gene knock outs (KOs) have no effect on antibiotic susceptibility

This component of this MSc study was aimed at further analyzing DD-CPase function. For this, antibiotic susceptibility of mutants lacking individual DD-CPase encoding genes was tested by MICs, as described in section 2.8. Single deletion mutants were obtained from Dr C. Ealand, who had previously carried out phenotypic characterisation on these strains. The data is shown in Table 3.3. Antibiotics were chosen based on ability to damage the cell wall as well as a few general TB drugs to determine any changes in permeability. This approach was aimed at trying to extrapolate function of the individual genes by antibiotic susceptibility, and thereby assessing any specific phenotypic differences resulting from the loss of DD-CPase-encoding genes. Neither determination of MICs using broth, Table 3.3, nor plating on solid media with antibiotics of varying concentrations (data not shown) revealed any differences in antibiotic susceptibilities. Most antibiotics tested in liquid culture resulted in a 2-fold variation between experiments, with the exception of Erythromycin and Cefoxitin which showed no variation in MIC values.

Table 3.3. MIC results of single DD-CPase KOs

	Amp	**Vanc**	**Ery**	**RIF**	**Cot**	**Cox**	**Cad**	**Ctx**	**Cap**	**D-cyc**
WT	150-300	1.56	0.1	0.155	93.75-187.52	20	256	250	100	52.5-26.25
ΔMSMEG_1661	150-300	1.56-3.125	0.1	0.155	93.75-187.52	20	256-128	125-250	100-50	52.5-26.25
ΔMSMEG_2433	150-300	3.125	0.1	0.155-0.31	93.75-187.52	20	256	250	100	52.5-26.25
ΔMSMEG_2432	150-300	1.56-3.125	0.1	0.31	93.75-187.52	20	256-128	250	100-50	52.5-26.25

MIC in µg/mL

The results are an average of 5 biological repeats

4. Discussion

Mtb is one of the most successful pathogens in human history, with TB disease dating back centuries, if not millennia. The rapid emergence of drug resistance is a problem in many bacterial organisms and the extensive number of antibiotics to which mycobacteria have developed resistance to - in such quick succession i.e. MDR, XDR and the most recent XXDR - is a point of particular concern (Velayati et al., 2009). The disease is further exacerbated by the lack of new drug candidates for treating individuals who carry these composite forms of drug resistance. Most of this resistance is due to the inherent features regarding mutability and adaptation in mycobacteria. As such, a better understanding of key aspects in mycobacterial metabolism is required for meaningful impact on TB drug development. In this study, we have chosen to study remodelling of the mycobacterial cell wall, particularly the PG component.

The overall cell wall structure of both gram positive and gram negative bacteria is generally complex, but the added layers present in the mycobacterial cell wall, such as the mycolic acids and arabinogalactan, make the mycobacterial wall vastly more complicated (Hett and Rubin, 2008). These unique features make the cell wall an interesting structural target for novel drug and vaccine development. Basic physical and metabolic constraints placed on the bacterial cell during growth and cell division demand that the cell wall remain dynamic with regards to composition and physical structure. The remodelling of various layers in the cell wall have garnered recent interest from the perspective of key steps in the cell division pathways of many bacterial species (Yang et al., 2012). Our laboratory has principally been active in studying the PG layer in the mycobacterial cell wall. The PG layer retains the capacity to be restructured by continuous rearrangement of the bonds between side chains to create space for the insertion of new PG units and the specialized secretion apparatus/porins (Typas et al., 2012). In many organisms the PG layer presents a permeability barrier in the

cell, Figure 1.3 (Sobhanifar et al., 2013), and has been of particular interest with regards to drug development since its biosynthesis involves a number of both membrane-bound and cytoplasmic enzymes which are unique to bacteria, such as the PBPs, the target for β-lactam antibiotics (Basu et al., 1992). Bacteria, including mycobacteria, have the ability to bypass or inactivate such antibiotics by the production of enzymes such as β-lactamases which inactivate β-lactams by a hydrolysis reaction, or by the action of efflux pumps to remove/pump out the antibiotic and both these mechanisms work in concert to ensure survival of the cell (Livermore, 1995, Jarlier and Nikaido, 1994).

Remodelling of PG is achieved by a class of enzymes termed hydrolases. This study focused specifically on low molecular weight PBPs termed DD-CPases. As stated previously, DD-CPases act on the terminal D-Ala residue on the pentapeptide side chain of PG and are associated with notable genetic redundancy in bacteria (Hammes and Seidel, 1978). In order to assess the function of these genes, single gene knockouts of MSMEG_1661, MSMEG_2432 and MSMEG_2433 were created (C. Ealand and B. Kana, unpublished). To further study effects of DD-CPase deficiency, we tested the antibiotic susceptibility profiles of these single DD-CPase gene knockouts. None of the deletion mutants (ΔMSMEG_2432; ΔMSMEG_2433; ΔMSMEG_1661) displayed an increase in susceptibility to antibiotics when compared to WT, Table 3.3. Other studies undertaken with these strains included growth kinetics, exposure to cell wall stresses, microscopy and biofilm formation, which resulted in the lack of any observable phenotypic abnormalities (Ealand and Kana, unpublished). Together, these data suggest that in these deletion mutants, the remaining DD-CPase-encoding genes play a compensatory role. In order to confirm this, double deletions in different combinations, as well as a triple deletion mutant would be required to dissect individual versus combinatorial biological roles.

The importance of PG remodelling in mycobacteria is demonstrated by the difference in abundance of the two types of cross-links between adjacent stem peptides (i.e. 4→3 and 3→3 cross-links), which are observed during different phases of growth (Lavollay et al., 2008). In mycobacteria, as in *E. coli*, there is an increase in the proportion of 3→3 cross-links at the onset of stationary phase, with a subsequent decline in 4→3 cross-links, (Lavollay et al., 2008, Hampshire et al., 2004, Lavollay et al., 2011). In *E. coli*, there is a very low abundance of 3→3 cross-links during exponential growth and it is only at the onset of the lag phase of growth that 3→3 cross-links become apparent, presumably due to nutritional deprivation or some other stress response (Templin et al., 1999). This type of cross-link causes the cell to increase in rigidity and reduced the susceptibility of the cell wall to PG hydrolases, consequently, it has been hypothesized that the organization of stem peptide cross-links in this manner may be important for the onset of, or exit from, dormancy in mycobacterial cells (Hett and Rubin, 2008).

Our reasoning for testing the antibiotic susceptibility of DD-CPases deletion strains was driven by the published evidence that shows a correlation between LMW PBPs and antibiotic resistance. The DacB enzyme from *E. coli* displays high levels of intrinsic resistance to penicillin (Gondre et al., 1973). A PBP5 mutant was more susceptible to antibiotics, specifically beta-lactams, which confirmed a role for this protein in the cell's intrinsic resistance to these antibiotics (Sarkar et al., 2010). Another study demonstrated that MICs to a number of antibiotics increased as amino acid mutations increased; specifically at positions 485 (methionine changed to threonine), 499, 629 (Valine substitution) and 466 (serine residue added) in PBP5 (Rice et al., 2004). Studies have also shown that during the onset of stationary phase in *E. coli*, *pbp3,* which encodes a high molecular weight PBP, gene expression is down-regulated, and the expression of a gene encoding a low molecular weight PBP, *pbp6*, is up-regulated with an increased amount of 3→3 cross-links (Boshoff and Barry,

2006, Dougherty and Pucci, 1994). Similarly, a gene encoding a high molecular weight PBP in *Pseudomonas aeruginosa*, *pbp3*, was also down-regulated and a gene encoding the low molecular weight PBP, *pbp2*, was up-regulated during the onset of stationary phase (Liao and Hancock, 1997). It is during stationary phase at which resistance to penicillin-binding drugs is high (Boshoff and Barry, 2006). The potential role of LMW PBPs, such as the DD-CPases, and changes in PG cross-linking during this stage is potentially interesting when considering drug resistance. In organisms such as *E. coli* and *B. subtilis*, the different DD-CPases function in a growth phase dependant manner as well (described in detail in introduction section 1.7.3.1) (Ghosh et al., 2008). This adds another layer of complexity to the functionality of these genes in the cell. However, the lack of information regarding these genes in mycobacteria makes it difficult to ascertain the mechanism of action of the specific DD-CPases in TB infection. Additionally, the lack of any differential increase or decrease in antibiotic susceptibility with the single deletion mutants in this study suggests that the remaining LMW PBPs compensate for the loss of a single gene in our mutants.

DacB and MSMEG_2433 in *M. smegmatis*

The rationale for choosing DacB and MSMEG_2433 for further analysis in this study is based on the following results from a study currently underway in our laboratory (Kana and Ealand, unpublished): (I) Of all the DD-CPases, MSMEG_2433 displays the highest homology to E. coli PBP5, with all necessary catalytic residues being conserved, (II) the gene encoding MSMEG_2433 is the most highly expressed DD-CPase in *M. smegmatis*, (III) deletion of *dacB* was not possible – suggesting that it is essential for growth and (IV) consistent with this notion, the *dacB* homologue in *M. tuberculosis* [Rv3627c - (Machowski et al., 2014)] is predicted to be essential from two separate studies (Sassetti et al., 2003, Griffin et al., 2011).

Of the 4 LMM PBPs in *E. coli*, the most well-characterized DD-CPase described so far is PBP5. Even though PBP5 is dispensable for growth, unlike *dacB* in *M. smegmatis*, it has been implicated in cell shape as well as resistance to beta-lactam antibiotics (Nelson and Young, 2001, Depardieu et al., 2007). Combinatorial PBP5 mutants, that lack other PBPs, display morphological abnormalities in cell length and diameter, as well as growth defects such as branching and budding, all of which are emphasized as the number of DD-CPase deletions increase (Nelson and Young, 2000, Nelson and Young, 2001). Over-expression of PBP5 causes defects in cell division, the production of rounded cells and ultimately cell lysis (Nelson and Young, 2000). In our study, we also noted morphological changes upon over-expression of the DacB-rsEGFP fusion, which led to the formation of longer cells.

Localization of DacB by fluorescence microscopy, with the use of fluorescent tags, revealed that this protein mainly localizes to a single cell pole, when over-expressed in *M. smegmatis*, Figures 3.22, 3.26-3.33. This dominance of monopolar localization was present when using both Venus and rsEGFP tags, as well as with both the episomal pSE100 and the modified integrative pTweety as the shuttle vectors. An interesting observation using the integrative vector was that at higher AHT concentrations, bipolar and bipolar with septal localization increased significantly to levels equivalent and greater than the monopolar localization. This could have been due to a marginal difference in gene expression at these levels, but could not be tested as technical difficulties were encountered when attempting to grow cultures consistently in liquid media for expression analysis, Figure 3.31D-G. In this study, expression of *dacB* could not be controlled using the 'Tet on' system (Guo et al., 2007) as the expression data for the pSE100 construct revealed that *dacB* was over-expressed, relative to wild type, under all AHT concentrations. Consequently, we can make no definitive conclusions regarding the localization of DacB when expressed at native levels. However, we hypothesize that over-expression of DacB, as achieved in this study may provide some insight on the

biological role of this protein. Indeed, a similar approach was taken to study PBP localization in *E. coli* and for other cell division proteins in mycobacteria (Nelson and Young, 2001, Kang et al., 2008, Maloney et al., 2009). Nelson and Young (2001) showed that *E. coli* PBP5 needs to be not only enzymatically active, but must also be localized to the correct position in order to function properly and hypothesized that proper localization could dictate which substrates, as well as the amount of substrates on which PBP5 acts. Wag31, a homologue of DivIVA, was shown to be essential in mycobacteria and involved in cell division of this organism (Cole et al., 1998, Jani et al., 2010, Kang et al., 2008). A mutational study of this gene demonstrated cells of abnormal morphologies, i.e. a swelling in one pole – indicative of the involvement of Wag31 in PG synthesis at the poles of the cell (Jani et al., 2010, Kang et al., 2008). Localization confirmed this finding since Wag31 localized to one pole (presumed to be the old pole) and less so to the alternate pole, with rare occurrences of septal localization (Kang et al., 2008, Meniche et al., 2014), quite similar to the results obtained in this study for DacB as well as MSMEG_2433. Wag31 was subsequently shown to interact with, as well as co-localize with, ParA (Ginda et al., 2013).

Cell division proteins in mycobacteria

ParA and ParB are segregation/partitioning proteins involved in the segregation of the chromosome (Fogel and Waldor, 2006). ParA localizes at various positions including polar; septal; quarter cell; as well as in a spiral fashion in some cells, whereas ParB indicated majority polar localization and occasional septal localization, similar to those observed for DacB (Maloney et al., 2009). Co-localization studies of ParA and ParB revealed polar co-localization, while ParA was shown to co-localize with the nucleoid at the septum, again pointing to a role for these proteins in the cell division process (Maloney et al., 2009). Wag31and ParA foci were shown to overlap, while the intensity of the ParA localization was proportional to that of Wag31 – indicating a dependency between these proteins and re-

iterating the role of Par proteins in the cell division process of mycobacteria (Kang et al., 2008, Ginda et al., 2013).

CrgA is also a mycobacterial cell division protein which interacts with other cell division proteins including FtsZ; FtsI; FtsQ and PBPA, and localizes to the cell membrane, poles and septum and it was hypothesized that the localization of this protein is dynamic with a dependence on the stage of cell division (Plocinski et al., 2013, Plocinski et al., 2012). The same study also demonstrated that FtsI localization was dependant on CrgA due to localization patterns being altered depending on the amount of CrgA/CrgA levels in the cell (Plocinski et al., 2011). PBPA, on the other hand, mainly indicated septal/midcell localization (Dasgupta et al., 2006).

Protein interactions and the cell wall

The existence and essentiality of protein-protein interactions has been well documented and demonstrated to be pivotal for a number of cellular processes. It has been suggested that many PBPs act as a complex in order to fully exert their function and for the cell to function optimally (Sauvage et al., 2008). To further understand this in mycobacteria, we sought to identify DD-CPase-interacting partners by using DacB and MSMEG_2433 as bait proteins in a library screen. These studies identified a number of potential interacting partners, with three being of particular interest due to the potential of these proteins to form complexes with the DD-CPases of interest, i.e. an acyltransferase; an ATP synthase; and a transcriptional regulator, Table 3.2. An interesting observation was that both DacB and MSMEG_2433 displayed the potential to interact with the TetR transcriptional regulator. This points to the possibility that both these DD-CPases, and potentially the other PBPs, are under the control of the same regulator and may possibly explain the ability of the cell to tolerate deletion of CPases with negligible effects on growth and antibiotic susceptibility. The interaction with an acyltransferase points to the possibility of a PG hydrolysing complex, as acyltransferase

activity is required for the formation of cross linkages by the transferral or polymerization of acyl chains (Rottig and Steinbuchel, 2013). Thus, a possible interaction could involve the trimming of the side chains by DacB, which would free the second D-Ala residue on which the acyltransferase could act in order to form a cross-link. At this point both these explanations are largely speculative and further work is required to confirm any of these ideas. Moreover, we can provide no logical explanation at this juncture for the possible interaction between DacB and an ATP synthase. Initiation and regulation of cell division are energy draining processes but there is no direct evidence from other organisms that PBPs regulate energy production in mycobacterial cells. An alternate, more attractive hypothesis is that both DacB and the ATP synthase are membrane/periplasmic proteins and the interaction between these two proteins in our screen in mainly based on non-specific hydrophobic interactions.

Enzymes involved in the synthesis and breakdown of PG can exert their function only by complex formation or by transitory protein interactions (Kana and Mizrahi, 2010). One of the most promising potential interacting partners of MSMEG_2433 was the PBP1A/1B (PonA2) protein. Sequencing received for two separate clones yielded a hit to PBP1A/1B.This could potentially point to a DD-CPase playing a role/ being a part of a synthesis/hydrolysis complex, which could work in concert with the previously identified RipA-RpfB-PonA complex. Hett et al. (2007) demonstrated that RpfB and RpfE interact with RipA (an endopeptidase) and furthermore, both RipA and RpfB co-localized at the septa of dividing cells. RipA was also shown to have hydrolase activity against the PG layer and the association between RpfB and RipA resulted in enhanced hydrolysis of PG. Depletion of RipA results in blockage of normal cell division, abnormal cell morphology, as well as an increased susceptibility to antibiotics targeting the cell wall (Hett et al., 2008). In order to further study the synergism between RpfB and RipA, studies were carried to establish which

other protein/s interact with this complex. PBP1, belonging to the HMW PBP family was shown to localize at the septa of dividing cells, with the RipA-RpfB complex. In addition, PBP1 was characterized as a bi-functional PG synthesizing enzyme with the ability to inhibit, and thus modulate, the RpfB-RipA synergistic interaction (Hett et al., 2010).

Such a complex, involving both PG hydrolases as well as PG synthases, is a direct indication of the importance of protein-protein interactions to maintain integrity of the cell wall and cellular homeostasis. A full understanding of this complex could provide a novel drug target, with DD-CPases being a potential target in order to affect the entire cascade of events. A model of the interaction of PonA2 and MSMEG_2433 and how it could affect the PBP1/RpfB/RipA complex can be proposed from our work, Figure 4.1. The hypothesis proposed is that the interaction between MSMEG_2433 and PonA2 occurs during PG hydrolysis and this DD-CPase acts in an antagonistic manner to the synthesizing properties of PonA2 in order to either ensure efficient PG hydrolysis or prevent the formation of inappropriate cross-links. This model was developed by the integration of our data for MSMEG_2433 into the model already proposed by Hett et al (2010).

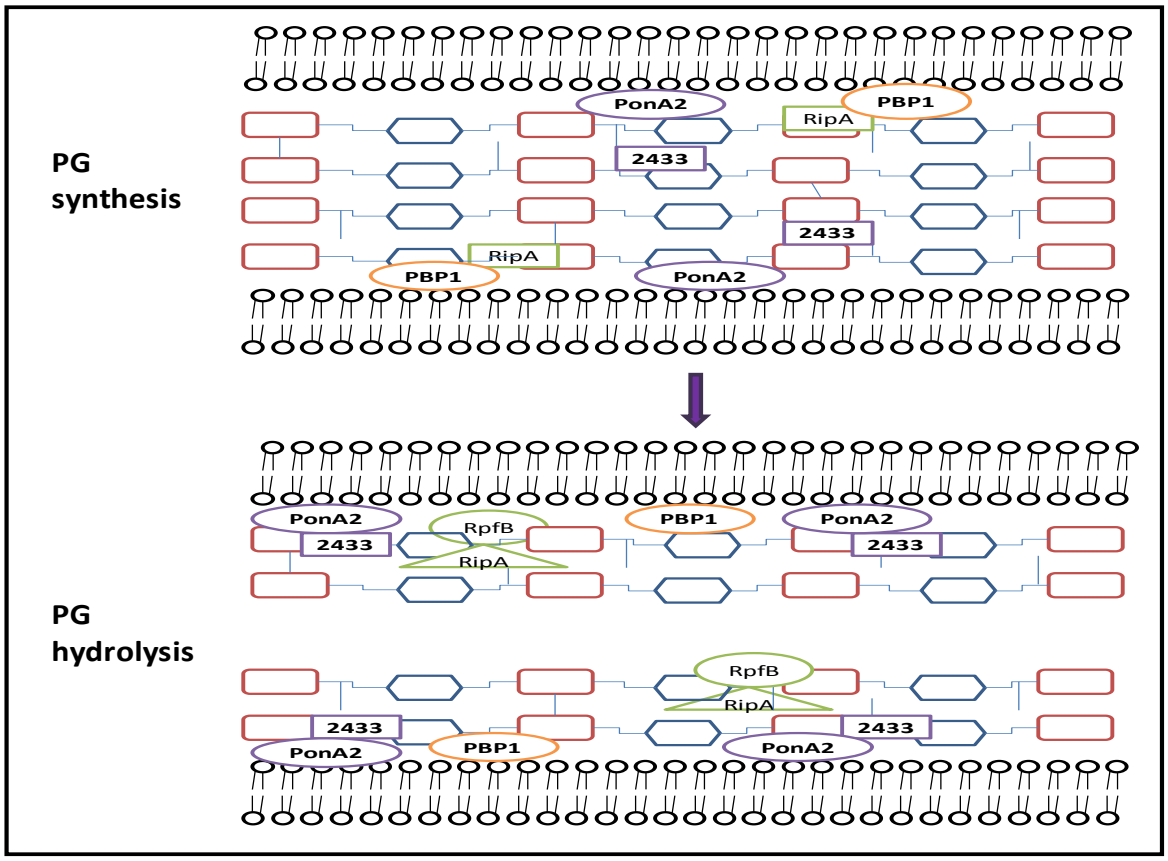


Figure 4.1. Model hypothesizing the interaction between MSMEG_2433 and PonA2 in the cell. The hypothesis is that MSMEG_2433 interacts with PG synthesizing enzyme PonA2 during PG hydrolysis and would thereby prevent this enzyme from synthesizing PG, in order to allow PG hydrolysis to take place efficiently. Adapted from Hett et al, 2010.

A number of HMW PBPs have been shown to be involved directly with cell division. In *E. coli*, the enzymes implicated in the formation and action of the divisome are reliant on a complexity of interactions involving over 12 proteins in a multi-protein network (Vollmer and Bertsche, 2008). These complexes include a number of Fts proteins, as well as amidases and PBPs, which all show septal localization. Müller and colleagues (2007) demonstrated that FtsN interacts with the existing complex of PBP1B and PBP3 (FtsI), which are PG synthases, and hypothesized that FtsN plays a role in modulating this complex, similar to the PBP1 modulation described earlier for mycobacteria. Evidence of such complexes is gaining interest in mycobacteria as a number of interactions between cell division proteins have been identified. (Muller et al., 2007). One such interaction in Mtb is between FtsZ and FtsW and FtsW in turn interacting with PBP3 (a HMW PBP) in a trimeric complex, with FtsW as the

bridging molecule (Datta et al., 2006). In both *M. smegmatis* and Mtb, the FtsZ-FtsW interaction is essential for Z-ring formation and cell division, with both proteins localizing to the septum and FtsW is thus hypothesized to serve as an anchor for FtsZ in order to ensure PG synthesis occurs during formation of the septum (Rajagopalan et al., 2005, Datta et al., 2002). The trimeric complex described is mediated by the proline residues of extracytoplasmic loops of FtsW and PBP3 which play a role in PG synthesis (Datta et al., 2006). In another study CswA (small membrane protein that plays a role in PG synthesis) from Mtb, which interacts with CrgA, has been hypothesized to interact with PBPs and thereby work in concert to control cell division (Plocinski et al., 2013).

The potential interacting partners of MSMEG_2433 were of particular interest and in addition to PBP1A/1B, our analysis identify other potentially interesting proteins such as a helicase and a ssDNA-binding protein, Table 3.2. Co-ordinating cell division with initiation and regulation of DNA replication is critical for successful cell division. In this context, our identification of components of the DNA replication machinery as potential interacting partners for MSMEG_2433 is appealing. Further conclusions in this regards require confirmation of these interactions though pull-down assays. Localization of MSMEG_2433 provided further evidence of the role of this protein in cell division as the protein seemed to be either dispersed in a diffused manner in a majority of cells or concentrated to one pole and the septum, possibly at the sites of cell elongation and division, Figures 3.37, 3.38 and 3.41. An interesting study in *E. coli* revealed that the branching phenotypes observed in PBP5 mutants could be related to cell division, in the absence of PBP5 the Z ring is incorrectly localized, resulting in increased branching, with this phenotype being exacerbated as the other DD-CPases are deleted (Potluri et al., 2012).

Concluding remarks

Taken together, the results from this study highlight an important role for DD-CPases in mycobacteria. This is evidenced by polar and polar/septal localization of both DacB and MSMEG_2433, a pattern of localization consistent with that seen of other key cell division proteins. In addition, these two DD-CPases possibly interact with other key components of the cell elongation machinery, such as PonA2, to mediate their action. This understanding could be pivotal in the formulation of novel vaccine as well as drug targets. This work is currently being progressed by another MSc student in order to confirm these interactions and subsequently assess interactions in proteins derived from Mtb. Collectively, these efforts may lead to the identification of new drug targets within PG metabolism in mycobacteria.

5. Appendices

Appendix A: Culture media and solutions

Sterilization of media and solutions were carried out either by filtering or autoclaving at 121 ºC for 10 min.

Bacterial growth

LB: 10 g tryptone, 5 g yeast extract, 10 g NaCl, 1 L sdH_2O

LA: 10 g tryptone, 5 g yeast extract, 10 g NaCl, 1.5 % agarose, 1 L sdH_2O

2 × TY: 20 g tryptone, 10 g yeast extract, 5 g NaCl, 1 L sdH_2O

Middlebrook 7H9: 4.7 g powder, 990 mL sdH_2O, 2 mL glycerol, 2 mL 25 % Tween80 (10 mL Tween80 dissolved in 40 mL sdH_2O, filter sterilized), 10 mL 100× glucose-salt (20 g glucose, 8.5 g NaCl dissolved in 100 mL sdH_2O)

Middlebrook 7H10: 19 g powder, 990 mL sdH_2O, 5 mL glycerol, 10 mL 100× glucose-salt

YPD broth: 20 g peptone, 10 g yeast extract, 0.003 % adenine hemisulfate (15 mL of filter sterilized 0.2 % stock solution), 940 mL sdH_2O, 2 % glucose (50 mL of filter sterilized 40 % stock solution)

YPDA: YPD including 20 g agar

Minimal SD base: 6.7 g yeast nitrogen base without amino acids, 20 g agar, 0.2 g appropriate dropout supplement, 950 mL sdH_2O, 2 % glucose

DNA manipulation solutions

TE buffer: 20 mL EDTA (0.5 M), 10 mL Tris HCl (1 M), sdH_2O

1 M Tris HCl: 121.1 g Tris, pH adjusted to 8.0 with HCl and made up to 1 L in sdH_2O.

0.5 M EDTA: 93.06 g, pH to 8.0 with NaOH, made up to 500 mL in sdH_2O.

NaCl/CTAB: 10 % N-cetyl-N, N, N-trimethyl ammonium bromide, 4.1 % NaCl, dissolved in sdH_2O

TAE buffer: 242g Tris dissolved in 500 mL sdH_2O, 100 mL 0.5 M EDTA (pH 8.0), 57.1 mL glacial acetic acid, made up to 1 L with sdH_2O

TfbI: 50 mM Manganese chloride, 30 mM potassium acetate, 10 mM calcium chloride, 100 mM rhubidium chloride, 15 % glycerol, pH adjusted to 5.8 using acetic acid (dilute), made up in sdH_2O

TfbII: 10 mM rhubidium chloride, 75 mM calcium chloride, 10 mM MOPS, 15% glycerol, pH adjusted to 6.5 with NaOH, made up in sdH_2O

Sodium acetate (3 M): 408.24 g/L sodium acetate dissolved in sdH_2O, pH adjusted to 5.2 with glacial acetic acid

Solution I: 20 mL 0.5 M glucose, 5 mL 1 M Tris HCl, 4 mL 0.5 M EDTA, made up to 200 mL with sdH_2O

Solution II: 1 mL 10 M NaOH, 2.5 mL 10 % SDS, made up to 25 mL with sdH_2O

Solution III: 60 mL potassium acetate, 11.5 mL glacial acetic acid, made up to 100 mL with sdH_2O

Southern Blot solutions

SSC (20 ×): 3M NaCl, 0.3M sodium citrate in sdH_2O

Maleic acid buffer: 116.1 g maleic acid powder, 87. 66 g NaCl, pH 7.5 with NaOH pellets, make up to 1 L with sdH_2O

Detection buffer: 0.1 M Tris-HCl, 0.1 M NaCl in sdH_2O (pH 9.5)

Antibody solution (Roche): Dilute 1 in 10 000 in blocking solution

CSPD (Roche): Disodium 2-chloro-5-(4-methoxyspiro (2-dioxetane-3,2 (2-dioxetane-3,2'-(5'-chloro)-tricyclo[3.3.1.1. 3, 7.]decan)-. 4-yl)-1-phenyl phosphate

Yeast solutions

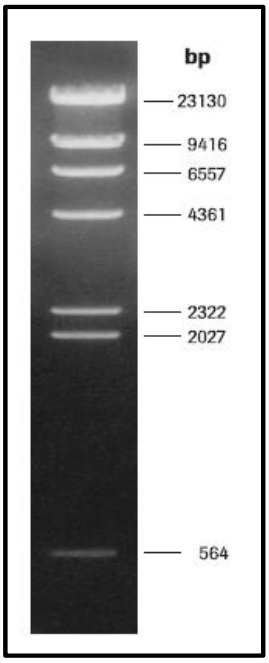
PEG/LiAC: 8 mL 50 % PEG 4000, 1 mL 10 × TE buffer, 1 mL 10 × LiAC

LiAC (10 ×): 1 M lithium acetate, pH adjusted to 7.5 with acetic acid (dilute)

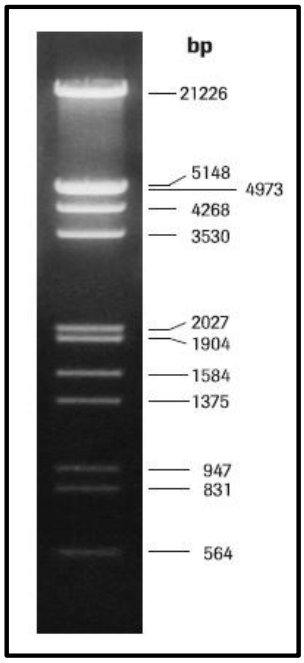
X-α-Gal: 20 mg/mL X-α-Gal dissolved in DMF

Appendix B: Molecular weight Markers

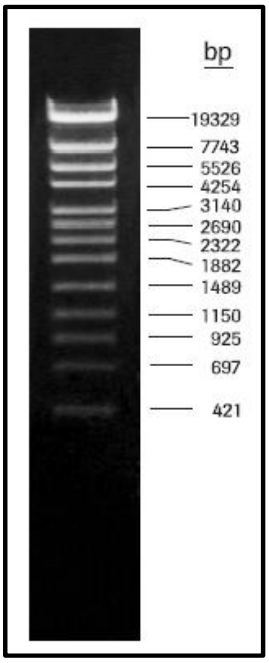
DNA molecular weight marker II



DNA molecular weight marker III



DNA molecular weight marker IV



Appendix C: Primers

Table C 1: Primers used to check site-specific integration of pMC1s

Primer	Sequence 5'- 3'	Amplicon
attL2	CTTGGATCCTCCCGCTGCGC	282 bp
attBS1	ACGTGGCGGTCCCTACCG	
attBS2	ACAGGATTTGAACCTGCGGC	320 bp
attL4	AATTCTTGCAGACCCCTGGA	

Appendix D: Library and Yeast Mating

Library Transformation Efficiency

Transformation efficiency (TE) = $\frac{no.of\ colonies\ on\ plate}{ηg\ of\ DNA\ plated}\ x\ 1000\ ηg/μg$

Yeast Mating Zygote formation

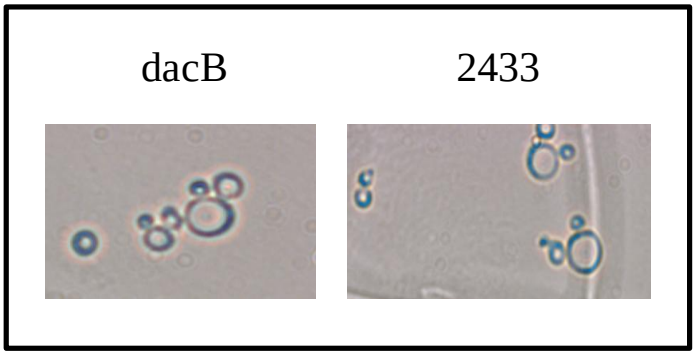


Figure D1: Image of zygote formation during yeast mating experiment, indicating the occurrence of mating of the yeast strains. Image was taken using a light microscope at 40 × magnification.

Calculations

Viability = No. of colonies (CFU) × Resuspension volume (mL) × Plating volume (mL) × Dilution factor

Mating efficiency $= \frac{No.of\ CFU/ml\ of\ diploids}{No.of\ CFU/ml\ of\ limiting\ partner}\ x\ 100$

= % diploids

DacB:

Prey viability = 207 × 12 × 10 × 1000
= 2.5×10^7 CFU/mL

Viability of diploids = 22 × 12 × 10 × 100
= 2.6×10^5 CFU/mL

Mating efficiency $= \frac{2.6 \times 10\text{^}5}{2.5 \times 10\text{^}7}\ x\ 100$
= 1.0 %

MSMEG_2433:

Prey viability = 218 × 12 × 10 × 1000
= 2.6×10^7 CFU/mL

Viability of diploids = 20 × 12 × 10 × 100
= 2.4×10^5 CFU/mL

Mating efficiency $= \frac{2.4 \times 10\text{^}5}{2.6 \times 10\text{^}7}\ x\ 100$
= 1.0 %

Appendix E: PCR confirmation of clones

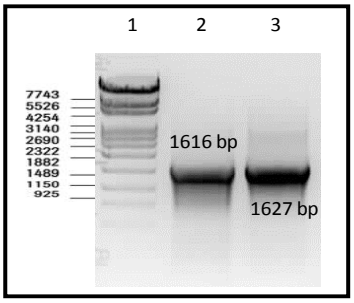


Figure E1: PCR of pSE2433-rsEGFP and pSE2433-Venus clones from *M. smegmatis* colony boil. Lane 1: Marker IV, Lane 2: *M. smegmatis* pSE100::2433_rseGFP clone C8, Lane 3: *M. smegmatis* pSE2433-Venus clone C8. Expected band: **1616bp**

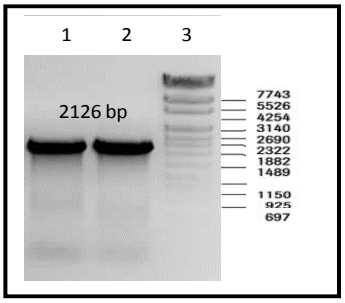


Figure E2: PCR of pSE*dacB*-mCherry clones from *M. smegmatis* colony boil. Lane 1: *M. smegmatis* clone C5, Lane 2: *M. smegmatis* clone C8, Lane 3: Marker IV. Expected size of PCR band: **2126bp**

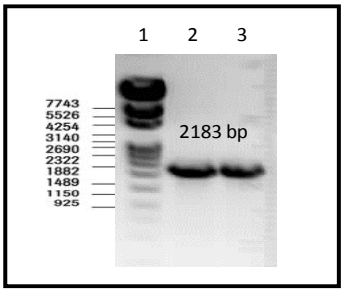


Figure E3: PCR of pSE*dacB*-Venus clone from *M. smegmatis* colony boil. Lane 1: Marker IV, Lane 2: *M. smegmatis* clone C3(i), Lane 3: *M. smegmatis* clone C3(ii). Expected band: **2183bp**

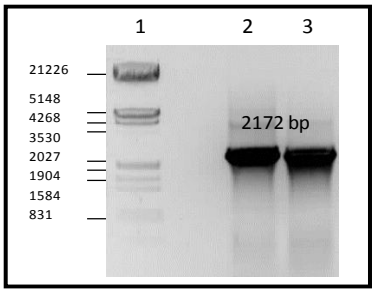


Figure E4: PCR of pSE*dacB*-rseGFP clones from *M. smegmatis* colony boil. Lane 1: Marker III, Lane 2: *M. smegmatis* clone C1, Lane 3: *M. smegmatis* clone C2. Expected band: **2172bp**

Appendix F: Repeated restriction digests

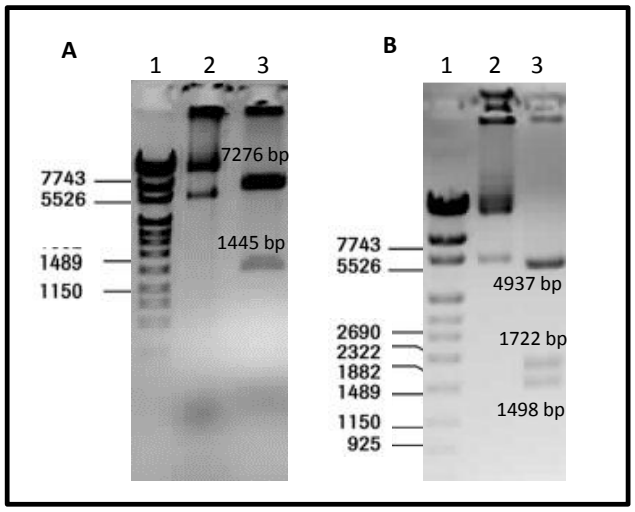


Figure F1: Repeated restriction digest of pGBKdacB and pGBK2433. **(A)** *Bam*HI + *Nde*I digest of pGBKdacB. **[Lane 1]** Roche marker IV, **[Lane 2]** uncut pGBKdacB, **[Lane 3]** *Bam*HI + *Nde*I. **(B)** *Hin*DIII digest of pGBK2433. **[Lane 1]** Roche marker IV, **[Lane 2]** uncut pGBK2433, **[Lane 3]** *Hin*DIII.

6. References

ADAMS, D. W. & ERRINGTON, J. 2009. Bacterial cell division: assembly, maintenance and disassembly of the Z ring. *Nat Rev Microbiol,* 7**,** 642-53.

AHO, S., ARFFMAN, A., PUMMI, T. & UITTO, J. 1997. A novel reporter gene MEL1 for the yeast two-hybrid system. *Anal Biochem,* 253**,** 270-2.

ALDRIDGE, B. B., FERNANDEZ-SUAREZ, M., HELLER, D., AMBRAVANESWARAN, V., IRIMIA, D., TONER, M. & FORTUNE, S. M. 2012. Asymmetry and aging of mycobacterial cells lead to variable growth and antibiotic susceptibility. *Science,* 335**,** 100-4.

ANDERSON, R. J., GROUNDWATER, P. W., TODD, A. & WORSLEY, A. J. 2012. Microorganisms. *In:* JOHN WILEY & SONS, L. (ed.) *Antimicrobial agents: Chemistry, Mode of action, Mechanisms of resistance and Clinical applications.* First ed.: John Wiley & Sons, Ltd.

ANUCHIN, A. M., MULYUKIN, A. L., SUZINA, N. E., DUDA, V. I., EL-REGISTAN, G. I. & KAPRELYANTS, A. S. 2009. Dormant forms of *Mycobacterium smegmatis* with distinct morphology. *Microbiology,* 155**,** 1071-9.

ATRIH, A., BACHER, G., ALLMAIER, G., WILLIAMSON, M. P. & FOSTER, S. J. 1999. Analysis of peptidoglycan structure from vegetative cells of *Bacillus subtilis* 168 and role of PBP 5 in peptidoglycan maturation. *J Bacteriol,* 181**,** 3956-66.

BANZHAF, M., VAN SAPAROEA, B. B., TERRAK, M., FRAIPONT, C., EGAN, A., PHILIPPE, J., ZAPUN, A., BREUKINK, E., NGUYEN-DISTECHE, M., DEN BLAAUWEN, T. & VOLLMER, W. 2012. Cooperativity of peptidoglycan synthases active in bacterial cell elongation. *Mol Biol,* 85**,** 179-194.

BASSO, L. A., DA SILVA, L. H., FETT-NETO, A. G., DE AZEVEDO, W. F., JR., MOREIRA IDE, S., PALMA, M. S., CALIXTO, J. B., ASTOLFI FILHO, S., DOS SANTOS, R. R., SOARES, M. B. & SANTOS, D. S. 2005. The use of biodiversity as source of new chemical entities against defined molecular targets for treatment of malaria, tuberculosis, and T-cell mediated diseases--a review. *Mem Inst Oswaldo Cruz,* 100**,** 475-506.

BASU, J., CHATTOPADHYAY, R., KUNDU, M. & CHAKRABARTI, P. 1992. Purification and partial characterization of a penicillin-binding protein from *Mycobacterium smegmatis*. *J Bacteriol,* 174**,** 4829-32.

BASU, J., MAHAPATRA, S., KUNDU, M., MUKHOPADHYAY, S., NGUYEN-DISTECHE, M., DUBOIS, P., JORIS, B., VAN BEEUMEN, J., COLE, S. T., CHAKRABARTI, P. & GHUYSEN, J. M. 1996. Identification and overexpression in *Escherichia coli* of a *Mycobacterium leprae* gene, *pon1*, encoding a high-molecular-mass class A penicillin-binding protein, PBP1. *J Bacteriol,* 178**,** 1707-11.

BI, E. F. & LUTKENHAUS, J. 1991. FtsZ ring structure associated with division in *Escherichia coli*. *Nature,* 354**,** 161-4.

BILLMAN-JACOBE, H., HAITES, R. E. & COPPEL, R. L. 1999. Characterization of a *Mycobacterium smegmatis* mutant lacking penicillin binding protein 1. *Antimicrob Agents Chemother,* 43**,** 3011-3.

BOSHOFF, H. I. & BARRY, C. E., 3RD 2006. Is the mycobacterial cell wall a hopeless drug target for latent tuberculosis? *Drug Discovery Today: Disease Mechanisms,* 3**,** 237 - 245.

BOTH, D., SCHNEIDER, G. & SCHNELL, R. 2011. Peptidoglycan remodeling in *Mycobacterium tuberculosis*: comparison of structures and catalytic activities of RipA and RipB. *J Mol Biol,* 413**,** 247-60.

BOURAI, N., JACOBS, W. R., JR. & NARAYANAN, S. 2012. Deletion and overexpression studies on DacB2, a putative low molecular mass penicillin binding protein from *Mycobacterium tuberculosis* H(37)Rv. *Microb Pathog,* 52**,** 109-16.

BRAMBILLA, L., MORAN-BARRIO, J. & VIALE, A. M. 2014. Low-molecular-mass penicillin binding protein 6b (DacD) is required for efficient GOB-18 metallo-beta-lactamase biogenesis in *Salmonella enterica* and *Escherichia coli*. *Antimicrob Agents Chemother,* 58**,** 205-11.

BRENNAN, P. J. 2003. Structure, function, and biogenesis of the cell wall of *Mycobacterium tuberculosis*. *Tuberculosis (Edinb),* 83**,** 91-7.

BRENNAN, P. J. & NIKAIDO, H. 1995. The envelope of mycobacteria. *Annu Rev Biochem,* 64**,** 29-63.

BUCHANAN, C. E. & LING, M. L. 1992. Isolation and sequence analysis of *dacB*, which encodes a sporulation-specific penicillin-binding protein in *Bacillus subtilis*. *J Bacteriol,* 174**,** 1717-25.

CABEEN, M. T. & JACOBS-WAGNER, C. 2005. Bacterial cell shape. *Nat Rev Microbiol,* 3**,** 601-10.

CAVA, F., KURU, E., BRUN, Y. V. & DE PEDRO, M. A. 2013. Modes of cell wall growth differentiation in rod-shaped bacteria. *Curr Opin Microbiol,* 16**,** 731-7.

CHAO, M. C., KIESER, K. J., MINAMI, S., MAVRICI, D., ALDRIDGE, B. B., FORTUNE, S. M., ALBER, T. & RUBIN, E. J. 2013. Protein complexes and proteolytic activation of the cell wall hydrolase RipA regulate septal resolution in mycobacteria. *PLoS Pathog,* 9**,** e1003197.

CHAO, M. C. & RUBIN, E. J. 2010. Letting sleeping dos lie: does dormancy play a role in tuberculosis? *Annu Rev Microbiol,* 64**,** 293-311.

CHOWDHURY, C., KAR, D., DUTTA, M., KUMAR, A. & GHOSH, A. S. 2012. Moderate deacylation efficiency of DacD explains its ability to partially restore beta-lactam resistance in *Escherichia coli* PBP5 mutant. *FEMS Microbiol Lett,* 337**,** 73-80.

CLAESSEN, D., EMMINS, R., HAMOEN, L. W., DANIEL, R. A., ERRINGTON, J. & EDWARDS, D. H. 2008. Control of the cell elongation-division cycle by shuttling of PBP1 protein in *Bacillus subtilis*. *Mol Microbiol,* 68**,** 1029-46.

COHEN-GONSAUD, M., BARTHE, P., BAGNERIS, C., HENDERSON, B., WARD, J., ROUMESTAND, C. & KEEP, N. H. 2005. The structure of a resuscitation-promoting factor domain from *Mycobacterium tuberculosis* shows homology to lysozymes. *Nat Struct Mol Biol,* 12**,** 270-3.

COLE, S. T., BROSCH, R., PARKHILL, J., GARNIER, T., CHURCHER, C., HARRIS, D., GORDON, S. V., EIGLMEIER, K., GAS, S., BARRY, C. E., 3RD, TEKAIA, F., BADCOCK, K., BASHAM, D., BROWN, D., CHILLINGWORTH, T., CONNOR, R., DAVIES, R., DEVLIN, K., FELTWELL, T., GENTLES, S., HAMLIN, N., HOLROYD, S., HORNSBY, T., JAGELS, K., KROGH, A., MCLEAN, J., MOULE, S., MURPHY, L., OLIVER, K., OSBORNE, J., QUAIL, M. A., RAJANDREAM, M. A., ROGERS, J., RUTTER, S., SEEGER, K., SKELTON, J., SQUARES, R., SQUARES, S., SULSTON, J. E., TAYLOR, K., WHITEHEAD, S. & BARRELL, B. G. 1998. Deciphering the biology of *Mycobacterium tuberculosis* from the complete genome sequence. *Nature,* 393**,** 537-44.

CRICK, D. C., MAHAPATRA, S. & BRENNAN, P. J. 2001. Biosynthesis of the arabinogalactan-peptidoglycan complex of *Mycobacterium tuberculosis*. *Glycobiology,* 11**,** 107R-118R.

DASGUPTA, A., DATTA, P., KUNDU, M. & BASU, J. 2006. The serine/threonine kinase PknB of *Mycobacterium tuberculosis* phosphorylates PBPA, a penicillin-binding protein required for cell division. *Microbiology,* 152**,** 493-504.

DATTA, P., DASGUPTA, A., BHAKTA, S. & BASU, J. 2002. Interaction between FtsZ and FtsW of *Mycobacterium tuberculosis*. *J Biol Chem,* 277**,** 24983-7.

DATTA, P., DASGUPTA, A., SINGH, A. K., MUKHERJEE, P., KUNDU, M. & BASU, J. 2006. Interaction between FtsW and penicillin-binding protein 3 (PBP3) directs PBP3 to mid-cell, controls cell septation and mediates the formation of a trimeric complex involving FtsZ, FtsW and PBP3 in mycobacteria. *Mol Microbiol,* 62**,** 1655-73.

DEB, C., LEE, C. M., DUBEY, V. S., DANIEL, J., ABOMOELAK, B., SIRAKOVA, T. D., PAWAR, S., ROGERS, L. & KOLATTUKUDY, P. E. 2009. A novel in vitro multiple-stress dormancy model for *Mycobacterium tuberculosis* generates a lipid-loaded, drug-tolerant, dormant pathogen. *PLoS One,* 4**,** e6077.

DEPARDIEU, F., PODGLAJEN, I., LECLERCQ, R., COLLATZ, E. & COURVALIN, P. 2007. Modes and modulations of antibiotic resistance gene expression. *Clin Microbiol Rev,* 20**,** 79-114.

DIACON, A. H., DAWSON, R., VON GROOTE-BIDLINGMAIER, F., SYMONS, G., VENTER, A., DONALD, P. R., VAN NIEKERK, C., EVERITT, D., WINTER, H., BECKER, P., MENDEL, C. M. & SPIGELMAN, M. K. 2012a. 14-day bactericidal activity of PA-824, bedaquiline, pyrazinamide, and moxifloxacin combinations: a randomised trial. *Lancet,* 380**,** 986-93.

DIACON, A. H., DONALD, P. R., PYM, A., GROBUSCH, M., PATIENTIA, R. F., MAHANYELE, R., BANTUBANI, N., NARASIMOOLOO, R., DE MAREZ, T., VAN HEESWIJK, R., LOUNIS, N., MEYVISCH, P., ANDRIES, K. & MCNEELEY, D. F. 2012b. Randomized pilot trial of eight weeks of bedaquiline (TMC207) treatment for multidrug-resistant tuberculosis: long-term outcome, tolerability, and effect on emergence of drug resistance. *Antimicrob Agents Chemother,* 56**,** 3271-6.

DIETRICH, J., LUNDBERG, C. V. & ANDERSEN, P. 2006. TB vaccine strategies--what is needed to solve a complex problem? *Tuberculosis (Edinb),* 86**,** 163-8.

DOMENECH, P., REED, M. B. & BARRY, C. E., 3RD 2005. Contribution of the *Mycobacterium tuberculosis* MmpL protein family to virulence and drug resistance. *Infect Immun,* 73**,** 3492-501.

DORHOI, A., REECE, S. T. & KAUFMANN, S. H. 2011. For better or for worse: the immune response against *Mycobacterium tuberculosis* balances pathology and protection. *Immunol Rev,* 240**,** 235-51.

DORMAN, S. E., GOLDBERG, S., STOUT, J. E., MUZANYI, G., JOHNSON, J. L., WEINER, M., BOZEMAN, L., HEILIG, C. M., FENG, P. J., MORO, R., NARITA, M., NAHID, P., RAY, S., BATES, E., HAILE, B., NUERMBERGER, E. L., VERNON, A., SCHLUGER, N. W. & TUBERCULOSIS TRIALS, C. 2012. Substitution of rifapentine for rifampin during intensive phase treatment of pulmonary tuberculosis: study 29 of the tuberculosis trials consortium. *J Infect Dis,* 206**,** 1030-40.

DOUGHERTY, T. J. & PUCCI, M. J. 1994. Penicillin-binding proteins are regulated by *rpoS* during transitions in growth states of *Escherichia coli*. *Antimicrob Agents Chemother,* 38**,** 205-10.

DOWNING, K. J., MISCHENKO, V. V., SHLEEVA, M. O., YOUNG, D. I., YOUNG, M., KAPRELYANTS, A. S., APT, A. S. & MIZRAHI, V. 2005. Mutants of *Mycobacterium tuberculosis* lacking three of the five rpf-like genes are defective for growth in vivo and for resuscitation in vitro. *Infect Immun,* 73**,** 3038-43.

DUCATI, R. G., RUFFINO-NETTO, A., BASSO, L. A. & SANTOS, D. S. 2006. The resumption of consumption -- a review on tuberculosis. *Mem Inst Oswaldo Cruz,* 101**,** 697-714.

DUEZ, C., VANHOVE, M., GALLET, X., BOUILLENNE, F., DOCQUIER, J., BRANS, A. & FRERE, J. 2001. Purification and characterization of PBP4a, a new low-molecular-weight penicillin-binding protein from *Bacillus subtilis*. *J Bacteriol,* 183**,** 1595-9.

DWORKIN, J. & SHAH, I. M. 2010. Exit from dormancy in microbial organisms. *Nat Rev Microbiol,* 8**,** 890-6.

EHRT, S., GUO, X. V., HICKEY, C. M., RYOU, M., MONTELEONE, M., RILEY, L. W. & SCHNAPPINGER, D. 2005. Controlling gene expression in mycobacteria with anhydrotetracycline and Tet repressor. *Nucleic Acids Res,* 33**,** e21.

FARNIA, P., MOHAMMAD, R. M., MERZA, M. A., TABARSI, P., ZHAVNERKO, G. K., IBRAHIM, T. A., KUAN, H. O., GHANAVEI, J., FARNIA, P., RANJBAR, R., POLESCHUYK, N. N., TITOV, L. P., OWLIA, P., KAZAMPOUR, M., SETAREH, M., SHEIKOLSLAMI, M., MIGLIORI, G. B. & VELAYATI, A. A. 2010. Growth and cell-division in extensive (XDR) and extremely drug resistant (XXDR) tuberculosis strains: transmission and atomic force observation. *Int J Clin Exp Med,* 3**,** 308-14.

FINE, P., CARNEIRO, IAM, MILSTIEN, JB, CLEMENTS, CJ 1999. Issues relating to the use of BCG in immunization programmes. *WHO***,** 45.

FLYNN, J. L. & CHAN, J. 2001. Tuberculosis: latency and reactivation. *Infect Immun,* 69**,** 4195-201.

FOGEL, M. A. & WALDOR, M. K. 2006. A dynamic, mitotic-like mechanism for bacterial chromosome segregation. *Genes Dev,* 20**,** 3269-82.

FOULQUIER, E., POMPEO, F., FRETON, C., CORDIER, B., GRANGEASSE, C. & GALINIER, A. 2014. PrkC-mediated phosphorylation of overexpressed YvcK protein regulates PBP1 protein localization in *Bacillus subtilis mreB* mutant cells. *J Biol Chem,* 289**,** 23662-9.

FRIRDICH, E. & GAYNOR, E. C. 2013. Peptidoglycan hydrolases, bacterial shape, and pathogenesis. *Curr Opin Microbiol,* 16**,** 767-78.

GANDHI, N. R., MOLL, A., STURM, A. W., PAWINSKI, R., GOVENDER, T., LALLOO, U., ZELLER, K., ANDREWS, J. & FRIEDLAND, G. 2006. Extensively drug-resistant tuberculosis as a cause of death in patients co-infected with tuberculosis and HIV in a rural area of South Africa. *Lancet,* 368**,** 1575-80.

GEBHARDT, H., MENICHE, X., TROPIS, M., KRAMER, R., DAFFE, M. & MORBACH, S. 2007. The key role of the mycolic acid content in the functionality of the cell wall permeability barrier in *Corynebacterineae*. *Microbiology,* 153**,** 1424-34.

GEE, C. L., PAPAVINASASUNDARAM, K. G., BLAIR, S. R., BAER, C. E., FALICK, A. M., KING, D. S., GRIFFIN, J. E., VENGHATAKRISHNAN, H., ZUKAUSKAS, A., WEI, J. R., DHIMAN, R. K., CRICK, D. C., RUBIN, E. J., SASSETTI, C. M. & ALBER, T. 2012. A phosphorylated pseudokinase complex controls cell wall synthesis in mycobacteria. *Sci Signal,* 5**,** ra7.

GHOSH, A. S., CHOWDHURY, C. & NELSON, D. E. 2008. Physiological functions of D-alanine carboxypeptidases in *Escherichia coli*. *Trends Microbiol,* 16**,** 309-17.

GHOSH, A. S. & YOUNG, K. D. 2003. Sequences near the active site in chimeric penicillin binding proteins 5 and 6 affect uniform morphology of *Escherichia coli*. *J Bacteriol,* 185**,** 2178-86.

GHOSH, J., LARSSON, P., SINGH, B., PETTERSSON, B. M., ISLAM, N. M., SARKAR, S. N., DASGUPTA, S. & KIRSEBOM, L. A. 2009. Sporulation in mycobacteria. *Proc Natl Acad Sci U S A,* 106**,** 10781-6.

GHUYSEN, J. M. 1991. Serine beta-lactamases and penicillin-binding proteins. *Annu Rev Microbiol,* 45**,** 37-67.

GINDA, K., BEZULSKA, M., ZIOLKIEWICZ, M., DZIADEK, J., ZAKRZEWSKA-CZERWINSKA, J. & JAKIMOWICZ, D. 2013. ParA of *Mycobacterium smegmatis* co-ordinates chromosome segregation with the cell cycle and interacts with the polar growth determinant DivIVA. *Mol Microbiol,* 87**,** 998-1012.

GLICKMAN, M. S. & JACOBS, W. R., JR. 2001. Microbial pathogenesis of *Mycobacterium tuberculosis*: dawn of a discipline. *Cell,* 104**,** 477-85.

GOMEZ, J. E. & MCKINNEY, J. D. 2004. *M. tuberculosis* persistence, latency, and drug tolerance. *Tuberculosis (Edinb),* 84**,** 29-44.

GONDRE, B., FLOURET, B. & VAN HEIJENOORT, J. 1973. Release of D-alanyl-D-alanine from the precursor of the cell wall peptidoglycan by a peptidase of *Escherichia coli* K 12. *Biochimie,* 55**,** 685-91.

GRIFFIN, J. E., GAWRONSKI, J. D., DEJESUS, M. A., IOERGER, T. R., AKERLEY, B. J. & SASSETTI, C. M. 2011. High-resolution phenotypic profiling defines genes essential for mycobacterial growth and cholesterol catabolism. *PLoS Pathog,* 7**,** e1002251.

GROTJOHANN, T., TESTA, I., LEUTENEGGER, M., BOCK, H., URBAN, N. T., LAVOIE-CARDINAL, F., WILLIG, K. I., EGGELING, C., JAKOBS, S. & HELL, S. W. 2011. Diffraction-unlimited all-optical imaging and writing with a photochromic GFP. *Nature,* 478**,** 204-8.

GUO, X. V., MONTELEONE, M., KLOTZSCHE, M., KAMIONKA, A., HILLEN, W., BRAUNSTEIN, M., EHRT, S. & SCHNAPPINGER, D. 2007. Silencing *Mycobacterium smegmatis* by using tetracycline repressors. *J Bacteriol,* 189**,** 4614-23.

GUPTA, R., LAVOLLAY, M., MAINARDI, J. L., ARTHUR, M., BISHAI, W. R. & LAMICHHANE, G. 2010. The *Mycobacterium tuberculosis* protein LdtMt2 is a nonclassical transpeptidase required for virulence and resistance to amoxicillin. *Nat Med,* 16**,** 466-9.

GUPTA, R. K. & SRIVASTAVA, R. 2012. Resuscitation promoting factors: a family of microbial proteins in survival and resuscitation of dormant mycobacteria. *Indian J Microbiol,* 52**,** 114-21.

HAINFELD, J. F., SPRINZL, M., MANDIYAN, V., TUMMINIA, S. J. & BOUBLIK, M. 1991. Localization of a specific nucleotide in yeast tRNA by scanning transmission electron microscopy using an undecagold cluster. *J Struct Biol,* 107**,** 1-5.

HAMMES, W. P. & SEIDEL, H. 1978. The activities in vitro of DD-carboxypeptidase and LD-carboxypeptidase of *Gaffkya homari* during biosynthesis of peptidoglycan. *Eur J Biochem,* 84**,** 141-7.

HAMPSHIRE, T., SONEJI, S., BACON, J., JAMES, B. W., HINDS, J., LAING, K., STABLER, R. A., MARSH, P. D. & BUTCHER, P. D. 2004. Stationary phase gene expression of *Mycobacterium tuberculosis* following a progressive nutrient depletion: a model for persistent organisms? *Tuberculosis (Edinb),* 84**,** 228-38.

HARPER, J. W., ADAMI, G. R., WEI, N., KEYOMARSI, K. & ELLEDGE, S. J. 1993. The p21 Cdk-interacting protein Cip1 is a potent inhibitor of G1 cyclin-dependent kinases. *Cell,* 75**,** 805-16.

HEIDRICH, C., TEMPLIN, M. F., URSINUS, A., MERDANOVIC, M., BERGER, J., SCHWARZ, H., DE PEDRO, M. A. & HOLTJE, J. V. 2001. Involvement of N-acetylmuramyl-L-alanine amidases in cell separation and antibiotic-induced autolysis of *Escherichia coli*. *Mol Microbiol,* 41**,** 167-78.

HETT, E. C., CHAO, M. C., DENG, L. L. & RUBIN, E. J. 2008. A mycobacterial enzyme essential for cell division synergizes with resuscitation-promoting factor. *PLoS Pathog,* 4**,** e1000001.

HETT, E. C., CHAO, M. C. & RUBIN, E. J. 2010. Interaction and modulation of two antagonistic cell wall enzymes of mycobacteria. *PLoS Pathog,* 6**,** e1001020.

HETT, E. C., CHAO, M. C., STEYN, A. J., FORTUNE, S. M., DENG, L. L. & RUBIN, E. J. 2007. A partner for the resuscitation-promoting factors of *Mycobacterium tuberculosis*. *Mol Microbiol,* 66**,** 658-68.

HETT, E. C. & RUBIN, E. J. 2008. Bacterial growth and cell division: a mycobacterial perspective. *Microbiol Mol Biol Rev,* 72**,** 126-56, table of contents.

HU, Z. & LUTKENHAUS, J. 2000. Analysis of MinC reveals two independent domains involved in interaction with MinD and FtsZ. *J Bacteriol,* 182**,** 3965-71.

HUNG, W. C., JANE, W. N. & WONG, H. C. 2013. Association of a D-alanyl-D-alanine carboxypeptidase gene with the formation of aberrantly shaped cells during the induction of viable but nonculturable *Vibrio parahaemolyticus*. *Appl Environ Microbiol,* 79**,** 7305-12.

HWANG, J. S., TAKAKU, Y., CHAPMAN, J., IKEO, K., DAVID, C. N. & GOJOBORI, T. 2008. Cilium evolution: identification of a novel protein, nematocilin, in the mechanosensory cilium of *Hydra* nematocytes. *Mol Biol Evol,* 25**,** 2009-17.

JACOBS, C. & SHAPIRO, L. 1999. Bacterial cell division: a moveable feast. *Proc Natl Acad Sci U S A,* 96**,** 5891-3.

JAMES, P., HALLADAY, J. & CRAIG, E. A. 1996. Genomic libraries and a host strain designed for highly efficient two-hybrid selection in yeast. *Genetics,* 144**,** 1425-36.

JANI, C., EOH, H., LEE, J. J., HAMASHA, K., SAHANA, M. B., HAN, J. S., NYAYAPATHY, S., LEE, J. Y., SUH, J. W., LEE, S. H., REHSE, S. J., CRICK, D. C. & KANG, C. M. 2010. Regulation of polar peptidoglycan biosynthesis by Wag31 phosphorylation in mycobacteria. *BMC Microbiol,* 10**,** 327.

JARLIER, V. & NIKAIDO, H. 1994. Mycobacterial cell wall: structure and role in natural resistance to antibiotics. *FEMS Microbiol Lett,* 123**,** 11-8.

JONES, L. J., CARBALLIDO-LOPEZ, R. & ERRINGTON, J. 2001. Control of cell shape in bacteria: helical, actin-like filaments in *Bacillus subtilis*. *Cell,* 104**,** 913-22.

JOYCE, G., WILLIAMS, K. J., ROBB, M., NOENS, E., TIZZANO, B., SHAHREZAEI, V. & ROBERTSON, B. D. 2012. Cell division site placement and asymmetric growth in mycobacteria. *PLoS One,* 7**,** e44582.

KAKKAR, A. K. & DAHIYA, N. 2014. Bedaquiline for the treatment of resistant tuberculosis: Promises and pitfalls. *Tuberculosis (Edinb),* 94**,** 357-362.

KANA, B. D., GORDHAN, B. G., DOWNING, K. J., SUNG, N., VOSTROKTUNOVA, G., MACHOWSKI, E. E., TSENOVA, L., YOUNG, M., KAPRELYANTS, A., KAPLAN, G. & MIZRAHI, V. 2008. The

resuscitation-promoting factors of *Mycobacterium tuberculosis* are required for virulence and resuscitation from dormancy but are collectively dispensable for growth in vitro. *Mol Microbiol,* 67**,** 672-84.

KANA, B. D. & MIZRAHI, V. 2010. Resuscitation-promoting factors as lytic enzymes for bacterial growth and signaling. *FEMS Immunol Med Microbiol,* 58**,** 39-50.

KANG, C. M., NYAYAPATHY, S., LEE, J. Y., SUH, J. W. & HUSSON, R. N. 2008. Wag31, a homologue of the cell division protein DivIVA, regulates growth, morphology and polar cell wall synthesis in mycobacteria. *Microbiology,* 154**,** 725-35.

KUMAR, P., ARORA, K., LLOYD, J. R., LEE, I. Y., NAIR, V., FISCHER, E., BOSHOFF, H. I. & BARRY, C. E., 3RD 2012. Meropenem inhibits D,D-carboxypeptidase activity in *Mycobacterium tuberculosis*. *Mol Microbiol,* 86**,** 367-81.

LAVOLLAY, M., ARTHUR, M., FOURGEAUD, M., DUBOST, L., MARIE, A., VEZIRIS, N., BLANOT, D., GUTMANN, L. & MAINARDI, J. L. 2008. The peptidoglycan of stationary-phase *Mycobacterium tuberculosis* predominantly contains cross-links generated by L,D-transpeptidation. *J Bacteriol,* 190**,** 4360-6.

LAVOLLAY, M., FOURGEAUD, M., HERRMANN, J. L., DUBOST, L., MARIE, A., GUTMANN, L., ARTHUR, M. & MAINARDI, J. L. 2011. The peptidoglycan of *Mycobacterium abscessus* is predominantly cross-linked by L,D-transpeptidases. *J Bacteriol,* 193**,** 778-82.

LEDERER, E., ADAM, A., CIORBARU, R., PETIT, J. F. & WIETZERBIN, J. 1975. Cell walls of Mycobacteria and related organisms; chemistry and immunostimulant properties. *Mol Cell Biochem,* 7**,** 87-104.

LIAO, X. & HANCOCK, R. E. 1997. Identification of a penicillin-binding protein 3 homolog, PBP3x, in *Pseudomonas aeruginosa*: gene cloning and growth phase-dependent expression. *J Bacteriol,* 179**,** 1490-6.

LIN, M. Y. & OTTENHOFF, T. H. 2008. Not to wake a sleeping giant: new insights into host-pathogen interactions identify new targets for vaccination against latent *Mycobacterium tuberculosis* infection. *Biol. Chem,* 389**,** 497-511.

LIVERMORE, D. M. 1995. beta-Lactamases in laboratory and clinical resistance. *Clin Microbiol Rev,* 8**,** 557-84.

LUKYANOV, K. A., CHUDAKOV, D. M., LUKYANOV, S. & VERKHUSHA, V. V. 2005. Innovation: Photoactivatable fluorescent proteins. *Nat Rev Mol Cell Biol,* 6**,** 885-91.

MACHOWSKI, E. E., SENZANI, S., EALAND, C. & KANA, B. D. 2014. Comparative genomics for mycobacterial peptidoglycan remodelling enzymes reveals extensive genetic multiplicity. *BMC Microbiol,* 14**,** 75.

MAINARDI, J. L., FOURGEAUD, M., HUGONNET, J. E., DUBOST, L., BROUARD, J. P., OUAZZANI, J., RICE, L. B., GUTMANN, L. & ARTHUR, M. 2005. A novel peptidoglycan cross-linking enzyme for a beta-lactam-resistant transpeptidation pathway. *J Biol Chem,* 280**,** 38146-52.

MALONEY, E., MADIRAJU, M. & RAJAGOPALAN, M. 2009. Overproduction and localization of *Mycobacterium tuberculosis* ParA and ParB proteins. *Tuberculosis (Edinb),* 89 Suppl 1**,** S65-9.

MARKIEWICZ, Z., BROOME-SMITH, J. K., SCHWARZ, U. & SPRATT, B. G. 1982. Spherical *E. coli* due to elevated levels of D-alanine carboxypeptidase. *Nature,* 297**,** 702-4.

MARRAKCHI, H., LANEELLE, M. A. & DAFFE, M. 2014. Mycolic acids: structures, biosynthesis, and beyond. *Chem Biol,* 21**,** 67-85.

MCDERMOTT, W. 1958. Microbial persistence. *Yale J Biol Med,* 30**,** 257-91.

MCDERMOTT, W. 1959. Inapparent infection: relation of latent and dormant infections to microbial persistence. *Public Health Rep,* 74**,** 485-99.

MCKENNEY, P. T., DRIKS, A. & EICHENBERGER, P. 2013. The *Bacillus subtilis* endospore: assembly and functions of the multilayered coat. *Nat Rev Microbiol,* 11**,** 33-44.

MCNEIL, M., DAFFE, M. & BRENNAN, P. J. 1990. Evidence for the nature of the link between the arabinogalactan and peptidoglycan of mycobacterial cell walls. *J Biol Chem,* 265**,** 18200-6.

MENDELSON, N. H. 1976. Helical growth of *Bacillus subtilis*: a new model of cell growth. *Proc Natl Acad Sci U S A,* 73**,** 1740-4.

MENICHE, X., OTTEN, R., SIEGRIST, M. S., BAER, C. E., MURPHY, K. C., BERTOZZI, C. R. & SASSETTI, C. M. 2014. Subpolar addition of new cell wall is directed by DivIVA in mycobacteria. *Proc Natl Acad Sci U S A,* 111**,** E3243-51.

MIGLIORI, G. B., DE IACO, G., BESOZZI, G., CENTIS, R. & CIRILLO, D. M. 2007. First tuberculosis cases in Italy resistant to all tested drugs. *Euro Surveill,* 12**,** E070517 1.

MORLOT, C., NOIRCLERC-SAVOYE, M., ZAPUN, A., DIDEBERG, O. & VERNET, T. 2004. The D,D-carboxypeptidase PBP3 organizes the division process of *Streptococcus pneumoniae*. *Mol Microbiol,* 51**,** 1641-8.

MUKAMOLOVA, G. V., KORMER, S. S., KELL, D. B. & KAPRELYANTS, A. S. 1999. Stimulation of the multiplication of *Micrococcus luteus* by an autocrine growth factor. *Arch Microbiol,* 172**,** 9-14.

MUKAMOLOVA, G. V., MURZIN, A. G., SALINA, E. G., DEMINA, G. R., KELL, D. B., KAPRELYANTS, A. S. & YOUNG, M. 2006. Muralytic activity of *Micrococcus luteus* Rpf and its relationship to physiological activity in promoting bacterial growth and resuscitation. *Mol Microbiol,* 59**,** 84-98.

MUKAMOLOVA, G. V., TURAPOV, O., MALKIN, J., WOLTMANN, G. & BARER, M. R. 2010. Resuscitation-promoting factors reveal an occult population of tubercle Bacilli in Sputum. *Am J Respir Crit Care Med,* 181**,** 174-80.

MUKAMOLOVA, G. V., TURAPOV, O. A., YOUNG, D. I., KAPRELYANTS, A. S., KELL, D. B. & YOUNG, M. 2002. A family of autocrine growth factors in *Mycobacterium tuberculosis*. *Mol Microbiol,* 46**,** 623-35.

MUKAMOLOVA, G. V., YANOPOLSKAYA, N. D., KELL, D. B. & KAPRELYANTS, A. S. 1998. On resuscitation from the dormant state of *Micrococcus luteus*. *Antonie Van Leeuwenhoek,* 73**,** 237-43.

MUKHERJEE, P., SUREKA, K., DATTA, P., HOSSAIN, T., BARIK, S., DAS, K. P., KUNDU, M. & BASU, J. 2009. Novel role of Wag31 in protection of mycobacteria under oxidative stress. *Mol Microbiol,* 73**,** 103-19.

MULLER, P., EWERS, C., BERTSCHE, U., ANSTETT, M., KALLIS, T., BREUKINK, E., FRAIPONT, C., TERRAK, M., NGUYEN-DISTECHE, M. & VOLLMER, W. 2007. The essential cell division protein FtsN interacts with the murein (peptidoglycan) synthase PBP1B in *Escherichia coli*. *J Biol Chem,* 282**,** 36394-402.

NELSON, D. E., GHOSH, A. S., PAULSON, A. L. & YOUNG, K. D. 2002. Contribution of membrane-binding and enzymatic domains of penicillin binding protein 5 to maintenance of uniform cellular morphology of *Escherichia coli*. *J Bacteriol,* 184**,** 3630-9.

NELSON, D. E. & YOUNG, K. D. 2000. Penicillin binding protein 5 affects cell diameter, contour, and morphology of *Escherichia coli*. *J Bacteriol,* 182**,** 1714-21.

NELSON, D. E. & YOUNG, K. D. 2001. Contributions of PBP 5 and DD-carboxypeptidase penicillin binding proteins to maintenance of cell shape in *Escherichia coli*. *J Bacteriol,* 183**,** 3055-64.

NIKITUSHKIN, V. D., DEMINA, G. R., SHLEEVA, M. O. & KAPRELYANTS, A. S. 2013. Peptidoglycan fragments stimulate resuscitation of "non-culturable" mycobacteria. *Antonie Van Leeuwenhoek,* 103**,** 37-46.

O'GARRA, A., REDFORD, P. S., MCNAB, F. W., BLOOM, C. I., WILKINSON, R. J. & BERRY, M. P. 2013. The immune response in tuberculosis. *Annu Rev Immunol,* 31**,** 475-527.

PAPP-WALLACE, K. M., ENDIMIANI, A., TARACILA, M. A. & BONOMO, R. A. 2011. Carbapenems: past, present, and future. *Antimicrob Agents Chemother,* 55**,** 4943-60.

PARK, J. T. 1995. Why does *Escherichia coli* recycle its cell wall peptides? *Mol Microbiol,* 17**,** 421-6.

PATRU, M. M. & PAVELKA, M. S., JR. 2010. A role for the class A penicillin-binding protein PonA2 in the survival of *Mycobacterium smegmatis* under conditions of nonreplication. *J Bacteriol,* 192**,** 3043-54.

PEDERSEN, L. B., MURRAY, T., POPHAM, D. L. & SETLOW, P. 1998. Characterization of DacC, which encodes a new low-molecular-weight penicillin-binding protein in *Bacillus subtilis*. *J Bacteriol,* 180**,** 4967-73.

PETREANU, L., HUBER, D., SOBCZYK, A. & SVOBODA, K. 2007. Channelrhodopsin-2-assisted circuit mapping of long-range callosal projections. *Nat Neurosci,* 10**,** 663-8.

PHAM, T. T., JACOBS-SERA, D., PEDULLA, M. L., HENDRIX, R. W. & HATFULL, G. F. 2007. Comparative genomic analysis of mycobacteriophage Tweety: evolutionary insights and construction of compatible site-specific integration vectors for mycobacteria. *Microbiology,* 153**,** 2711-23.

PINHO, M. G., KJOS, M. & VEENING, J. W. 2013. How to get (a)round: mechanisms controlling growth and division of coccoid bacteria. *Nat Rev Microbiol,* 11**,** 601-14.

PLOCINSKI, P., ARORA, N., SARVA, K., BLASZCZYK, E., QIN, H., DAS, N., PLOCINSKA, R., ZIOLKIEWICZ, M., DZIADEK, J., KIRAN, M., GORLA, P., CROSS, T. A., MADIRAJU, M. & RAJAGOPALAN, M. 2012. *Mycobacterium tuberculosis* CwsA interacts with CrgA and Wag31, and the CrgA-CwsA complex is involved in peptidoglycan synthesis and cell shape determination. *J Bacteriol,* 194**,** 6398-409.

PLOCINSKI, P., MARTINEZ, L., SARVA, K., PLOCINSKA, R., MADIRAJU, M. & RAJAGOPALAN, M. 2013. *Mycobacterium tuberculosis* CwsA overproduction modulates cell division and cell wall synthesis. *Tuberculosis (Edinb),* 93 Suppl**,** S21-7.

PLOCINSKI, P., ZIOLKIEWICZ, M., KIRAN, M., VADREVU, S. I., NGUYEN, H. B., HUGONNET, J., VECKERLE, C., ARTHUR, M., DZIADEK, J., CROSS, T. A., MADIRAJU, M. & RAJAGOPALAN, M. 2011. Characterization of CrgA, a new partner of the *Mycobacterium tuberculosis* peptidoglycan polymerization complexes. *J Bacteriol,* 193**,** 3246-56.

POPHAM, D. L., GILMORE, M. E. & SETLOW, P. 1999. Roles of low-molecular-weight penicillin-binding proteins in *Bacillus subtilis* spore peptidoglycan synthesis and spore properties. *J Bacteriol,* 181**,** 126-32.

POTLURI, L. P., DE PEDRO, M. A. & YOUNG, K. D. 2012. *Escherichia coli* low-molecular-weight penicillin-binding proteins help orient septal FtsZ, and their absence leads to asymmetric cell division and branching. *Mol Microbiol,* 84**,** 203-24.

PRIGOZHIN, D. M., MAVRICI, D., HUIZAR, J. P., VANSELL, H. J. & ALBER, T. 2013. Structural and biochemical analyses of *Mycobacterium tuberculosis* N-acetylmuramyl-L-alanine amidase Rv3717 point to a role in peptidoglycan fragment recycling. *J Biol Chem,* 288**,** 31549-55.

RAJAGOPALAN, M., MALONEY, E., DZIADEK, J., POPLAWSKA, M., LOFTON, H., CHAUHAN, A. & MADIRAJU, M. V. 2005. Genetic evidence that mycobacterial FtsZ and FtsW proteins interact, and colocalize to the division site in *Mycobacterium smegmatis*. *FEMS Microbiol Lett,* 250**,** 9-17.

RAMASWAMY, S. V., REICH, R., DOU, S. J., JASPERSE, L., PAN, X., WANGER, A., QUITUGUA, T. & GRAVISS, E. A. 2003. Single nucleotide polymorphisms in genes associated with isoniazid resistance in *Mycobacterium tuberculosis*. *Antimicrob Agents Chemother,* 47**,** 1241-50.

RAYMOND, J. B., MAHAPATRA, S., CRICK, D. C. & PAVELKA, M. S., JR. 2005. Identification of the *namH* gene, encoding the hydroxylase responsible for the N-glycolylation of the mycobacterial peptidoglycan. *J Biol Chem,* 280**,** 326-33.

RICE, L. B., BELLAIS, S., CARIAS, L. L., HUTTON-THOMAS, R., BONOMO, R. A., CASPERS, P., PAGE, M. G. & GUTMANN, L. 2004. Impact of specific *pbp5* mutations on expression of beta-lactam resistance in *Enterococcus faecium*. *Antimicrob Agents Chemother,* 48**,** 3028-32.

ROTTIG, A. & STEINBUCHEL, A. 2013. Acyltransferases in bacteria. *Microbiol Mol Biol Rev,* 77**,** 277-321.

RUGGIERO, A., TIZZANO, B., PEDONE, E., PEDONE, C., WILMANNS, M. & BERISIO, R. 2009. Crystal structure of the resuscitation-promoting factor (DeltaDUF)RpfB from *M. tuberculosis*. *J Mol Biol,* 385**,** 153-62.

RUSSELL-GOLDMAN, E., XU, J., WANG, X., CHAN, J. & TUFARIELLO, J. M. 2008. A *Mycobacterium tuberculosis* Rpf double-knockout strain exhibits profound defects in reactivation from chronic tuberculosis and innate immunity phenotypes. *Infect Immun,* 76**,** 4269-81.

SANI, M., HOUBEN, E. N., GEURTSEN, J., PIERSON, J., DE PUNDER, K., VAN ZON, M., WEVER, B., PIERSMA, S. R., JIMENEZ, C. R., DAFFE, M., APPELMELK, B. J., BITTER, W., VAN DER WEL, N. & PETERS, P. J. 2010. Direct visualization by cryo-EM of the mycobacterial capsular layer: a labile structure containing ESX-1-secreted proteins. *PLoS Pathog,* 6**,** e1000794.

SANTI, I., DHAR, N., BOUSBAINE, D., WAKAMOTO, Y. & MCKINNEY, J. D. 2013. Single-cell dynamics of the chromosome replication and cell division cycles in mycobacteria. *Nat Commun,* 4**,** 2470.

SANTOS, J. M., LOBO, M., MATOS, A. P., DE PEDRO, M. A. & ARRAIANO, C. M. 2002. The gene *bolA* regulates *dacA* (PBP5), *dacC* (PBP6) and *ampC* (AmpC), promoting normal morphology in *Escherichia coli*. *Mol Microbiol,* 45**,** 1729-40.

SARKAR, S. K., CHOWDHURY, C. & GHOSH, A. S. 2010. Deletion of penicillin-binding protein 5 (PBP5) sensitises *Escherichia coli* cells to beta-lactam agents. *Int J Antimicrob Agents,* 35**,** 244-9.

SASSETTI, C. M., BOYD, D. H. & RUBIN, E. J. 2003. Genes required for mycobacterial growth defined by high density mutagenesis. *Mol Microbiol,* 48**,** 77-84.

SAUVAGE, E., KERFF, F., TERRAK, M., AYALA, J. A. & CHARLIER, P. 2008. The penicillin-binding proteins: structure and role in peptidoglycan biosynthesis. *FEMS Microbiol Rev,* 32**,** 234-58.

SCHOMBURG, D. & SALZMANN, M. 1991. N-Acetylmuramoyl-L-alanine amidase. *In:* HEIDELBERG, S. B. (ed.) *Enzyme Handbook 4.* Springer Berlin Heidelberg.

SCHOONMAKER, M. K., BISHAI, W. R. & LAMICHHANE, G. 2014. Nonclassical transpeptidases of *Mycobacterium tuberculosis* alter cell size, morphology, the cytosolic matrix, protein localization, virulence, and resistance to beta-lactams. *J Bacteriol,* 196**,** 1394-402.

SENZANI, S. & KANA, B. D. Unpublished. Ami1 and Ami2 of *Mycobacterium smegmatis*. CBTBR, Univeristy of Witwatersrand, NHLS.

SEVERIN, A., SCHUSTER, C., HAKENBECK, R. & TOMASZ, A. 1992. Altered murein composition in a DD-carboxypeptidase mutant of *Streptococcus pneumoniae*. *J Bacteriol,* 174**,** 5152-5.

SHAH, I. M., LAABERKI, M. H., POPHAM, D. L. & DWORKIN, J. 2008. A eukaryotic-like Ser/Thr kinase signals bacteria to exit dormancy in response to peptidoglycan fragments. *Cell,* 135**,** 486-96.

SHANER, N. C., CAMPBELL, R. E., STEINBACH, P. A., GIEPMANS, B. N., PALMER, A. E. & TSIEN, R. Y. 2004. Improved monomeric red, orange and yellow fluorescent proteins derived from *Discosoma sp.* red fluorescent protein. *Nat Biotechnol,* 22**,** 1567-72.

SHANER, N. C., STEINBACH, P. A. & TSIEN, R. Y. 2005. A guide to choosing fluorescent proteins. *Nat Methods,* 2**,** 905-9.

SHLEEVA, M., MUKAMOLOVA, G. V., YOUNG, M., WILLIAMS, H. D. & KAPRELYANTS, A. S. 2004. Formation of 'non-culturable' cells of *Mycobacterium smegmatis* in stationary phase in response to growth under suboptimal conditions and their Rpf-mediated resuscitation. *Microbiology,* 150**,** 1687-97.

SHLEEVA, M. O., BAGRAMYAN, K., TELKOV, M. V., MUKAMOLOVA, G. V., YOUNG, M., KELL, D. B. & KAPRELYANTS, A. S. 2002. Formation and resuscitation of "non-culturable" cells of *Rhodococcus rhodochrous* and *Mycobacterium tuberculosis* in prolonged stationary phase. *Microbiology,* 148**,** 1581-91.

SIDDERS, B. & STOKER, N. G. 2007. Mycobacteria: Biology. *Encyclopedia of Life Sciences* [Online].

SINGH, B., GHOSH, J., ISLAM, N. M., DASGUPTA, S. & KIRSEBOM, L. A. 2010. Growth, cell division and sporulation in mycobacteria. *Antonie Van Leeuwenhoek,* 98**,** 165-77.

SINGH, B., NITHARWAL, R. G., RAMESH, M., PETTERSSON, B. M., KIRSEBOM, L. A. & DASGUPTA, S. 2013. Asymmetric growth and division in *Mycobacterium spp.*: compensatory mechanisms for non-medial septa. *Mol Microbiol,* 88**,** 64-76.

SMITH, J. D., KUMARASIRI, M., ZHANG, W., HESEK, D., LEE, M., TOTH, M., VAKULENKO, S., FISHER, J. F., MOBASHERY, S. & CHEN, Y. 2013. Structural analysis of the role of *Pseudomonas*

aeruginosa penicillin-binding protein 5 in beta-lactam resistance. *Antimicrob Agents Chemother,* 57**,** 3137-46.
SMITH, T. J., BLACKMAN, S. A. & FOSTER, S. J. 2000. Autolysins of *Bacillus subtilis*: multiple enzymes with multiple functions. *Microbiology,* 146 (Pt 2)**,** 249-62.
SNAPPER, S. B., MELTON, R. E., MUSTAFA, S., KIESER, T. & JACOBS, W. R., JR. 1990. Isolation and characterization of efficient plasmid transformation mutants of *Mycobacterium smegmatis*. *Mol Microbiol,* 4**,** 1911-9.
SOBHANIFAR, S., KING, D. T. & STRYNADKA, N. C. 2013. Fortifying the wall: synthesis, regulation and degradation of bacterial peptidoglycan. *Curr Opin Struct Biol,* 23**,** 695-703.
SPRATT, B. G. 1983. Penicillin-binding proteins and the future of beta-lactam antibiotics. The Seventh Fleming Lecture. *J Gen Microbiol,* 129**,** 1247-60.
SQUEGLIA, S., D'AURIA, G. & BERISIO, R. 2013. *Structural and functional characterization of proteins involved in bacterial cell growth and division.* PhD, University of Naples "Federico II".
STEYN, A. J., COLLINS, D. M., HONDALUS, M. K., JACOBS, W. R., JR., KAWAKAMI, R. P. & BLOOM, B. R. 2002. *Mycobacterium tuberculosis* WhiB3 interacts with RpoV to affect host survival but is dispensable for in vivo growth. *Proc Natl Acad Sci U S A,* 99**,** 3147-52.
STIEL, A. C., ANDRESEN, M., BOCK, H., HILBERT, M., SCHILDE, J., SCHONLE, A., EGGELING, C., EGNER, A., HELL, S. W. & JAKOBS, S. 2008. Generation of monomeric reversibly switchable red fluorescent proteins for far-field fluorescence nanoscopy. *Biophys J,* 95**,** 2989-97.
TAKAYAMA, K., WANG, C. & BESRA, G. S. 2005. Pathway to synthesis and processing of mycolic acids in *Mycobacterium tuberculosis*. *Clin Microbiol Rev,* 18**,** 81-101.
TAMERIS, M. D., HATHERILL, M., LANDRY, B. S., SCRIBA, T. J., SNOWDEN, M. A., LOCKHART, S., SHEA, J. E., MCCLAIN, J. B., HUSSEY, G. D., HANEKOM, W. A., MAHOMED, H., MCSHANE, H. & TEAM, M. A. T. S. 2013. Safety and efficacy of MVA85A, a new tuberculosis vaccine, in infants previously vaccinated with BCG: a randomised, placebo-controlled phase 2b trial. *Lancet,* 381**,** 1021-8.
TELENTI, A. 1997. Genetics of drug resistance in tuberculosis. *Clin Chest Med,* 18**,** 55-64.
TELENTI, A., IMBODEN, P., MARCHESI, F., LOWRIE, D., COLE, S., COLSTON, M. J., MATTER, L., SCHOPFER, K. & BODMER, T. 1993. Detection of rifampicin-resistance mutations in *Mycobacterium tuberculosis*. *Lancet,* 341**,** 647-50.
TEMPLIN, M. F., URSINUS, A. & HOLTJE, J. V. 1999. A defect in cell wall recycling triggers autolysis during the stationary growth phase of *Escherichia coli*. *EMBO J,* 18**,** 4108-17.
THANKY, N. R., YOUNG, D. B. & ROBERTSON, B. D. 2007. Unusual features of the cell cycle in mycobacteria: polar-restricted growth and the snapping-model of cell division. *Tuberculosis (Edinb),* 87**,** 231-6.
TODD, J. A. & ELLAR, D. J. 1983. Identification of penicillin-binding protein 5a of *Bacillus megaterium* KM as a DD-carboxypeptidase. *Biochem J,* 214**,** 653-5.
TRAAG, B. A., DRIKS, A., STRAGIER, P., BITTER, W., BROUSSARD, G., HATFULL, G., CHU, F., ADAMS, K. N., RAMAKRISHNAN, L. & LOSICK, R. 2010. Do mycobacteria produce endospores? *Proc Natl Acad Sci U S A,* 107**,** 878-81.
TRUEBA, F. J. 1982. On the precision and accuracy achieved by *Escherichia coli* cells at fission about their middle. *Arch Microbiol,* 131**,** 55-9.
TUFARIELLO, J. M., MI, K., XU, J., MANABE, Y. C., KESAVAN, A. K., DRUMM, J., TANAKA, K., JACOBS, W. R., JR. & CHAN, J. 2006. Deletion of the *Mycobacterium tuberculosis* resuscitation-promoting factor Rv1009 gene results in delayed reactivation from chronic tuberculosis. *Infect Immun,* 74**,** 2985-95.
TYPAS, A., BANZHAF, M., GROSS, C. A. & VOLLMER, W. 2012. From the regulation of peptidoglycan synthesis to bacterial growth and morphology. *Nat Rev Microbiol,* 10**,** 123-36.
VAN CREVEL, R., OTTENHOFF, T. H. & VAN DER MEER, J. W. 2002. Innate immunity to *Mycobacterium tuberculosis*. *Clin Microbiol Rev,* 15**,** 294-309.

VAN DER LINDEN, M. P., DE HAAN, L., HOYER, M. A. & KECK, W. 1992. Possible role of *Escherichia coli* penicillin-binding protein 6 in stabilization of stationary-phase peptidoglycan. *J Bacteriol,* 174**,** 7572-8.

VELAYATI, A. A., MASJEDI, M. R., FARNIA, P., TABARSI, P., GHANAVI, J., ZIAZARIFI, A. H. & HOFFNER, S. E. 2009. Emergence of new forms of totally drug-resistant tuberculosis bacilli: super extensively drug-resistant tuberculosis or totally drug-resistant strains in iran. *Chest,* 136**,** 420-5.

VERSCHOOR, J. A., BAIRD, M. S. & GROOTEN, J. 2012. Towards understanding the functional diversity of cell wall mycolic acids of *Mycobacterium tuberculosis*. *Prog Lipid Res,* 51**,** 325-39.

VIJAY, S., NAGARAJA, M., SEBASTIAN, J. & AJITKUMAR, P. 2014. Asymmetric cell division in *Mycobacterium tuberculosi*s and its unique features. *Arch Microbiol,* 196**,** 157-68.

VOLLMER, W. & BERTSCHE, U. 2008. Murein (peptidoglycan) structure, architecture and biosynthesis in *Escherichia coli*. *Biochim Biophys Acta,* 1778**,** 1714-34.

VOLLMER, W., BLANOT, D. & DE PEDRO, M. A. 2008a. Peptidoglycan structure and architecture. *FEMS Microbiol Rev,* 32**,** 149-67.

VOLLMER, W., JORIS, B., CHARLIER, P. & FOSTER, S. 2008b. Bacterial peptidoglycan (murein) hydrolases. *FEMS Microbiol Rev,* 32**,** 259-86.

WANG, S., FURCHTGOTT, L., HUANG, K. C. & SHAEVITZ, J. W. 2012. Helical insertion of peptidoglycan produces chiral ordering of the bacterial cell wall. *Proc Natl Acad Sci U S A,* 109**,** E595-604.

WAYNE, L. G. 1994. Dormancy of *Mycobacterium tuberculosis* and latency of disease. *Eur J Clin Microbiol Infect Dis,* 13**,** 908-14.

WAYNE, L. G. & SOHASKEY, C. D. 2001. Nonreplicating persistence of *Mycobacterium tuberculosis*. *Annu Rev Microbiol,* 55**,** 139-63.

WHO 2013. Global Tuberculosis Report 2013. World Health Organisation.

YANG, D. C., TAN, K., JOACHIMIAK, A. & BERNHARDT, T. G. 2012. A conformational switch controls cell wall-remodelling enzymes required for bacterial cell division. *Mol Microbiol,* 85**,** 768-81.

YOUNG, K. D. 2010. Bacterial shape: two-dimensional questions and possibilities. *Annu Rev Microbiol,* 64**,** 223-40.

ZHANG, Y. 2005. The magic bullets and tuberculosis drug targets. *Annu Rev Pharmacol Toxicol,* 45**,** 529-64.

ZUMLA, A., GEORGE, A., SHARMA, V., HERBERT, N. & BARONESS MASHAM OF, I. 2013. WHO's 2013 global report on tuberculosis: successes, threats, and opportunities. *Lancet,* 382**,** 1765-7.